Technical Report 747/2024/ENG

RESEARCH OF FRACTURE CONNECTIVITY IN THE BUKOV URF

Final Report

Authors: Milan Zuna et al.

Prague, 2024

REPORT NAME: Research of fracture connectivity in the Bukov URF – Final Report

PROJECT NAME: Research of fracture connectivity in the Bukov URF

PROJECT IDENTIFICATION: Final Report

CONTRACT NUMBER: *SO 2019 – 031*

TEAM OF AUTHORS: Milan Zuna[1], Libor Gvoždík[4], Martin Milický[4], Karel Sosna[3], Ondřej Švagera[2], Filip Jankovský[1], Jaroslav Řihošek[2], Petr Kabele[5]

ÚJV Řež, a. s.[1], Czech Geological Survey[2], SG Geotechnika a.s.[3], PROGEO, s.r.o.[4], ČVUT Praha[5],

BIBLIOGRAPHICAL REFERENCE: ZUNA M., GVOŽDÍK L., MILICKÝ M., SOSNA K., ŠVAGERA O., JANKOVSKÝ F., ŘIHOŠEK J., KABELE P. (2024): Research of fracture connectivity in the Bukov URF – Final Report. TR SÚRAO 747/2024.

Jan Smutek	**Milan Zuna**
SÚRAO	Main project manager ("Fracture connectivity in the Bukov URF")

SÚRAO

SÚRAO

Contents

List of Abbreviations:

ABI	Acoustic Borehole Imaging
CVŘ	Research Center Rež
CEC	Cation Exchange Capacity
CGS	Czech Geological Survey
DFN	Discrete Fracture Network
ST	Sub-Task
EC	Electric Conductivity
ECPM	Equivalent Continuum Porous Media
Eh	Oxidation-Reduction Potential (relative to the hydrogen electrode)
EIZ	Excavation Influence Zone
EURAD (FUTURE)	EU Programme Fundamental Understanding of Radionuclide Retention
Fsc	Fluorescein Sodium Salt / Uranine
GeoPET	Positron Emission Tomography (adapted for rock samples)
GHB	General Head Boundary
GRYF	GRYF HB, spol. s r.o.
HPLC	High Performance Liquid Chromatography
HTO	Tritiated Water
DGR	Deep Geological Repository
HZDR	Helmholtz-Zentrum Dresden-Rossendorf
ISE	Ion Selective Electrode
IUGS	International Union of Geological Sciences
LDO	Liquid Dissolved Oxygen
µCT	Computerized Tomography
MOVE	MOVE Modeling Software (PE Limited, Petex)
OBI	Optical Borehole Imaging
ORP	Oxidation-Reduction Potential (without correction)
Bukov URF	Bukov Underground Research Facility
RAW	Radioactive Waste
RWT	Rhodamine WT
SG	Structural-Geological
SGW2	Synthetic Granite Water (type 2)
SPECT	Single-Photon Emission Computed Tomography
SÚRAO	Radioactive Waste Repository Authority (Správa úložišť radioaktivních odpadů)
TACR	Technology Agency of the Czech Republic
TR	Technical Report
ÚJV	ÚJV Řež a.s.
URF	Underground Research Facility
WPT	Water Pressure Test
WTW	WTW (Germany)
ZK2	Test Chamber ZK2 (Bukov URF)
FR	Final Report
18F	Fluorine-18
3D	Three-Dimensional

Abstract

This final report summarizes the progress of the work performed and results achieved within the project “Research of fracture connectivity in Bukov URF” implemented by the company ”Fracture connectivity in Bukov URF” between 2019 and 2024.

The main aim of the project was to obtain data for the development of hydrogeological and transport models to simulate groundwater flow in the rock mass at a depth of approximately 550 m. In general terms, then apply and validate a comprehensive workflow from the implementation of the boreholes, their characterization, instrumentation, and testing of hydraulic and transport parameters. At the same time, the work included a laboratory program focusing on the description of representative rock types, geochemistry of fracture fillings, and geomechanical parameters. Another part of the laboratory tests was focused on the study of transport parameters of selected tracers (diffusion, sorption) and transport experiments on natural fracture drill core samples.

The selected rock block for the study of the fracture network is adjacent to the test chamber ZK-2 situated in the Bukov URF. Firstly, a detailed characterization of the rock block was performed, which included detailed structural measurements, photo documentation, processing of structures in the MOVE software, and subsequent development of a 3D structural geological model. Based on the characterization of the rock block, three monitoring boreholes S-27, S-31, and S-36 were drilled. The boreholes were characterized in detail using a suite of logging methods, geological description of the drill cores and study of rock samples. The existing S-8 borehole was also used for monitoring.

Hydrogeological parameters were studied primarily by means of water pressure tests and hydraulic tests. Based on the complete characterization and the resulting 3D geometric model, the main potentially conductive structures were selected, and the main study intervals were defined. Multipacker systems containing four measurement intervals were subsequently installed in each borehole, where continuous monitoring of water pressure conditions was implemented. In the next phase of the project, hydraulic tests were performed between the boreholes using both pulse tests and long-term injection tests. After the evaluation of the tests, the models were updated, flow simulations were performed, and then tracer tests with conservative tracers were designed and implemented. Attention was focused on intervals with both a highly conductive fractured zone and a less conductive fractured zone, with transport distances being approximately 13.8 m and 28 m, respectively.

As part of the project, geological (GeoDFN), hydrogeological (HydroDFN), and transport models of the studied block of rock were constructed, which were gradually updated and refined based on the available data from the characterization work and the hydraulic and tracer tests.

The report includes a summary of the experience and recommendations for further activities or similar future projects.

Keywords

Deep geological repository, Bukov URF, tracer test, fracture, migration, transport, laboratory experiments, modeling, GeoDFN model, HydroDFN model

1 Introduction

This report summarizes the progress of the work performed and the results achieved in six sub-tasks and in individual stages of the project (Stages 1 to 28) (Tab. 1). The work plan and continuity of work within the selected Bukov URF block was described in detail in interim report No. 1 in the form of an implementation project (Zuna et al. 2020). Subsequently, the activities and interim results were described in the interim reports of the project and the final report (Tab. 1).

Tab. 1 Overview of the sub-tasks and technical reports

Sub-task	Stage	TR Number	Citation
1	1–3	459/2020	Zuna et al. 2020
2	4–9	521/2020	Zuna et al. 2020b
3	10–20	551/2021	Zuna et al. 2021
4	21–23	630/2022	Zuna et al. 2022
5	24–26	702/2023	Zuna et al. 2023
6	26–28	747/2024	Zuna et al. 2024

1.1 Project Scope

The subject of the project was research and development work leading to the acquisition of information about the speed and nature of the groundwater flow, the connectivity of fracture networks and, in general, the methodology and conservative nature of the mathematical models used.

The main requirement was to test the following complex workflow:

1) Compilation of a conceptual hydrogeological model and a preliminary mathematical flow model of the rock block of interest,
2) In-situ tests in boreholes in the rock block of interest, and
3) Calibration and verification of the models

At present, it is necessary to obtain real data from the corresponding environment of the DGR in order to determine whether the expert estimates of rock properties, on which current hydrogeological and transport models are based, correspond to reality. It is important to test the environment corresponding to the rock mass at the location of the storage sites in the DGR (without significant hydraulically conductive fault zones) and, conversely, discrete fault structures.

The subject of the work was to characterize the geology of the rock block of interest, perform technical work and instrumentation, and evaluate the experimental work using a mathematical model.

The research activity according to the previous paragraph included:

- Study of existing knowledge of similar projects in the Czech Republic and abroad,

- Geological characterization of the rock block of interest and the boreholes,
- Processing of the implementation project and the project quality plan,
- Performance of technical works (e.g., drilling work, characterization of boreholes,)
- Instrumentation of the experiment (monitoring of pressure ratios),
- Performance of in-situ tests and measurements (water pressure tests, hydraulic tests, tracer tests),
- Mathematical modeling,
- Final evaluation

1.2 Project Implementation

In the first phase, attention was focused on the study of similar projects in laboratories abroad and in the Czech Republic. Relevant projects performed in crystalline rocks were selected for the study, mainly from the Grimsel Test Site and the Äspo Hard Rock Laboratory. Part of the research was also a laboratory program focusing on the study of transport parameters, experimental instrumentation, test parameters, and numerical and model approaches to the evaluation of tracer tests. The study forms part of interim report No. 1 - part 1 (Zuna et al. 2020).

Subsequently, work began on the detailed characterization of the selected rock block in the Bukov URF (the area between corridors ZK-2, BZ1-XII, and BZ-XIIJ) and the surrounding area. The first part of the work focused on summarizing the previous data and results from the Bukov URF obtained over the years within related projects. The individual methods used in the geological and geotechnical investigations performed in the area were described with an emphasis on the obtained data, including their description within the geological and structural characterization of the Bukov URF, and the main results were summarized. The detailed characterization of the rock block of interest included detailed in-situ structural measurements using a geological compass, acquisition of high-resolution photographic material of the individual walls, processing of the measured structures in the MOVE software, and subsequent creation of a 3D structural-geological model. This model was used to predict the progress of fragile structures and surface-parallel structures and allowed for a qualified estimate for the position of the proposed drilling works. The work focusing on the characterization of the rock mass and the rock block is part of interim report No. 1 – part 2 (Kryl et al. 2020). One of the aims of the characterization of the experimental block was to propose locations for the drilling of the first characterization borehole based on SG measurements of foliation and significant brittle structures. Based on the geological characterization, the first borehole S-27 with a length of 58.1 m was drilled.

After drilling the borehole, it was thoroughly cleaned, and characterized using a suite of well-logging methods, and detailed geological characterization of the drill core and rock samples was also performed. The well-logging was performed to obtain information on the lithology, rock failures, geomechanical properties of the encountered rocks, and the character of faults in the rock mass. The well-logging utilized a set of measurement methods (well camera, OBI optical television, ABI acoustic television, natural gamma well-logging, neutron-neutron well-logging, density well-logging, magnetic susceptibility well-logging, electrical well-logging, induction well-logging, cavernometry, inclinometry, thermometry, resistivimetry, and wave acoustic well-logging). Hydrogeological conditions in the borehole were determined by the method of diluting a tracer liquid. The borehole was further characterized by water pressure tests (WPT) using a mobile system. WPT were performed in the borehole at selected test intervals. Based on the results of all characterization methods and the resulting 3D geometric model, suitable intervals were selected for sealing the borehole and performing subsequent measurements/tests. In the next stage, a multipacker system containing four packers and thereby four measuring intervals (three between the packers and one between the last packer and the borehole bottom) was constructed. Piezometers for online monitoring of water pressure (Geokon model 4500C) were installed in all measurement intervals.

In the following stage, two more boreholes (S-31 and S-36) were drilled and characterized using the same procedure as for borehole S-27 (well-logging measurements, WPT, etc.). In borehole S-31, a fault zone was encountered at a depth of 9–12 m, which represented a significant risk for the installation of the multipacker system. Therefore, it was decided to stabilize the borehole by injecting it with epoxy resin and then redrilling the injected part of the borehole. This stabilization was successful, and the borehole could be further measured by WPT.

Subsequently, an interval WPT was performed in the boreholes. In the newly drilled boreholes (S-31, S-36), selected intervals were tested by a suite of tests (pulse test, injection pressure test, drop test). The aim of the hydraulic tests in boreholes S-31 and S-36 was to characterize and quantify the hydraulic properties in the selected sections of the boreholes. Knowledge of these parameters is necessary for the mathematical hydraulic models of flow and transport of substances in the rock environments. The obtained parameters were also used to evaluate the hydraulic conductivity.

After evaluating all the test results, multipacker systems were installed at the selected depths. The multipackers allow simultaneous measurement of groundwater pressure and sampling, or injecting, water from two different areas of the interval in the tested floor. In order to determine the hydraulic connection of the studied boreholes (S-27, S-31, S-36) with the existing borehole S-8. This borehole was also characterized and equipped with a multipacker system with two monitoring intervals. After all the boreholes were equipped, hydraulic connectivity tests were performed between the individual borehole intervals.

Structural-geological and petrological analysis was performed along the drill cores. Individual planar structural elements (fissures, shear fractures, longitudinal fractures, fracture zones, tectonic faults, and reactivated foliation) of the drill cores were also described. Structural and lithological data were clearly summarized in a well log elaborated in LogPlot7 software. Laboratory analyses of representative rock types were conducted on selected parts of the drill cores to determine the petrology, mineralogy, and geomechanical parameters of the rock matrix, and fillings of the studied fracture zones, etc.

Another part of the work focused on constructing a conceptual model of the rock block of interest. The spatial orientation of the three boreholes (S-27, S-31, and S-36) was designed to provide information on the 3D layout of all important structures in the block of interest, while also providing relevant information for hydraulic and subsequent tracer tests. The detailed results of the works performed during sub-task 3 (Stages 10 to 20) are summarized in the report of Zuna et al. 2021.

After the installation of all multipackers in boreholes S-27, S-31, S-36, and S-8 (Stage 22), the phase of monitoring pressure ratios in all the test intervals followed. In the first phase, the establishment of pressure ratios in the boreholes was monitored when all intervals were closed. Furthermore, the flow rates from selected open intervals and the induced pressure responses in the other intervals of the multipackers were also measured. The next stage focused on hydraulic tests between the individual boreholes. Pressure tests, pulse tests, and then longer-term hydraulic injection tests were performed in selected floors of the boreholes. The stable ratios at the end of the tests were used to evaluate the hydraulic conductivity of the tested sections.

Laboratory tests in Stage 25 focused on studying the sorption properties of selected tracers on rock material (rock, fracture fillings) and diffusion experiments on the rock matrix. Laboratory transport experiments were also conducted on samples of drill cores with fractures. The transport was visualized using µCT analysis and subsequent measurements were taken by GeoPET tomography (^{18}F). For in-situ experiments, the use of salts (KCl and KI) was verified in the laboratory, including the simultaneous measurement of conductivity (EC) and iodide concentration using ISE. Further work focused on the collection and analysis of fracture and vein filling samples obtained from boreholes S-27, S-31, and S-36 (Zuna et al. 2023). Attention was also paid to the differences in hydrochemical parameters in the studied intervals, especially the EC and pH values, which have an influence on the behavior of the tracer and the balance of the tracer when salts are used (conductivity measurements). During the measurement, flow rates from the individual intervals were monitored and hydrochemical parameters (EC, pH, Eh, LDO) were measured in the flow cell.

Based on the evaluation of hydraulic tests and predictive models, tracer tests were performed, focusing primarily on the active zones with hydraulic communication at selected intervals. For the tracer tests, instrumentation was developed, tested, and used both for the tracer tests themselves and for monitoring during and after the tracer tests. Detection systems for measuring flow, concentrations of iodide, dyes (e.g., fluorescein), and conductivity were tested as part of the laboratory and tracer tests. During Stage 26, three in-situ tracer tests were performed and evaluated using the conservative tracers KCl, KI, and fluorescein at concentrations of 0.01 M KCl to 0.1 M KI. Both conductive intervals (S31_ 2 to S36_3) and intervals with a less conductive fault (S31_1 to S36_3ab) were tested. The distance between the intersections of the fractures with the boreholes was roughly 28 m, i.e., twice as long as the distance of the intersections in the test (S31_2 to S36_3) (Zuna et al. 2023).

In the final phase of the project, the numerical model (E27) was finalized, which followed on from the modeling work performed in the previous stages 12, 21, and 24. These stages focused on the preparation of the fracture network geometry and flow simulation. The aim of the work in Stage 27 was to complete the numerical model, verify and update the hydraulic parameters, and determine the transport parameters of specific semi-deterministic fractures based on the tracer tests.

To conclude, the knowledge and experiences gained were summarized and recommendations for further activities were formulated. A summary of recommendations for the possible use of the existing test chamber (ZK-2), including instrumentation and suggestions for further potential experiments, was also included.

2 Geological Characterization

During the preparation of experiments and drilling works in the Bukov URF, a detailed structural-geological characterization of the rock block was performed. The aim was to obtain detailed information on the geological structure of the block and to propose the optimal location of the first characterization borehole. Detailed information is included in technical report No. 1 - part 2 (Zuna et al. 2020). From the dataset of 430 measurements of fragile structures, 118 more significant discontinuous fractures, 100 continuous fractures, and two faults were plotted in the characterization 3D SG model. The filling of individual fragile structures was most commonly defined by calcite, chlorite with locally precipitated limonite and, in the case of shear faults and fractures, clays.

Petrographic characterization of the rocks in corridors ZK-2, BZ1-XII, and BZ-XIIJ distinguished three main lithological types, i.e., biotite paragneiss, amphibole-biotite paragneiss, and migmatite. The foliation construction is flatly parallel in all corridors, with a variable inclination. The fracture system consists of continuous and discontinuous fractures with two main directions: NNE-SWW and WNW-ESE (Fig. 1), and three significant fault structures were mapped.

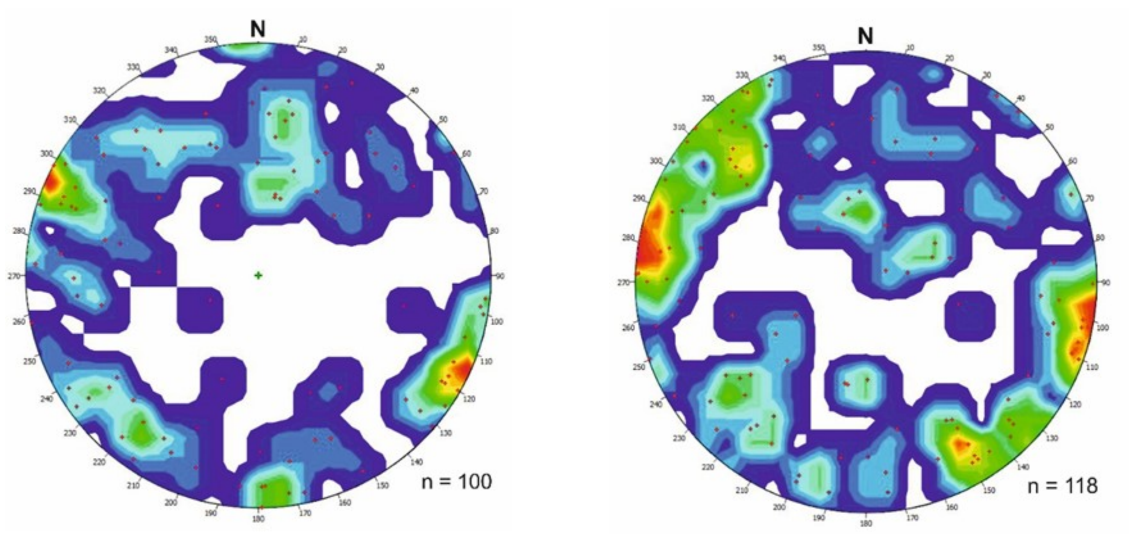

Fig. 1 Pole diagrams showing the general direction of the slope and the slope of continuous (left) and discontinuous (right) fractures in individual corridors of the studied section. The contours in the diagram were calculated in the MOVE program and show the poles of the surfaces of the individual in-situ measurements in the Bukov URF.

The next phase of the work included detailed high-resolution photographic documentation of all corridors with the aim of creating 3D photogrammetric models for visualization and analysis of the structural data.

The modeling process involved several steps:

1. Photographic documentation:

Over 1000 images of corridors were taken in high resolution.

2. Processing:

The images were divided into processable sections (individual corridors) and processed in the Agisoft Metashape program into the form of a point cloud and then a 3D mesh model with a realistic photo texture (Fig. 2).

3. Positioning:

The models were positioned in the S-JTSK Křovák East-North georeferencing system (EPSG: 5514) and on the Bukov URF ground plan obtained from DIAMO s.p.

4. Data output:

Based on the measurement database of all structural data documented underground, selected representative data for the GeoDFN model were plotted in the models Fig. 3). A detailed description of the measured data is included in TR 459/2020 (part 2 - Kryl et al. 2020).

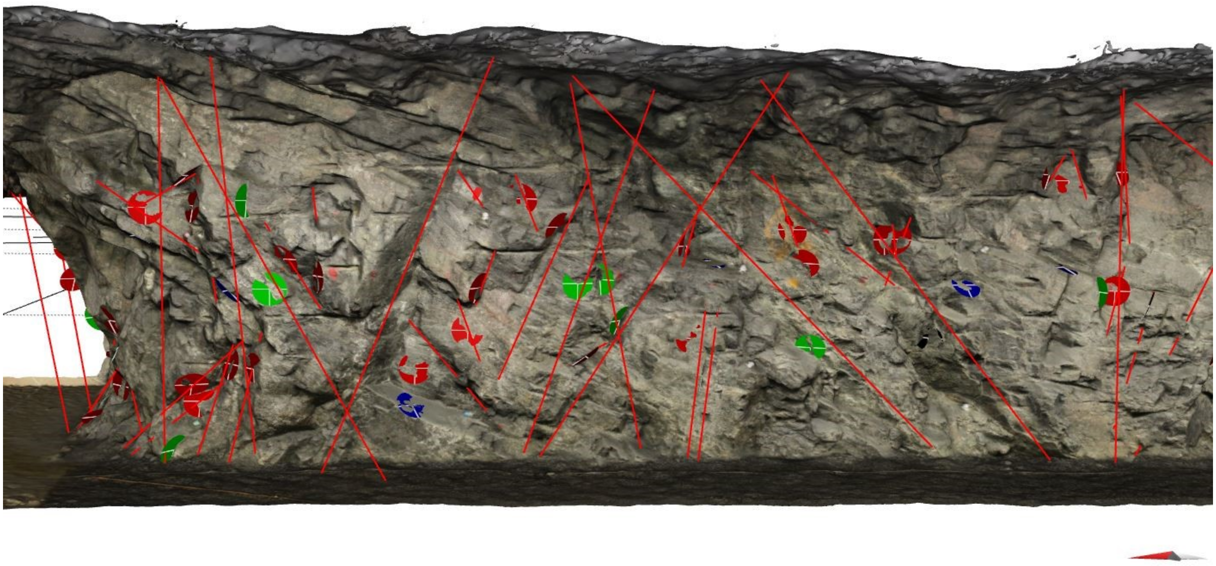

Fig. 2 Example of a part of the photogrammetric model complied in MOVE with the marked orientations of the individual structural measurements (blue – foliation, red – discontinuous fractures, green – continuous fractures, red line – course of the whole visible surface of the fracture)

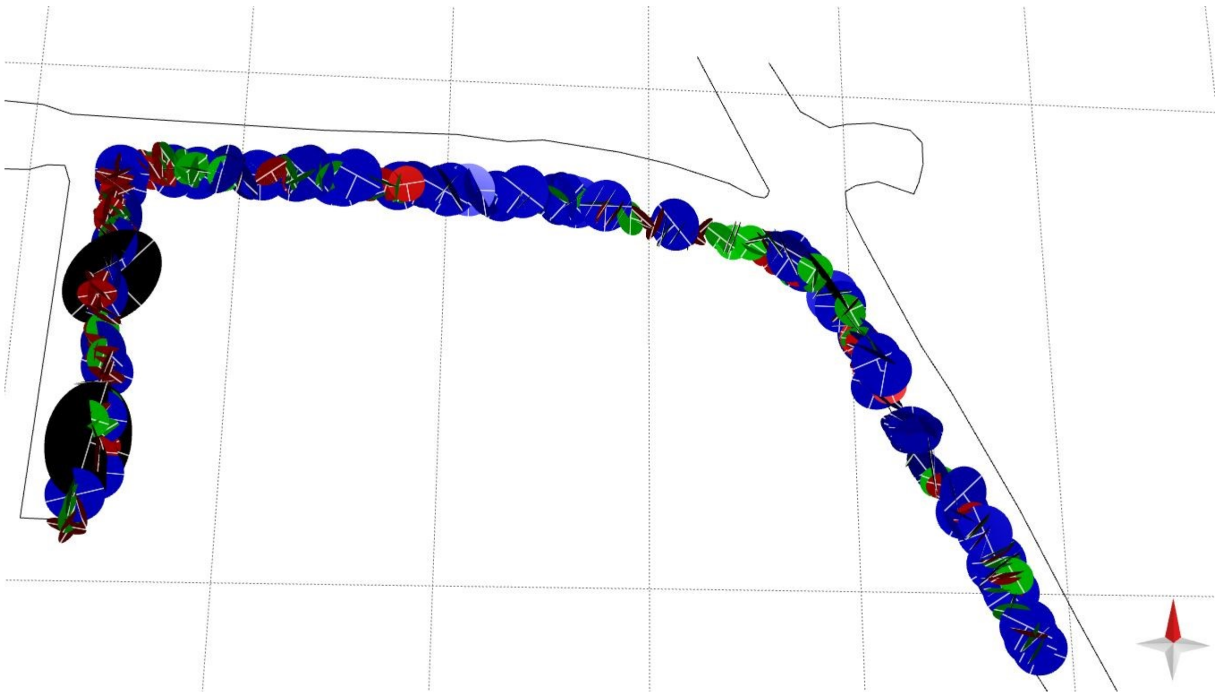

Fig. 3 Illustration of all measured and plotted structures in the studied block in the Bukov URF (blue – foliation, red – discontinuous fractures, green – continuous fractures, black – faults)

Based on structural measurements and visualizations, a 3D structural-geological model of the rock block of interest was created. The model and its subsequent iterations enabled interactive visualization and analysis of the structural data, facilitating planning of the experiments and drilling work.

Based on the model, the optimal location of characterization borehole 1 (S-27) was proposed, mainly with regard to:

- Structural and lithological homogeneity,
- Perpendicular orientation to the foliation,
- Presence of significant fragile structures.

The 3D geological model was then updated with each new borehole, and the data from it was used in the subsequent modeling work. More information about this procedure is included in Section 6.2 of this report.

3 Design and Drilling of Boreholes

Before starting the drilling work, the workplace was prepared. Tracks were installed in the test chamber ZK-2, an iron structure was created for the drilling and attaching the drilling rig, and lighting, electrical, and network connections were provided.

A detailed characterization of the selected block was performed based on the structural-geological mapping (measurement of foliation and important fragile structures). From the results, the first 3D SG model was constructed with suggested alterative locations and the orientation of borehole 1 (S-27). The choice of the location for drilling borehole 1 depended mainly on factors such as structural and lithological homogeneity (predictable foliation and uniform lithology in the first few meters of the borehole), perpendicular orientation to the foliation (minimizing the risk of the drill bit slipping), the presence of any significant fragile structures with a potential for transporting water near the mouth of the borehole (minimizing the damage caused by the borehole collapsing, reachability of the conductive structure in the first few meters) and at a sufficient range of the borehole across the experimental block so that the results of well-logging, SG, and petrographic documentation of the drill core may be used to adjust the SG model. After precisely marking out the borehole, drilling work was performed (Diamo s.p., GEAM Dolní Rožínka). Detailed information on the drilling and characterization of borehole 1 (S-27) is included in technical report No. 2 (Zuna et al. 2020b).

Fig. 4 Preparing corridor ZK-2, installation of the tracks

Fig. 5 Installation of the drilling rig in chamber ZK-2

After drilling and characterizing borehole 1, it was subsequently possible to better understand the propagation of significant brittle structures to the depth of the experimental block and to correlate the assumed petrological characteristics of the rock mass in the experimental block.

The main aim of sub-task 3 was to drill boreholes 2 (S-31) and 3 (S-36) and their detailed characterization. Based on the characterization of the site of interest, the location and inclination of boreholes S-31 and S-36 were specified. Drilling work began after stabilization of the pressure conditions in the multipacker test intervals of borehole 1 (S-27). During the drilling work, the response of the drilling work in the surrounding boreholes was measured to clarify the connection of the boreholes and individual fracture systems. Detailed information on the drilling of boreholes S-31 and S-36 is provided in technical report No. 3 (Zuna et al. 2021).

After drilling each borehole, the borehole was repeatedly flushed out using the drilling rig and subsequently flushed out (with pressurized water) from the bottom of the borehole and pumped out using an Airlift (flushing of drilling water and mud). Groundwater from borehole S-1 was used for flushing out borehole.

During the drilling work, the drill core was precisely placed into core boxes and manually oriented (orientation marked with a grinding wheel on the core). After the drilling work was completed, the drill cores were transported to the material documentation warehouse of SÚRAO.

After drilling the boreholes, the work focused on their detailed characterization (see Section 4). A structural-geological and petrological analysis of the drill core was performed. The individual lithologies encountered in the boreholes were separated macroscopically and samples were taken from them for microscopic analysis in order to update the lithological determination and narrow the lithological variability. Individual structural elements such as fault zones, fractures, foliation, and reactivated foliation were identified and described on the drill cores. Individual structures were also measured with a geological compass and an attempt was made to correlate and reorient these measurements in relation to the spatial location of the boreholes. After the petrological and structural geological characterization, the drill cores were used to take larger core samples for further analytical and laboratory work (e.g., ÚJV Řež a.s., SG Geotechnika a.s.).

Fig. 6 Drilling work – placing the drill core into the drill core boxes

Fig. 7 Material documentation of the borehole

4 Characterization of Boreholes

4.1 Geological Characterization of Drill cores

Geological characterization of the drill cores consisted in the macro and microscopic description of the rock and the identification of the main lithological types. For the microscopic description and to update the macroscopic description, a set of cuttings was made from each borehole. The structural documentation focused mainly on the description of the type and character of the filling of individual structures. Since the drill core was not sampled as oriented, it was necessary to use information on the orientation of the structural data exclusively from the ABI40 well-logging measurements. For each borehole, the borehole column was processed to contain information on the description of the drill core. Details and individual outputs and condition surveys are part of TR 521/2020 (Zuna et al. 2020) and TR 551/2021 (Zuna et al. 2021).

A summary of the performed work is given below:

Borehole S-27:

- Four main lithologies were identified: biotite-amphibole paragneiss, biotite paragneiss, amphibolite, and migmatite.
- A total of 289 structural elements were documented (fractures, faults, foliation).
- A total of 193 structural elements were measured with a compass and a correlation test was performed with data from the ABI40 and it was possible to assign the measured data to the fractures.

Borehole S-31:

- Three main lithologies were identified: biotite-amphibolic paragneiss, migmatite and amphibolite.
- A total of 350 structural elements were documented.
- A total of 337 structural elements were measured with a compass - frequency correlation test with ABI40.

Borehole S-36:

- Three main lithologies were identified: biotite-amphibolic paragneiss, migmatite, and amphibolite.
- A total of 413 structural elements were documented.
- The orientation of the structural elements on the core was no longer measured, based on inconclusive results from the tests on drill cores S-27 and S-31, and only the data from the ABI 40 acoustic camera was used.

Microscopic analysis:

- Performed on cuttings from the samples taken.
- Served to update the lithological determination and narrow down the lithological variability (Fig. 8).

Borehole logs:

Processed in LogPlot7 software for each borehole (Fig. 9).

- Location, stationing, and orientation of the borehole.
- Information on lithology and structural elements.
- Results of measurements with the ABI40 acoustic television.
- Sinusoids for calculating the spatial orientation of structural elements from ABI40.

After characterization, the drill cores were made available taking larger samples for geochemical analysis, mechanical testing, and isotopic analysis.

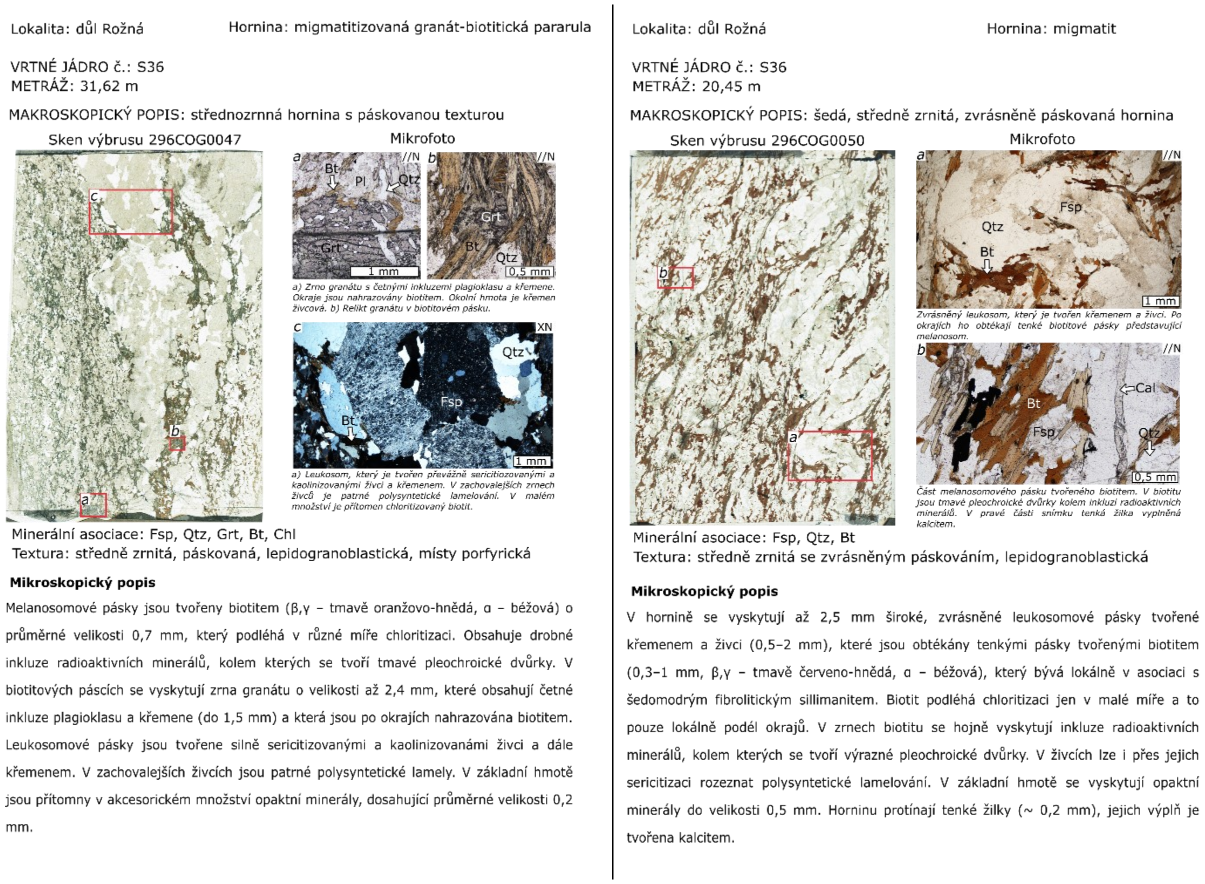

Fig. 8 Example of condition surveys characterizing the individual lithologies of borehole S-36

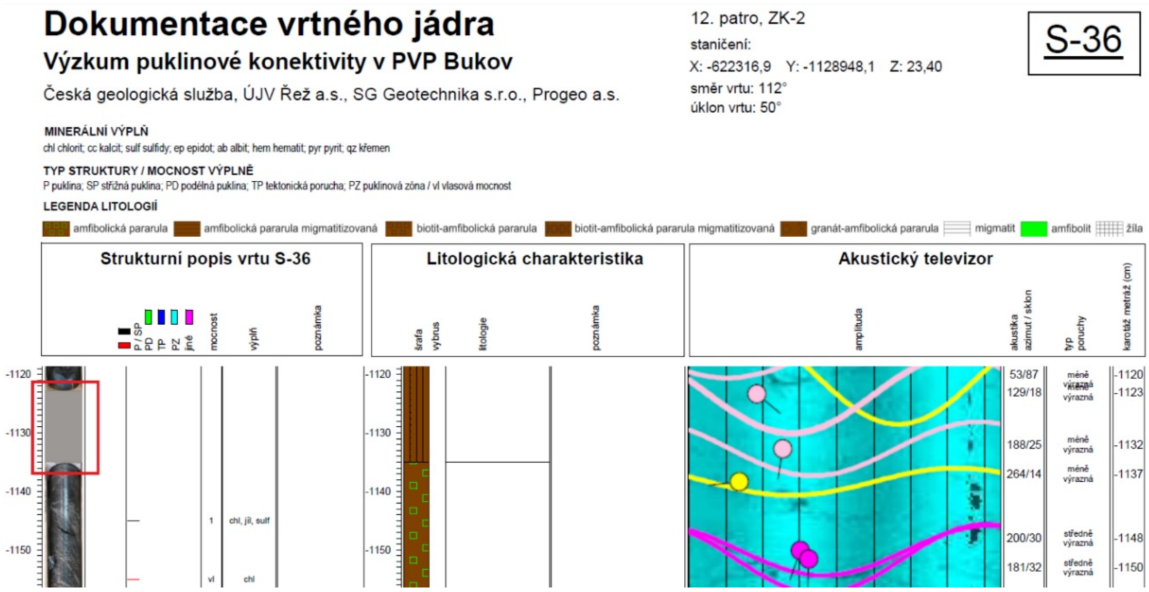

Fig. 9 Overview of the processed borehole column S-36 with added information from the acoustic television

4.2 Reorientation and Correlation of the Drill Core Based on Data from the Acoustic Television

Another aspect of the structural-geological description of the boreholes was testing the possibility of working with an unoriented drill core and performing its reverse reorientation based on the course of foliation surfaces and the results of well-logging using ABI and in borehole S-36 also OBI. The results and recommendations when correlating data from measurements on unoriented drill cores with well-logging measurements performed in boreholes S-27, S-31, and S-36 are as follows:

Borehole S-27

- The orientation of borehole S-27 was measured by well inclinometry and geodetic surveying of the moth of the borehole with an assumed linear course.
- Discrepancies between these measurements and local inclinometric compass fluctuations due to iron sulfide mineralization were detected.
- In-situ geodetic surveying of the borehole was determined to be the best method with an azimuth of 91° and an inclination of 31°. Well-logging data were converted to this azimuth.
- A direct measurement of the structures in borehole S-27 was performed and compared to the acoustic television data.

Borehole S-31

- Reorientation of the data from the drill core of borehole S-31 was performed based on the recording from the acoustic camera.
- Structural data were measured with a geological compass in sample boxes.
- A discrepancy between the orientation of the structural elements on the drill core and the recording from the acoustic camera was found.

- Manual reorientation of the drill core according to the ABI records and measurement of structural elements with a compass was found to be neither sufficient nor accurate.
- Relevant data for the orientation of structural elements must be obtained from correctly performed well-logging using the ABI method.

Borehole S-36

- The optical television method (OBI) was used in combination with the acoustic television (ABI).
- OBI makes it possible to better evaluate tectonic disturbances, as it provides an optical comparison between the wall of the borehole stem and the drill core.
- Structural characterization of the log core is necessary in terms of determining the filling, power and type of structural elements.

Manual reorientation of the drill core and measurement of structural elements with a compass is not recommended due to it being inaccurate and time-consuming.

- A combination of ABI and OBI well-logging methods is crucial for identifying structural elements and determining their orientation.
- Structural characterization of the drill core is important for determining the filling, thickness, and character of structural elements, including determining the lithological composition.
- The borehole column serves as a comprehensive overview of the encountered rock environment.

For future characterizations and development of a methodology for the description of the drill cores, we recommend the following:

- Prioritize well-logging methods (ABI, OBI) to obtain the orientation of structural elements.
- Use non-magnetic centrators (when measuring with the ABI40).
- Use OBI for a more detailed assessment of tectonic disturbances in their fillings and correlation with the drill core.
- Combine the results of well-logging with a complex structural and petrological analysis of the drill cores.

4.3 Well-logging

In addition to the records from the ABI and OBI, characterization of the boreholes involved a wide range of well-logging methods applied in the boreholes. Their main objectives were to:

- Verify and refine the lithological profiles compiled according to the drill cores,
- Determine the spatial orientation (inclination and azimuth) of areas of discontinuity (fracture or fault zones) by acoustic television and subsequently by OBI,
- Determine the basic physical properties of rocks in the borehole profile with a step of 5 cm (in particular specific volume weight, natural radioactivity of rocks, specific electrical resistance of rocks, conductivity of rocks, neutron properties, susceptibility, and others),
- Determine the degree of rock failure, both chemical (weathering and weathering) and tectonic rock failure (determination of fault zones, or smaller individual fractures),

- Determine the basic geomechanical properties of rocks based on acoustic and density well-logging (bulk weight, velocity of propagation of longitudinal and transverse seismic waves, Young's modulus of the elasticity of rocks, shear modulus, Poisson's number, if applicable),
- Determine the basic hydrodynamic conditions in the borehole,
- Determine the properties of the liquid in the borehole (resistivity, temperature and transparency),
- Determine the actual diameter of the borehole, identify open fractures, sections of non-cohesive rock where the rock has fallen from the borehole wall,
- Determine the spatial course of the borehole.

To meet the requirements for well-logging, a relatively wide suite of well-logging methods was chosen, which included:

- *Optical television inspection* – television inspection of borehole walls and optical verification of fault zones,
- *ABI40 acoustic television* – under favorable conditions, this method enables the separation of areas of discontinuity in the borehole profile (mainly fractures) and the determination of their spatial orientation (inclination and azimuth),
- *Gamma well-logging* (natural radioactivity) – for the basic breakdown of the lithological profile,
- *Neutron-neutron well-logging* (determination of water content in rocks, both free and chemically bound in clay minerals – connection with the degree of chemical weathering of the rock or rock failure),
- *Density well-logging* (determination of specific bulk density and separation of fractured rock sections),
- *Magnetic susceptibility well-logging* (exclusion of rocks with a higher content of ferromagnetic materials and strongly altered rocks),
- *Electrical well-logging RAP010 and RAP041* in a potential arrangement with probe lengths of 41 cm and 10 cm - determination of the apparent electrical resistivity of rocks - breakdown of rocks according to lithology and degree of fracturing,
- *Induction well-logging* probe length 50 cm and 80 cm - determination of rock conductivity - division of rocks according to lithology and degree of fracturing - the method may also be used to measure in dry sections of boreholes. This method replaces electrical well-logging in dry boreholes and in boreholes cased with a plastic casing,
- *Wave acoustic well-logging* – this method enables the registration of complete wave images and the evaluation of the speed of longitudinal and transverse waves, which in favorable conditions leads to the calculation of Poisson's number and other geomechanical modules (Young's modulus ED_ALT and shear modulus GD_ALT),
- *Cavernometry* – measurement of borehole diameter, detection of open fractures and sections of unstable rock,
- *Inclinometry* – measurement of the spatial course of the borehole with an inclinometer with continuous recording of inclination and azimuth,
- *Thermometry*, continuous measurement of the water temperature in the borehole, serves to determine the locations of inflows or losses,

- *Resistivimetry* - determination of the electrical resistivity of the borehole liquid - conductivity,
- *A suite of resistivimetry methods for hydrogeology*, i.e., resistivimetry by filtration. Inflows into the boreholes (hydrogeological conditions) were determined by the method of diluting a tracer liquid.

Based on selected geophysical methods, the well-logging profile was divided into five categories according to the degree of rock failure. Measuring using optical (OBI) and acoustic (ABI) television, determined the orientation of all discontinuity surfaces, which subsequently served to update the structural 3D model of the block of interest. Using well-logging measurements, the locations of inflows were verified in both boreholes under intact hydraulic conditions. Data on the technical condition of the borehole and its spatial orientation were also provided (Zuna et al. 2021).

4.4 Conclusions from the Characterization Methods

The following conclusions were made from the three methods used (measurement of structures directly on the walls of the Bukov URF, measurement of structures directly on the drill core, and measurement of structures by acoustic television):

1) None of the methods alone shows the real state of the complete fracture network;

2) A limitation of measurement on the walls in a single floor of the mine is the inability of measuring sub-horizontal fractures in real frequency;

3) A limitation of direct measurement on the drill core is the neglect of steep fractures running parallel to the long axis of the borehole;

4) A limitation of direct measurement on the drill core is also often the accuracy of measuring individual structures, which may be slightly inaccurate in terms of inclination and azimuth due to the small area measured. An advantage is having a dataset measured directly on the walls of the underground work available for subsequent data correlation and correction. A possible solution is targeted drilling, whereby it is possible to determine the exact location and orientation of the core relative to the course of the borehole (azimuth and inclination);

5) A limitation of the acoustic television well-logging method is its inability to distinguish subparallel fractures from foliations from the resulting data, as well as the high frequency of foliations compared to other structures;

6) Another limitation of well-logging lies in the fact that it is extremely important to be certain of the orientation of the borehole, which is a number that is subsequently used in the calculation of the orientations of the individual structures/inhomogeneities, which are subsequently important for comparing with directly measured structural data. Well-logging data are also used as input data for the 3D model; therefore, it is necessary to be certain of their orientation;

7) A comparative study based on all three methods, performed on at least two semi-parallel boreholes, which, taking into account all the above-mentioned limitations, allowing the real parameters of the fracture/fault network to be plotted in 3D space seems an ideal solution;

8) Additional methods to the above procedure may include a comparison of OBI, ABI, and drill core scan data. All these methods allow the captured disturbances to be plotted using sinusoids and may therefore be compared with each other. A condition for the correct interpretation of data from these methods is a completely accurate measurement of the azimuth and inclination of the borehole and subsequent orientation of the drill core, either using a specialized tool for oriented drilling or a combination of the methods mentioned in this section, i.e., inclinometry, orientation of the drilling rig with a compass, geodetic orientation of the wellhead.

5 Multipacker and Measurement System – Monitoring

Further activities focused on the development and production of the multipacker system. The multipacker system for boreholes S-27, S-31, S-36, and S-8 consists of the following components: 4× stainless packer from Geopro, 4× pressure bushings, stainless pipes and a measuring center (Note: for borehole S-8, two packers and pressure bushings were used). Underneath each packer is a pressure bushing that contains four outlets. This solution makes it possible to simultaneously measure groundwater pressure and sample water from two different locations on the tested floor. The pressurization of the packers is ensured by polyamide tubes with an outer and inner diameter of 6 and 3 mm (up to 100 bar), respectively. A polyamide tube with an outer and inner diameter of 6/4 mm (up to 58 bar) designed for injection or collection of water is led into the space between the packers. Geokon model 4500C vibrating string piezometers with a diameter of 11 mm and a range of 7 bar placed directly in the well space between the packers are used to monitor the pressure. After each measurement, the data were stored in the internal memory of the measuring center and are sent via remote online access.

Based on the results of the hydraulic tests, well-logging methods and interpreted geological models, suitable intervals for the construction of the multipacker systems were selected. The multipacker systems were successfully installed in corridor ZK-2 in boreholes S-27, S-31, and S-36 with defined intervals (four measurement intervals). These intervals were used to measure pressure ratios and subsequently conduct hydraulic and transport tests. During the hydraulic tests, the pressure ratios were measured in the multipacker systems.

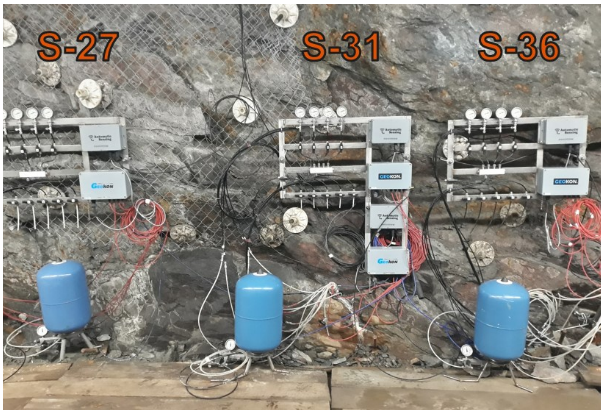

Fig. 10 Control panels of boreholes S-27, S-31, and S-36 in gallery ZK-2

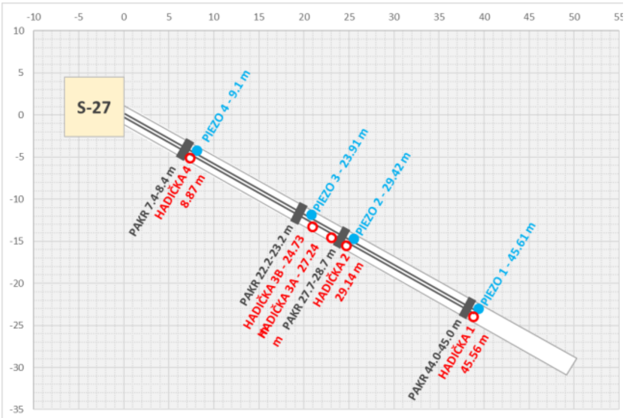

Fig. 11 Diagram of the multipacker in borehole S-27

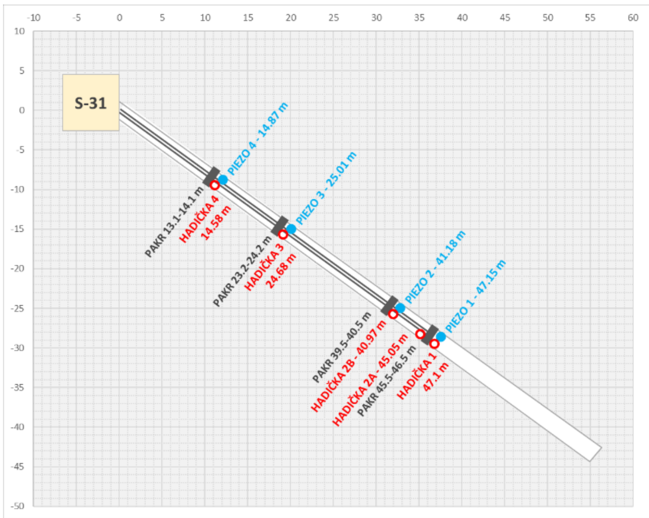

Fig. 12 Diagram of the multipacker in borehole S-31

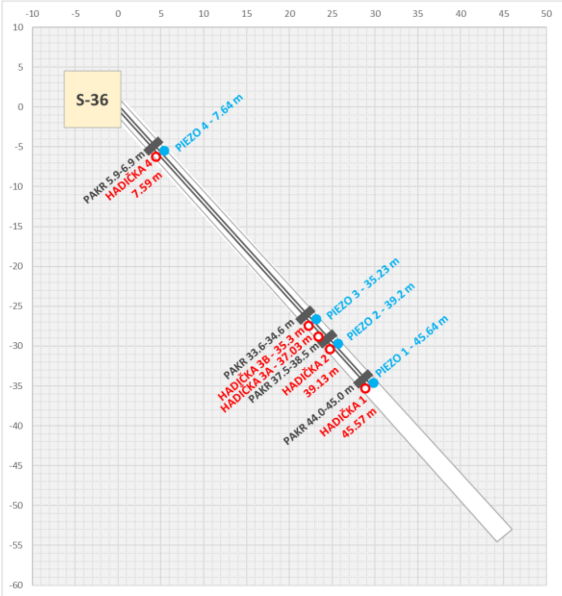

Fig. 13 Diagram of the multipacker in borehole S-36

Tab. 2 Details of the installation of multipacker S-27

Packer	Depth of the sealing part (m)	Piezometer depth (m)	Injection tube depth (m)	Injection tube length (m)
1	44.00–45.00	45.61	45.56	46.50
2	27.72–28.72	29.42	29.14	30.20
3	22.19–23.19	23.91	27.24	28.80
			24.73	25.50
4	7.42–8.42	9.10	8.87	10.00

Tab. 3 Details of the installation of multipacker S-31

Packer	Depth of the sealing part (m)	Piezometer depth (m)	Injection tube depth (m)	Injection tube length (m)
1	45.50–46.50	47.15	47.10	48.00
2	39.52–40.52	41.18	45.05	46.30
			40.97	42.00

3	23.24–24.24	25.01	24.68	25.50
4	13.14–14.14	14.87	14.58	15.50

Tab. 4 Details of the installation of multipacker S-36

Packer	Depth of the sealing part (m)	Piezometer depth (m)	Injection tube depth (m)	Injection tube length (m)
1	44.00–45.00	45.64	45.57	48.00
2	37.47–38.47	39.20	39.13	42.00
3	33.55–34.55	35.23	37.03	39.00
			35.30	37.00
4	5.91–6.91	7.64	7.59	12.00

Tab. 5 Details of the installation of multipacker S-8

Packer	Depth of the sealing part (m)	Piezometer depth (m)	Injection tube depth (m)	Injection tube length (m)
1	29.90-30.40	30.94	30.98	36.00
2	2.23–2.73	3.37	3.43	10.00

Pressure monitoring took place for almost 3.5 years (from installation to the end of the project). In addition to the groundwater pressure data from the intervals, the atmospheric pressure and temperatures in the intervals and the test chamber were also measured (Fig. 14).

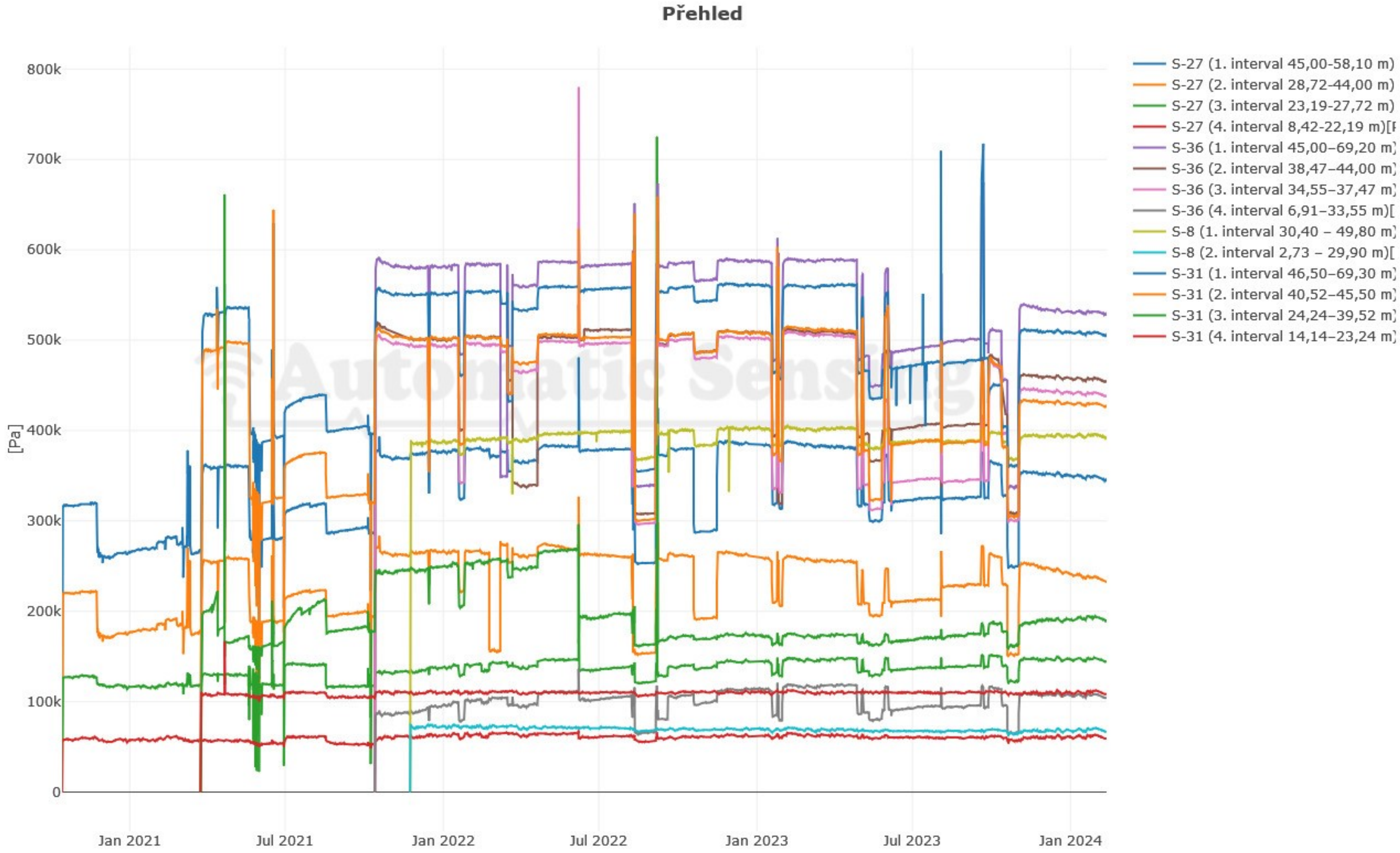

Fig. 14 Pressure monitoring – response to hydraulic tests and tracer tests

6 Model of the Rock Block of Interest

During the project performance, a geological, hydrogeological and transport model of the examined rock block was compiled, which was gradually updated and modified based on the available data from the characterization work and the hydraulic and tracer tests.

6.1 Conceptual Model of the Rock Block of Interest

The creation of the conceptual geological (Geo) and hydrogeological (Hydro) DFN model is described in detail in the interim technical report TR 551/2021 (Zuna et al. 2021). The aim of Stage 12 was, based on limited input data (mainly archival data from earlier field work and monitoring, but also from the newly drilled boreholes), to propose a model concept of the rock block of interest in the Bukov URF, which will serve as a tool for planning drilling works and experiments that they are necessary for a better understanding of the properties of the rock environment and its behavior.

6.1.1 Geological Model

MOVE software was used to construct the geological model. The model covers an area of 40 × 60 × 60 m, and integrates data from various different sources (Fig. 15):

- Structural measurement:
  Detailed mapping and measurement of the orientation of structural elements (faults, foliation, fractures) on the walls of corridors in a given block. Approximately 250 structural measurements were documented and digitized, with an emphasis on the exact orientation and characteristics of the fractures (type, length, termination).
- Well-logging data:
  Acoustic television results from boreholes S-27 and S-31, which provide detailed information on the structure and properties of the rock along the borehole profiles. Well-logging data include acoustic images of the borehole walls from which the occurrence and properties of fractures, foliation and other geological structures may be interpreted.

Deterministic structures

The model includes a representation of important deterministic structures, such as faults, reactivated foliation, and/or fault zones. These structures are created in the MOVE program using various methods, such as extrapolation of structural measurements, the creation of ribbons and areal extensions. Three main faults and two fault zones that affect the hydrogeological properties of the block were identified and modelled. The foliation was divided into three generations according to orientation and character. The model was divided into three main rock types: biotite-amphibolic paragneiss, migmatite and amphibolite.

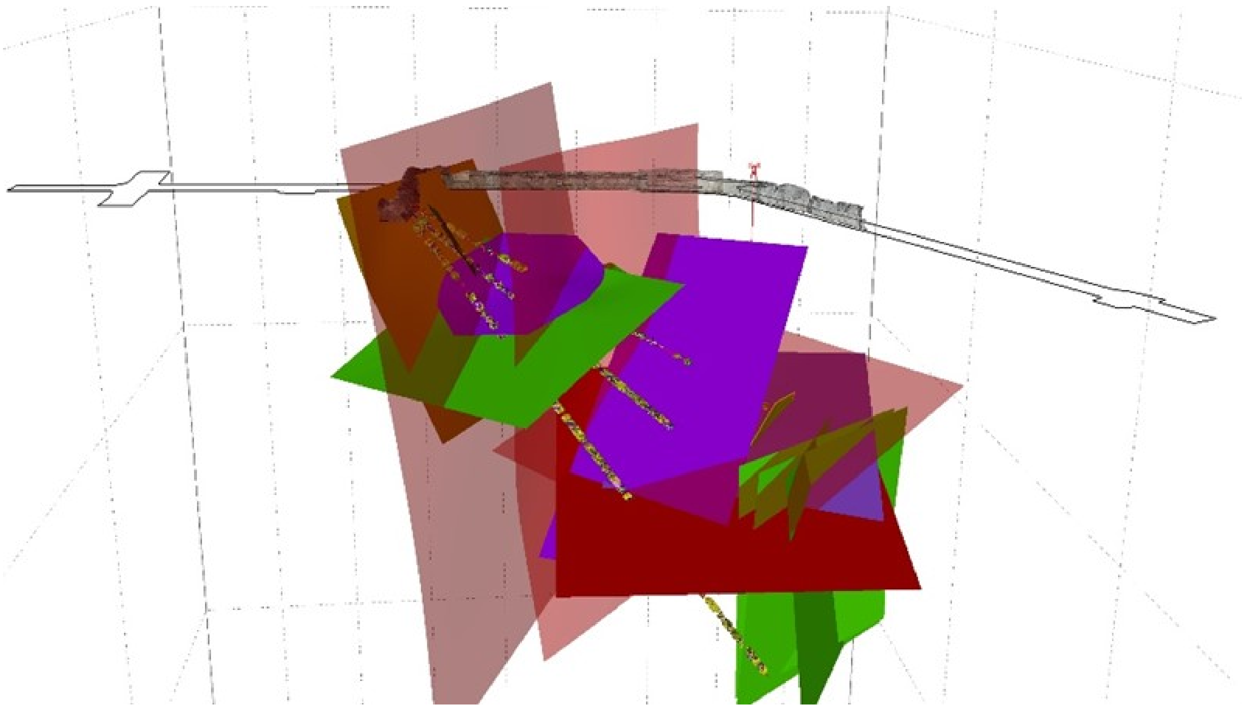

Fig. 15 3D model with plotted structural data for all drilled boreholes and surface meshes of significant fault zones identified by the acoustic camera in the boreholes and their connection to significant structures on the walls of the corridors

Stochastic DFN model

To simulate the fracture network in the given block, a stochastic DFN model was created using the DFraM program (Fig. 16) (Švagera et al. 2017). The model distinguishes five populations of fractures based on their orientation (dip and strike). For each population, parameters such as the density of the fractures, their longitudinal and orientational distribution and the nature of termination are defined. In total, 425 fracture feet from the mapping were analyzed and divided into five populations with respect to their orientation and nature of termination. Statistical parameters of the length and density of fractures were determined for each population (Tab. 6 and Tab. 7).

Tab. 6 DFN network parameters showing the mean strike, dip, the position of the center of the data cluster (μx,y,z), and the concentration parameter (κ) for individual populations

Pop	n	Strike	Dip	μx	μy	μz	κ
1	113	15.14	89.55	−0.965	0.261	−0.008	15.852
2	119	63.56	89.47	0.445	−0.895	0.009	8.808
3	126	312.05	83.34	0.665	0.738	0.116	8.926
4	35	109.31	42.69	−0.224	−0.640	0.735	21.381
5	23	130.87	8.87	−0.101	−0.117	0.988	15.438

Tab. 7 DFN network parameters determining the minimum size of the radius of the circle described in a single fracture (x_{min}), concentration parameter (α) and fracture density per m^3 (P_{30})

Populace	1	2	3	4	5
x_{min} [m]	0.406	0.491	0.315	0.379	0.757
α [-]	3.221	3.594	3.029	2.771	4.651
P_{30} $\left[\frac{1}{m^3}\right]$	0.335	0.339	0.552	0.067	0.037

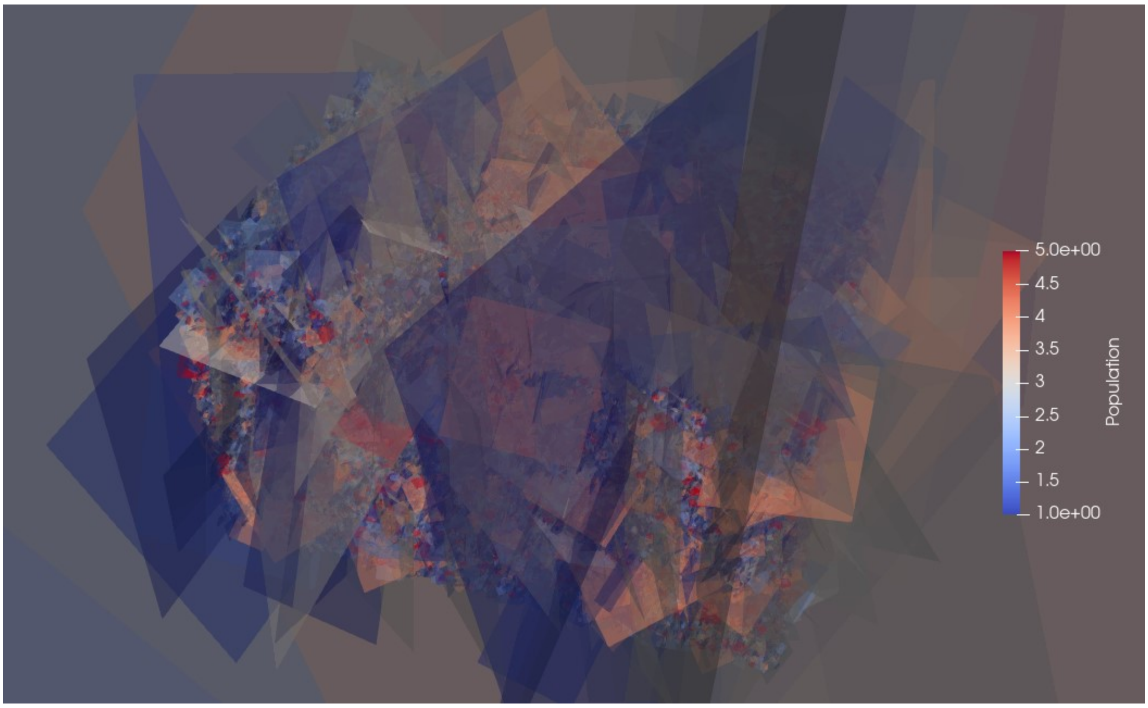

Fig. 16 Output of the DFN model in the ParaView program environment

Validation of the DFN model includes a comparison with the observed data from the mapping and borehole profiles (Fig. 17 and Fig. 18). A key aspect is the analysis of intersections of the fractures with the boreholes and correlation with the well-logging data. The validation results demonstrate a good agreement between the model and reality, thereby confirming its reliability for further analyses. A comparison of simulated and observed fracture frequencies and lengths was made, with good agreement for all populations. The intersections of the fractures with the boreholes were analyzed and correlated with the well-logging data, confirming a realistic representation of the fracture network in the model (Fig. 19).

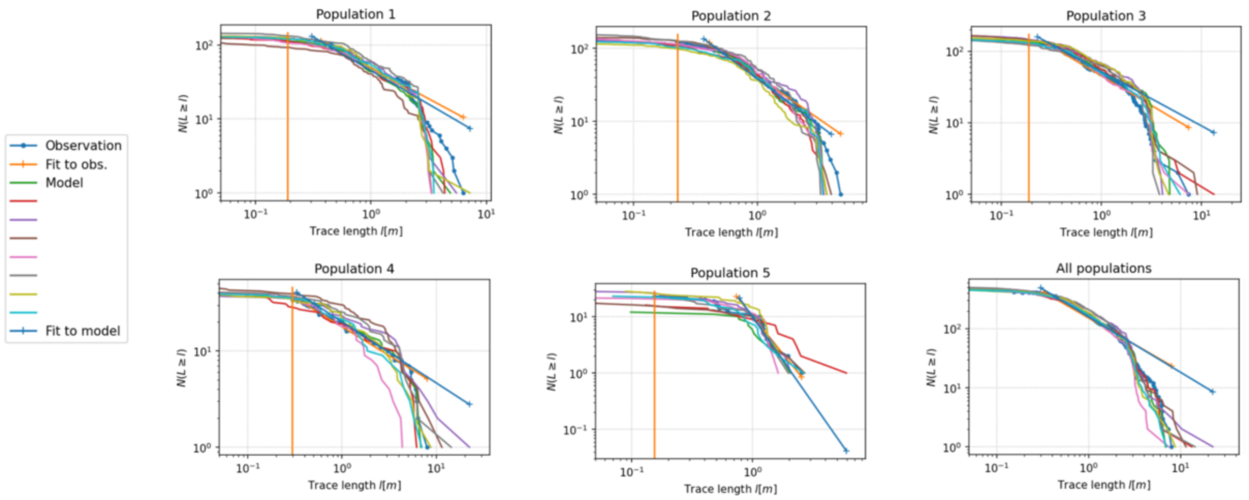

Fig. 17 Graphs comparing frequencies and trace lengths on the observation windows and calculated by the model for individual populations together with interpolated best fit curves

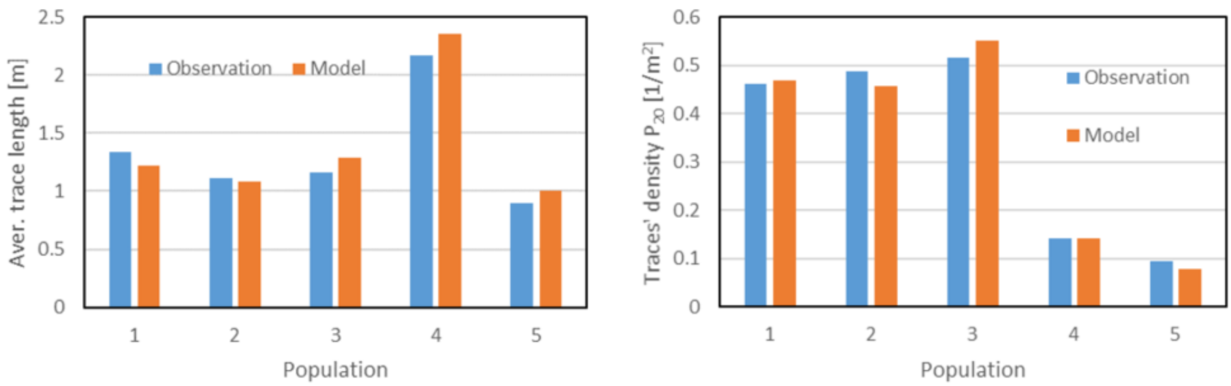

Fig. 18 Comparison of the average trace lengths of the fractures and their density between direct field observation (blue bars) and the DFN model (orange bars)

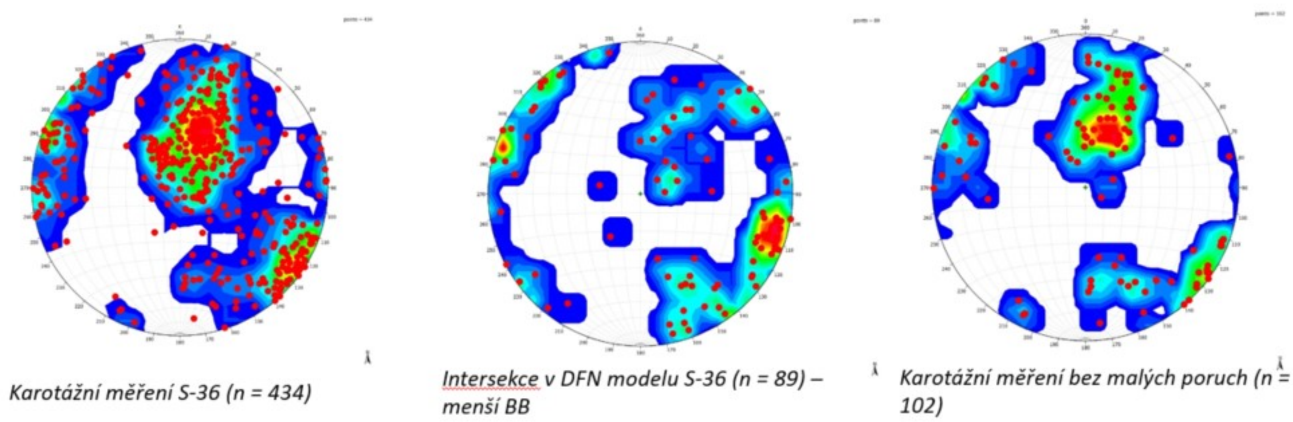

Fig. 19 Comparison of the poles of the discontinuities measured by the ABI40 method and the intersection of the calculated DFN model on a virtual borehole, and an apparent agreement when filtering out very small

faults and/or foliations from the log measurements of the projection of the poles of the surfaces onto the lower hemisphere in the Schmidt surface view

The conceptual model enables a detailed visualization and analysis of the geological structure of the block. It provides valuable information on the distribution and character of structural elements, the fracture network and lithological variations. This information served as a basis for planning experiments, optimizing the location of measuring devices and hydrogeological tests with regard to the geological heterogeneities and hydrogeological parameters.

6.1.2 Hydrogeological Model

A hydrogeological model of the rock block of interest (HydroDFN) was designed on the same scale and extent as the GeoDFN model defined by shafts BZ1-XII, BZ-XII-J, and ZK2 with a slight overlap beyond the boundary of the studied block, see Fig. 20. The main reason for expanding the model domain was to specify unaffected boundary conditions at the boundary of the hydrogeological model. The HydroDFN model of the rock block is processed in the DFN module of ConnectFlow (formerly NAPSAC).

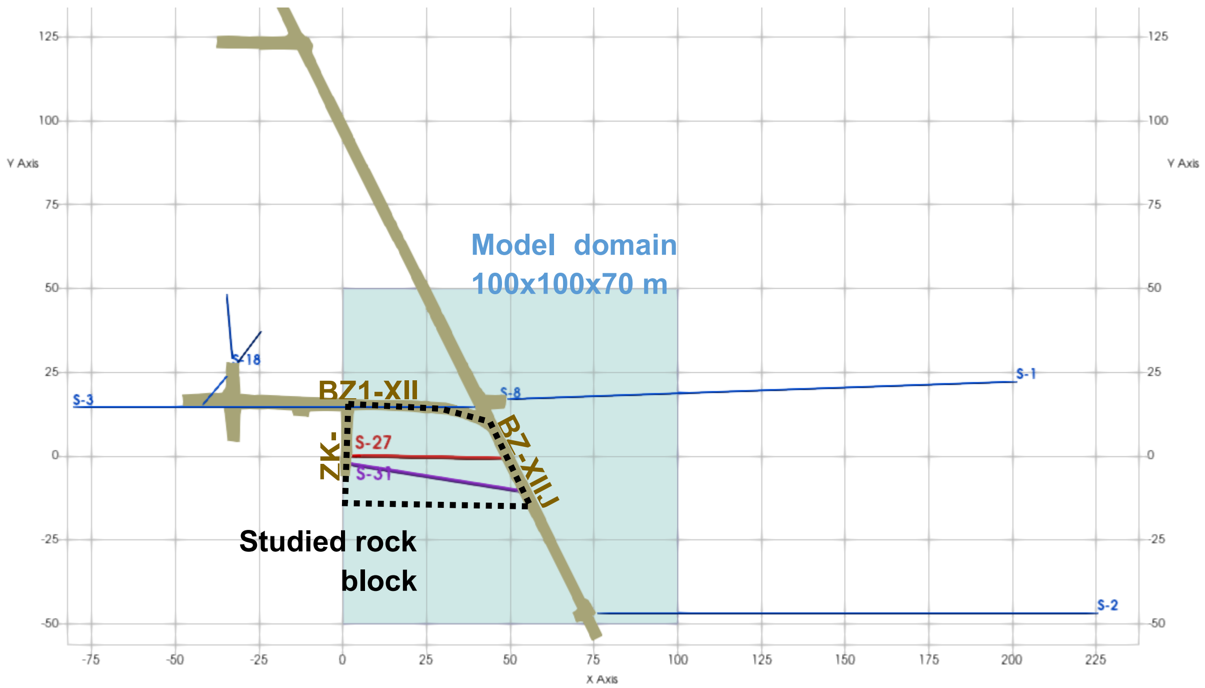

Fig. 20 Delineation of the studied rock block (black dashed line) and the extent of the model domain of the HydroDFN model (blue line)

Geometry of the fracture network

The construction of the HydroDFN model in terms of geometry (size, number, shape of fractures) directly follows on from the outputs from the Geo DFN modeling, which formed the primary input for the HydroDFN modeling. The geometry of the fracture network in the rock block was divided into two areas:

1) Fracture network in the central area of the studied rock block. The boundary of this rock block is firmly defined and includes primarily deterministically defined fractures mapped based on field work (shaft, new boreholes). At the same time, the model of the studied rock block includes stochastic fracture datasets representing brittle failure of the rock. Some larger faults are also entered stochastically (non-deterministically), which complete the fracture network in places where data is missing and where deterministically defined fractures are not entered. "Deterministic" fractures may also be partially stochastically (semi-) defined, i.e., the intersection, slope and direction of the fractures are specified from the characterization, while their size is generated randomly. The geometry of the fracture network in the area of the studied rock block is prepared and generated as part of the work on the Geo-DFN model and is transferred to the HydroDFN model, including all the outputs.
2) Fracture network in the envelope zone (buffer) around the studied rock block for the purpose of entering the boundary conditions. The outer zone contains only stochastically generated fractures with the parameters of the datasets entered into the central area of the studied rock block. For computational reasons, the fracture network in this outer zone is simplified, e.g., to reduce the number of fracture intersections and speed up the calculation, only larger fractures are included. The geometry of the stochastic fracture network in the buffer zone of the studied rock block was directly generated in the ConnectFlow program.

Hydraulic parameters of the fracture network

The transmissivity (or hydraulic expansion) values of conductive fracture are calibrated in the model based on the results of measurements of the multipacker system and water pressure tests, etc. The conceptual procedure is such that in the basic model variants, a constant hydraulic expansion is assigned over the entire area of the fracture, depending on the size of the fracture but it may change (according to the thickness distribution), i.e., the distribution of hydraulic expansion parameters is the subject of model calibrations. If the model fails to be calibrated using a constant opening in the fracture surface, a variable fracture opening is used in subsequent model variants. The entry of variable expansion is assumed only for larger structural elements or for elements with a known course entered deterministically. Variable expansion is generated in the fracture surface using probabilistic functions available and implemented directly in the ConnectFlow program, or with the help of scripts or other tools (e.g., GSTools).

Defining the boundary conditions at the boundary of the model

While the spatial definition of the rock block for the creation of the geological model was essentially unambiguous (a rock block in which drilling work takes place), the definition of the hydrogeological model is more complex, as it is necessary to take into account the flow regime of groundwater flowing into the block of interest from the rock mass. The entire area of the Bukov URF is intensively drained not only due to the tunnel and shafts, but also to older open boreholes. The long boreholes S-1 and S-2 in particular drain a large amount of groundwater from the rock and, together with the boreholes S-8 and S-18, connect the fracture network in the vicinity of the studied block and deform the pressure field. Based on measurements of the multipacker system in the first borehole S-27, a pressure of only 0.5 m above the wellhead of the borehole was detected at a distance of 25 m from the shaft. The rock and fractures in the vicinity of the shaft may not be entirely water bearing (up to a distance of approximately 20-30 m), which may complicate both the experiments and tests conducted (the free space will be filled first) and modeling (unsaturated fractures have completely different parameters).

No comprehensive hydrogeological assessment of the Bukov URF, which is important for defining the boundary conditions, has been elaborated. This may have been used as a basis for detailed work on a smaller rock block (the current monitoring collects data, but does not evaluate it in context). The boundary conditions, i.e., inflows from the rock mass (see Fig. 21) were set based on the results from the measuring of pressures and outflows from the boreholes during the hydraulic tests. Tunnel eyes and open boreholes, which drain the whole structure and through which groundwater flows from the model block, are specified by a pressure boundary condition, i.e., the value of the hydraulic height corresponds to the geodetic height. Boreholes and shafts are entered in the model as engineering objects of the type “borehole” and “shaft” (not using fractures). The measured value of the flow from the fractures and from the boreholes to the shaft is used as a calibration parameter when adjusting the model.

When simulating the hydraulic tests or water pressure tests, a boundary condition of known flow or pressure is used, where only one of the values is entered and the other is used in the model calibration.

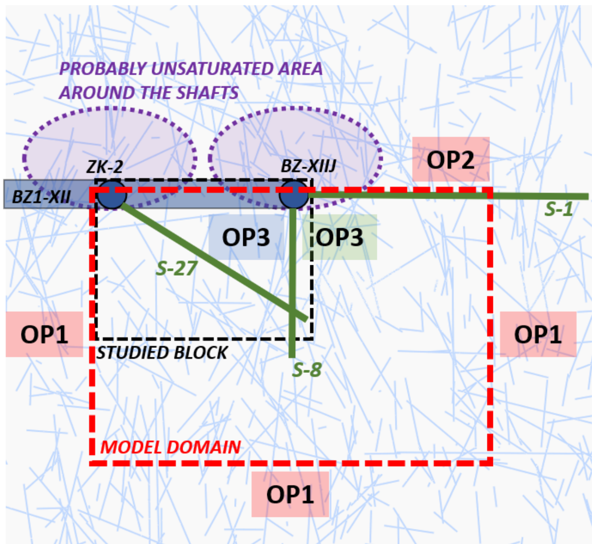

- OP1 - inflow to the rock block of interest - the type of boundary condition (constant pressure or flow) will be specified during model implementation
- OP2 - probably zero flow across the upper boundary (also to be specified during model implementation)
- OP3 - pressure boundary condition in the shafts and open boreholes (H = 21 m)

Fig. 21 Schematic rendition of the boundary conditions of the HydroDFN model

Regional hydrogeological model

During the processing of the detailed HydroDFN model of the block of interest, a simplified “regional” model of the surroundings of the Bukov URF was also created to enter boundary conditions and the total inflow at the boundary of the HydroDFN model of the rock block of interest. The model includes the wider surroundings of the Rožná mine, within approximately 500 m of the Bukov URF, see Fig. 22, and is connected to the detailed fracture network of the rock block of interest.

From the point of view of geometry and boundary conditions (Fig. 23), the “regional” model is significantly simplified; however, it includes the main balance elements of the area, i.e., the overflow of water from the subsurface zone into the rock mass and drainage into the mine.

Fig. 22 Layout of the supplementary regional model

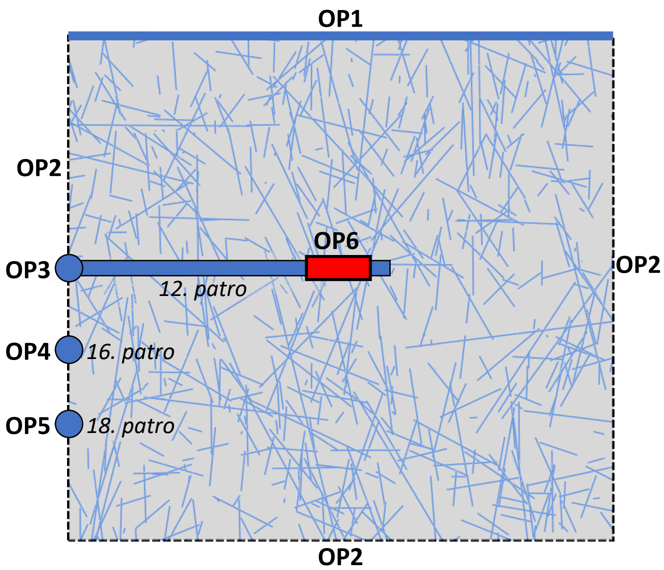

- OP1 – constant head H = 500 m (terrain)
- OP2 – no flow boundary
- OP3 – constant head H = 21 m (12th floor)
- OP4 – constant head H = -186 m (16th floor)
- OP5 – constant head H = -286 m (18th floor)
- OP6 – constant head H = 21 m (Bukov URF)

Fig. 23 Schematic rendition of the boundary conditions of the regional model

The "regional" model was primarily processed as a DFN fracture model in ConnectFlow. The geometric parameters of the fracture network were taken from previous works. The hydraulic parameters of the fractures were optimized when calibrating the model to the measured total inflows to the Bukov URF (SÚRAO monitoring) and the measured pressures in the new boreholes S-27 and S-31. Fig. 24 shows a section through the model domain and the fracture network of the regional model.

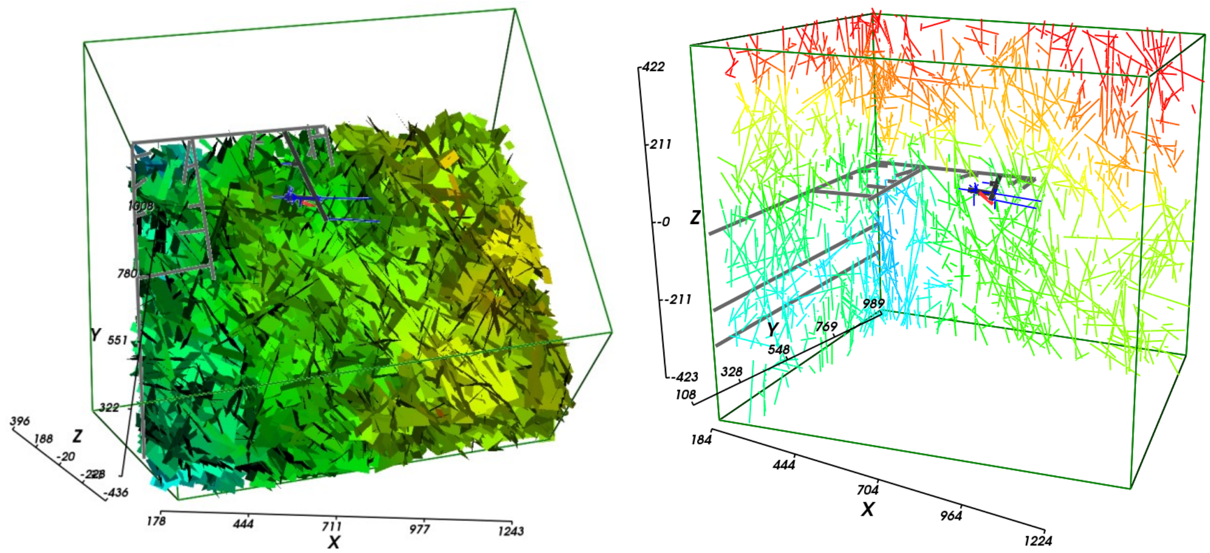

Fig. 24 Cross-section of the regional HydroDFN model at the level of the Bukov URF - the extent of the regional model 1200 × 1000 × 1000 m also includes part of the 12th, 16th, and 18th floors of the Rožná mine

6.2 Basic Numerical Model

The basic numerical model was processed as part of Stage 21 and is described in detail in interim technical report No. 630/2022. The basic model was based on the proposed conceptual model and the newly obtained structural data from the boreholes.

6.2.1 Identification of Parameters and Generation of the Stochastic sGeoDFN Model (version k01)

Structural-geological data measured by CGS were used to identify the parameters of the model. These data included a data set with the vertices of a total of eight observation windows located on the walls of the corridors. Subsequently, a data set with information on 416 fractures focused on the observation windows. The record for each fracture contained, among other things, its identifier, the slope and direction of the fracture, the coordinates of the end points of the trace, information about the termination of the fracture, the identifier of the observation window and the inclusion of the fracture in the geological population.

Statistical tests of the fracture orientation models

For individual fracture populations, it was necessary to verify whether their orientation may be modeled using the commonly used Fisher distribution, or using another statistical model.

The data were first divided into five populations (A–E) (Fig. 25) based on the type of trail termination. Statistical tests showed that none of these populations showed a dominant orientation and the data rather corresponded to a belt (equatorial) distribution with low concentration. The hypothesis of equal distribution was rejected for all populations.

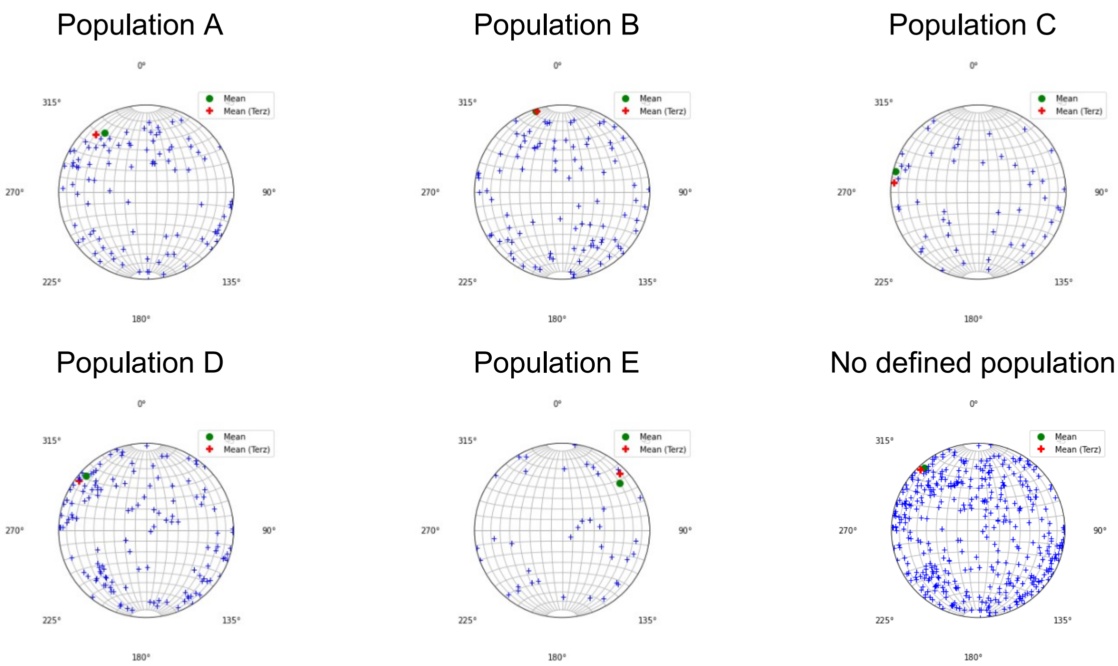

Fig. 25 Stereograms of fracture poles for populations A–E defined by type of trace termination

Furthermore, the fractures were divided into five populations (1–5) (Fig. 26) based on the dominant orientation. Stereograms of the fracture poles showed the cluster character of the distribution for all populations. Analysis of the direction matrix confirmed the cluster character with a medium concentration around the dominant direction. The hypothesis of equal distribution was again rejected for all populations.

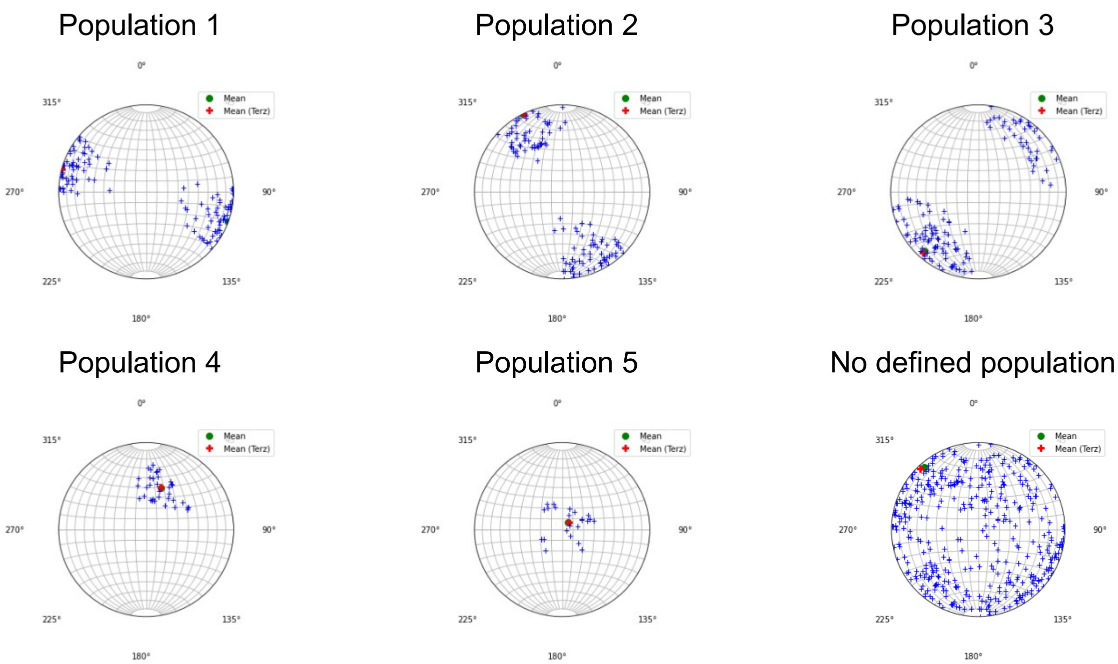

Fig. 26 Stereograms of fracture poles for population 1–5 defined according to dominant orientation

The performed analysis shows that if the fractures of the investigated rock block are divided into populations exclusively according to the type of trace termination, then the individual populations do not meet the criteria for a uniform distribution model but mostly show the character of a strip (equatorial) distribution, but with a weak directional concentration. During the creation of sGeoDFN models, further work was performed with the division of fractures into populations 1–5, which were determined based on the dominant orientations according to the methodology of (Kabele et al. 2017) and (Švagera et al. 2017), showing a bipolar character with medium concentration; therefore, they are described well using Fisher distribution (Fisher at al.1993).

Analysis of fracture termination

A basic analysis of fracture termination between individual populations was performed. Populations A–E were found to be correctly defined based on the type of trace termination, but their hierarchy could not be reliably determined with regard to termination.

Determining the Fisher distribution parameters for populations 1–5

Fisher distribution parameters for populations 1–5 were determined as the highest likelihood estimates with respect to Terzaghi's correction (Terzaghi 1965). Differences between the main directions with and without correction were minimal.

Determination of the volume density and parameters of the thickness distribution of fractures for the populations 1–5

Volume density and thickness distribution parameters of the fractures for populations 1–5 were determined using linear regression and generation of stochastic DFN models. The optimized parameters are given in Tab. 8.

Tab. 8 Optimized thickness distribution parameters for populations 1–5

Pop	$a_{min}(x_{min})$ (m)	α (-)	P_{30} [a] $(1/\mathrm{m}^3)$	P_{32} [a] $(\mathrm{m}^2/\mathrm{m}^3)$
1	0.254	3.111	0.837	1.234
2	0.327	3.387	0.571	0.719
3	0.198	3.135	1.45	1.229
4	0.237	2.682	0.115	0.903
5	0.629	4.841	0.058	0.096

[a] Values P_{30} and P_{32} are determined for square fractures with a thickness distribution of sizes in the interval $a \langle a_{min}, 1000\rangle$ m; a is the radius of the circumcircle.

The optimized parameters were used to generate a stochastic sGeoDFN model of the rock mass block of interest (version k01). The model contains square fractures in populations 1–5 with a maximum length of 1414 m. The centers of the fractures were located by a Poisson process. The model was transferred into .vtk format including the verification and validation protocol.

6.2.2 Structural-Geological Model – Identification of Continuous Structures Based on Data from the Boreholes and Corridor Walls

This section deals with the creation of a structural-geological model for the studied rock mass block. The aim is to identify and describe continuous structures in the rock mass, which play a key role in its hydrogeological properties.

The model is based on data from the boreholes and walls of corridors in the block. Well-logging methods, including acoustic television (ABI40), were used to map the fractures and tectonic faults. Based on these data, a total of 43 continuous structures were defined and visualized.

The compilation of the model involved the following steps:

1. Identification of structures:

- Data from the ABI40 was analyzed in individual boreholes and structures with the same/similar orientation and course were identified.
- Only medium and very pronounced structures, as well as tectonic faults and fractures, were taken into account (Fig. 27).
- The orientation and inclination of the structures were verified using additional logging methods and primary records.

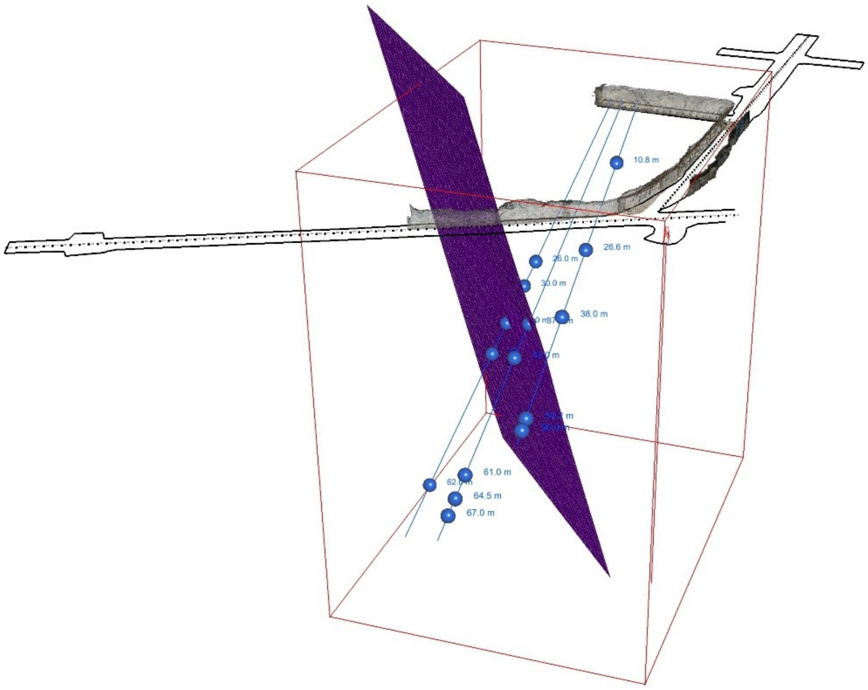

Fig. 27 Visualization of deterministic structure No. 21 in the 3D model, blue spheres represent areas of inflows to boreholes determined by well-logging

2. Surface construction:

- Identified structures in individual boreholes were transformed into lines.
- An initial surface in the form of a mesh (triangulation) was created for each structure.
- Areas were extrapolated using the method of extrapolation in the strike and dip of the edges of the triangles of the mesh.
- To simplify and minimize the subjectivity of the modeler, the surfaces were resampled to a grid with a cell size of 2 × 2 meters.

3. Exporting the data:

Data from the model were exported to create a semi-deterministic GeoDFN model. The exported files included the coordinates of the intersections of the structures with the boreholes and corridors, the orientation and slope of the structures, the depth of occurrence, and the population in which the structures fall.

Furthermore, the in-situ structural and well-logging measurements were correlated with the stochastic GeoDFN model. The DFN model was created in the DFraM program and imported into the MOVE software. The orientations and frequencies of structures in both models were compared.

The agreement of the DFN model with the data from the well-logging measurements is good, but there are differences in the frequencies of the structures (Fig. 28 and Fig. 29). The well-logging data show a higher frequency of structures, especially in the foliation cluster. The reason is that the acoustic camera also captures small fissures and fractures that are not relevant to the hydrogeological properties of the rock mass.

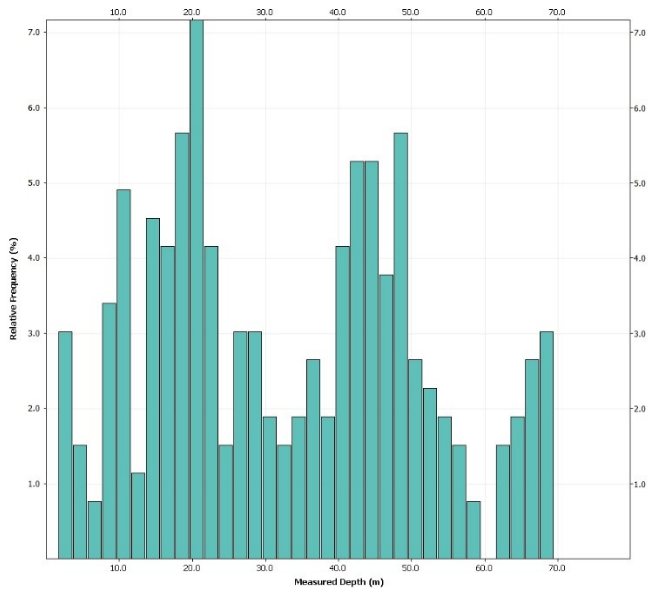

Fig. 28 Graph of the relative frequency of the structures from the well-logging after filtering out filled and less pronounced structures versus the measured depth of the boreholes, overall for boreholes S-27 to S-36 with the column width corresponding to a 2-m borehole

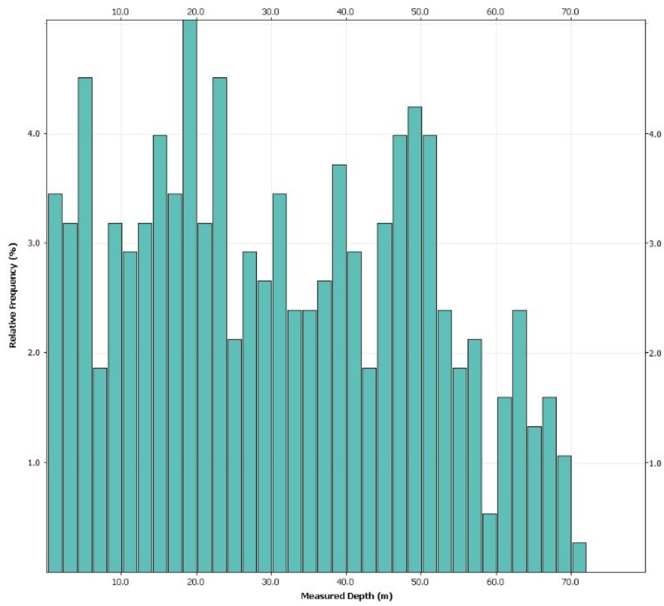

Fig. 29 Graph of relative frequency of the structures from the sGeoDFN model versus the measured depth of the boreholes, overall for boreholes S-27 to S-36 with the column width corresponding to a 2-m borehole

The sGeoDFN model, which is based on field documentation of the walls of the corridors, shows a lower frequency of structures. This is because only relevant structures are considered in the geological documentation and fractures or induced fissures with a length of less than 20 cm are not considered.

Furthermore, some of the structures are only captured in the well-logging data and vice versa. This is due to the limitations of both methods. The well-logging data are influenced by the diameter of the borehole and the inability to determine the length and spatial continuity of the structures. The field documentation, on the other hand, is limited to the available exposed sections of the corridors.

To optimize the model, it was necessary to consider the limitations of both approaches and to choose appropriate data filtering methods. It is important to preserve the relevant structures for the hydrogeological properties of the rock mass and also to eliminate small fractures and structures that do not affect the flow of water.

6.2.3 Semi-Deterministic dGeoDFN Model

Information on continuous (deterministic) structures, which were evaluated from the boreholes and tunnel walls, as described in the previous section, was used for conditioning the GeoDFN model. Conditioning the geometric description of the structures on the recorded intersections with the boreholes and corridor walls allows the existing observations to be considered deterministically in the model, while the characteristics that cannot be directly observed (e.g., the position of the center or the extent of the structures) are still modeled stochastically. Since the resulting model includes both deterministic and stochastic elements, it is referred to as a semi-deterministic GeoDFN model (dGeoDFN).

Procedure for compiling the dGeoDFN model:

1. Data processing:

Information on continuous structures (position, orientation, dimensions) was obtained from the boreholes and tunnel walls. A basic geometric model (surface) representing its shape and extent was created for each structure. Data on the intersections of the structures with the boreholes and the tunnel walls were used to define the conditions for compiling the dGeoDFN model.

2. Compiling the dGeoDFN model:

The proposed algorithm generated random radii and center points for the structures based on the surfaces of the basic geometric models and considering the observed data. Two outputs of the dGeoDFN model were created with minimum radii of 5 m and 10 m, respectively.

Since the size of the structures is governed by a thickness probability distribution, which generally has different parameter values for each geological fracture population, the outer cycle of the algorithm runs through each population:

1) A cycle through the individual populations: A sufficiently large sample of random radius values is generated for a given fracture population $\{r\}$ from the thickness distribution with the relevant parametersr_{min} and α. Experience to-date has shown us that a sample size of 1000 values should be sufficient (Fig. 30).
2) An internal cycle through individual deterministic structures of a given population:
   a) From sample $\{r\}$ one value r_i is randomly selected (Fig. 30).
   b) For the selected value r_i, a search is performed for all the potential fracture centers on the surface of the basic geometric model of the structure within the extent of the model area (Fig. 31 (a)), which are in conformity with the observation, i.e., satisfy the conditions:
      - Distance from all points where the structure was NOT recorded $r_{nr} > r_i$ (Fig. 31 (b)),
      - Distance from all points where the structure WAS recorded $r_r \leq r_i$ (Fig. 31 (c)).
   c) If the result is an empty set, then another value r_i is chosen from sample $\{r\}$ and the operations are repeated from point 2) a). If the result is not an empty set, then:
      - The selected value r_i is saved as the selected radius for the given structure and this value is taken out of sample $\{r\}$ so that it cannot be used for another structure of the given population.

- One point C_i (point shown in orange on Fig. 31 (d)) is randomly selected from the set of searched potential centers, and is saved as the center of the given structure.
- The surface of the basic geometric model is cropped by a spherical surface with center C_i and radius r_i. This creates the final geometric model of the given structure (Fig. 31 (e)).

d) Return to point 2).

3) Return to point 1).

This algorithm was implemented in the Python programming language in the dDFN_size_and_clip.py program as part of the DFN_tools script package. The output of the calculation is a protocol that includes information about the calculation process and the basic characteristics of the generated semi-deterministic structures, a file in .csv format with the characteristics of the structures and a file in .vtp format that contains the dGeoDFN model, i.e., the geometric representation of individual structures (PolyData type).

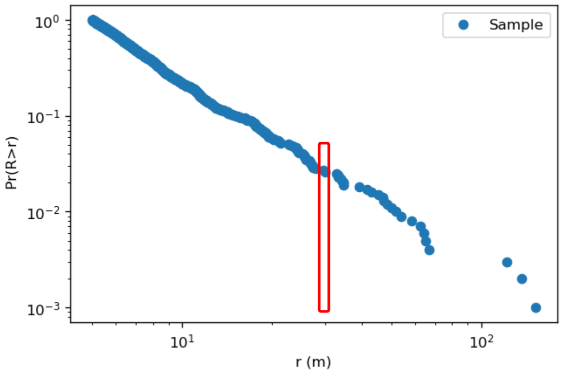

Fig. 30 A sample of random radius values $\{r\}$ from the thickness distribution. A randomly selected value according to point 2) a) is marked in red

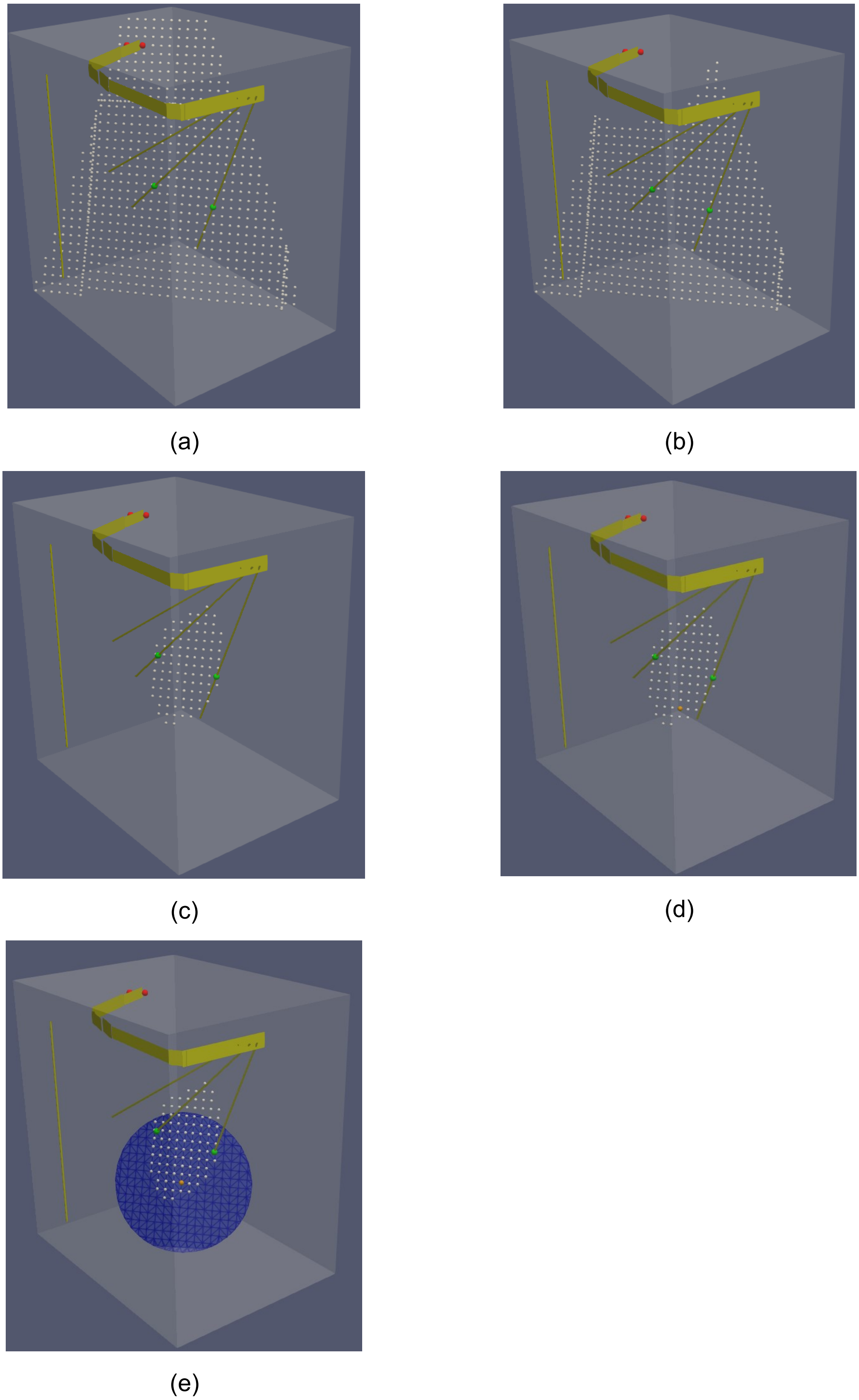

Fig. 31 Gradual generation of the semi-deterministic model of continuous structure (fractures)

3. Integration of the sGeoDFN and dGeoDFN models:

Before further use of the complied sGeoDFN and dGeoDFN models, it is necessary to considered that both networks describe a fracture system in a partially overlapping area of the rock mass around the corridors and boreholes on which structural-geological measurements were made. Specifically, the sGeoDFN model was generated for an area of 130 m × 130 m × 100 m, while the dGeoDFN model covers a smaller block of 60 m × 45 m × 65 m. The original sGeoDFN model includes all stochastically generated fractures whose sizes are bounded from below by the parameter value a_min (in the order of tens of cm, see Tab. 8), but they are practically not limited from above. However, the semi-deterministic dGeoDFN model includes fractures larger than the r_min value, i.e., 5 or 10 m. Hence, it is clear that both models contain duplicate (in the statistical sense) structures. Therefore, these duplicates must be removed from the stochastic sGeoDFN model before integrating both networks into the resulting GeoDFN model.

Duplicate structures (larger than 5 m or 10 m) that were located in the area covered by the dGeoDFN model were removed from the sGeoDFN model.

Subsequently, the integrated model (Fig. 32) contained both stochastic structures from the sGeoDFN model (less than 5 m or 10 m) and deterministic structures from the dGeoDFN model (greater than 5 m or 10 m).

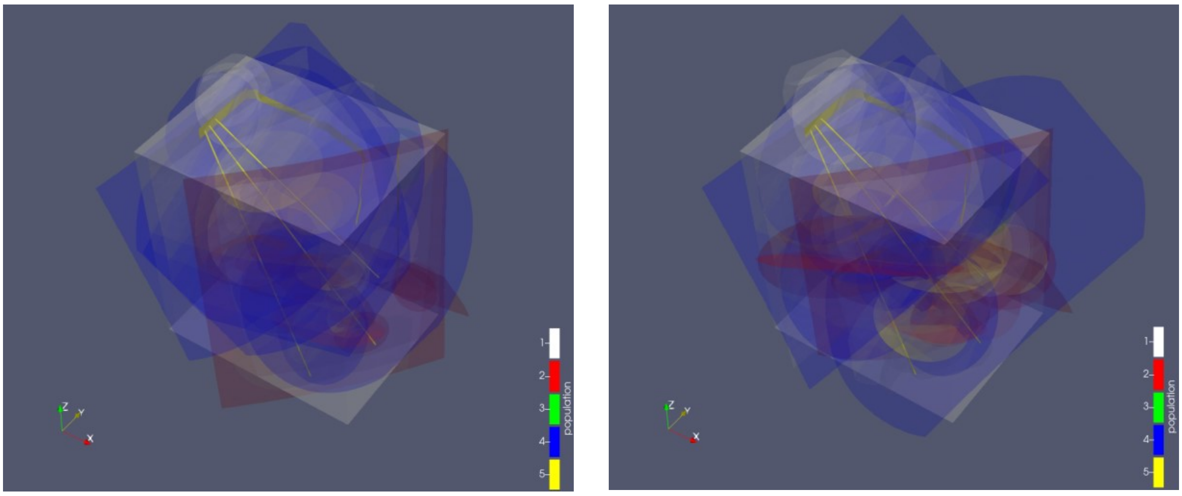

(a) (b)

Fig. 32 3D visualization of the semi-deterministic dGeoDFN model version d01s_v06 (a) r_{min} = 5 m, (b) r_{min} = 10 m

6.2.4 HydroDFN model

Work on the hydrogeological model of the area of interest (the HydroDFN model) was performed in two parallel branches at the stage of processing the basic numerical model, which overlapped and complemented each other in several smaller areas:

- Regional HydroDFN model (approximately 1 × 1 × 1 km in size). The aim was to define the pressure and balance conditions at the boundary of the rock block of interest, to analyze the influence of selected parameters of the fracture network on the results of the flow model, which will be applied/used during the following stages of the detailed model optimization,

- Detailed HydroDFN model of the rock block of interest (130 × 130 × 100 m in size). The aim was to verify and prepare procedures for constructing the geometry of the fracture network of the HydroDFN model based on the outputs of the GeoDFN modeling

After completing the work on the basic geological GeoDFN model (stochastic and deterministic, see Sections 6.2.1 to 6.2.3), the basic HydroDFN model was prepared, the initial calibration of the model was performed, and the flow was simulated. Subsequently, the parameters of the HydroDFN fracture network were upscaled to the ECPM model, the flow was simulated, and the results were compared and evaluated.

Regional HydroDFN model

The regional HydroDFN model of the surroundings of the Bukov URF (for the needs of the project, the regional model is simplified, it is not a full-fledged model of the area) is the basis and input for processing a credible detailed HydroDFN model of the rock block of interest. The basic function of this regional model is to define the pressure and balance (size of inflow) conditions at the edges of the defined block of rock, which is investigated and processed in more detail in the project. The regional model includes the area of the Rožná mine within approximately 500 m of the Bukov URF, see Fig. 22.

The newly drilled boreholes S-27, S-31, and S-36 are also included in the regional model. They are entered with a single packer interval (with a packer at the mouth of the borehole), i.e., they are not a boundary condition but hydraulically connect the fractures intersecting the borehole. This was used to analyze, compare, and evaluate the pressure ratios during variant simulations and basic calibration of the model. The regional HydroDFN model is processed entirely in the ConnectFlow program, i.e., including the generation of the fracture network. This is in contrast to the detailed HydroDFN model, where the input geometry of the fracture network is created in the MOVE (deterministic network) and DFRAM (stochastic network) programs. The input geometric parameters for generating the fracture network in the basic model were taken from previous works on the order sheet "T8 – Transport of radionuclides from a deep repository/Testing of conceptual and computational models" (Gvoždík et al. 2020), but the procedure for generating the HydroDFN fracture network was modified as follows:

- Due to the regional scale of the model (1100 × 900 × 1000 m in size), larger fractures were generated, i.e., 50 × 50 to 500 × 500 m in size
- The input statistical parameters for the generation of fractures were preserved, i.e., nine populations of fractures, parameters of the Fisher distribution for the directions (orientation) of the fractures, parameters of the thickness distribution for the size and number of fractures; however, the exponent of the power distribution remains the same, the P32 parameter is recalculated for the new range of fracture sizes,
- The number of fractures was optimized for the number of intersections in boreholes and shafts (according to the WPT and well-logging measurements, the number of conductive fractures or conductive zones in boreholes is (4–6), documented inflows from fractures/zones in shafts from Bukov URF is approximately 30). The optimized input parameters for the generation of stochastic fractures in the regional HydroDFN are presented in Tab. 9. Depending on the network implementation (10 different stochastic networks were generated), the average number of intersections of fractures with the

boreholes is 1–5, and the number of intersections of fractures with the corridors of the Bukov URF is 20–50.

Tab. 9 Optimized input parameters for generating stochastic fractures in the regional HydroDFN model

Population	**Fisher distribution**			**Power law distribution**			
	Strike (°)	**Dip (°)**	**κ (-)**	**α (-)**	**L_1 (m)**	**L_2 (m)**	**$P_{32}[L_1,L_2]$ ($m^2 \cdot m^{-3}$)**
1	222.9	85.4	35.1	3.328	50	500	0.01892
2	49.6	36.9	2.7	3.062	50	500	0.02633
3	313.7	3.4	28.6	3.8	50	500	0.00056
4	316.8	87.5	25.4	3.789	50	500	0.00032
5	133.4	62.3	2.9	3.382	50	500	0.00259
6	346.3	88.6	18.7	3.042	50	500	0.01184
7	1.0	78.2	3.8	3.001	50	500	0.00745
8	269.5	88.6	17.3	3.607	50	500	0.00151
9	86.0	83.3	4.0	3.296	50	500	0.00646

The regional HydroDFN model contains approximately 7100 fractures divided into 120,000 minor fractures, with approximately 370,000 intersections between the minor fractures. A section generated by the regional HydroDFN model is shown in Fig. 33.

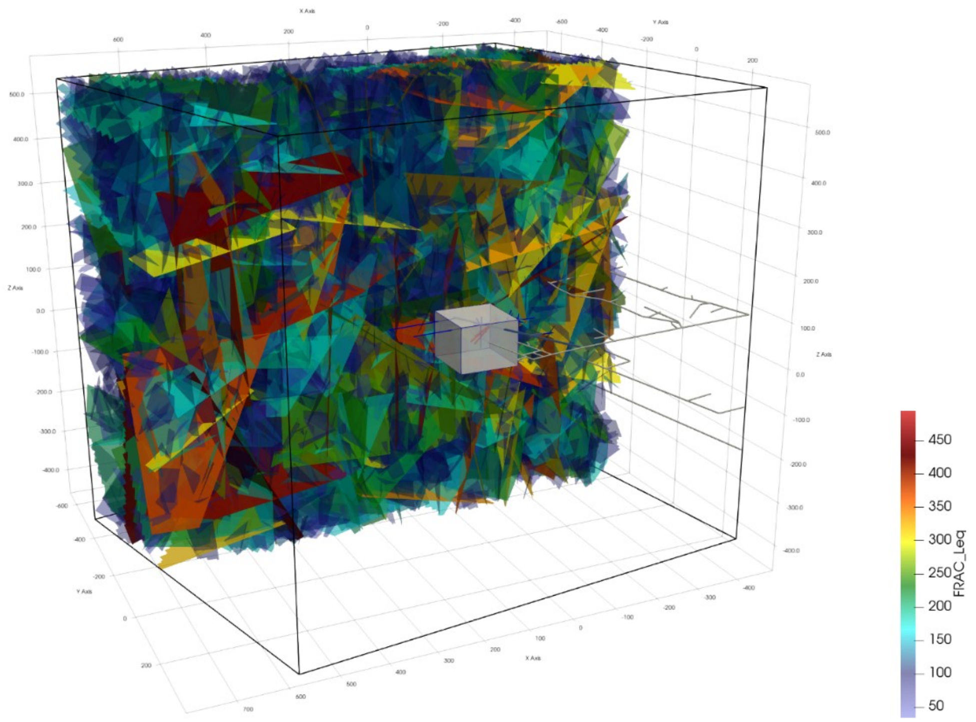

Fig. 33 Cross-section through the regional HydroDFN model (the size of the generated fractures Frac_L_{eq} is distinguished by color) - northern view, the area of the detailed model, boreholes in the Bukov URF and mine corridors are also shown (visualization in ParaView)

The regional groundwater flow model was compiled in 12 variants, in which the influence of selected parameters on the model results was analyzed and evaluated. An overview of the model variants is given in Tab. 10.

Tab. 10 Overview of model variants of the regional model with the values of the tested parameters

Model variant	L_1 [m]	L_2 [m]	$P_{32}(L_1,L_2)$	$\sigma_{ln(T)}$	Comment
Regio.0	50	500	P32	0.0	correlated transmissivity
Regio.1	50	500	P32	3.0	semi-correlated transmissivity
Regio.2	50	500	1.2 × P32	3.0	
Regio.3	50	500	1.5 × P32	3.0	
Regio.4	50	500	1.2 × P32	3.5	
Regio.5	20	500	1.2 × P32	3.5	lower L_1
Regio.6	10	500	P32*	3.5	lower L_1, P32 not scaled
Regio.7	50	500	P32	1.0	
Regio.8(1*)	50	500	P32	3.0	Regio.1 without levels 16 a 18
Regio.9(6*)	10	500	P32*	3.5	Regio.6 with calibrated Q - higher T
Regio.10(7*)	50	500	P32	1.0	Regio.7 with calibrated Q - higher T
Regio.11(6**)	10	500	P32*	0.0	Regio.6 with correlated T

The numerical calculation of the groundwater flow is performed in the ConnectFlow program as a separate process, whereby the input is the generated geometric model, including the boundary conditions. Calculation of the flow in the basic model variant “Regio.0” for a single fracture network takes 6-7 minutes. The higher variability of fracture transmissivity and the higher number of fractures and intersections make the calculation longer, e.g., in the case of the model variant “Regio.5”, the calculation time was 18–22 minutes.

The evaluation of the results of the regional model focused on the following:

- An analysis and comparison of pressure ratios in the newly drilled boreholes (measured overpressure values in boreholes packed at the mouth are in the range of 5–10 m, i.e., measured pressure height 27–32 m at a geodetic height of the borehole mouth of 22 m,
- An analysis and comparison of the size of inflows to the Bukov URF (based on operational monitoring data, the measured total inflow into the Bukov URF is approximately 3.3 l/s).

The variants Regio.9 and Regio.10 correspond best to the measured data, for which the transmissivities of the model fractures intersecting boreholes S-8, S-27, S-31, and S-36 were also evaluated. For variant Regio.9, where inflows to the Bukov URF were calculated in the range of 1.1 to 14.0 l/s, only fractures from five selected implementations of the networks with inflows of 2.5 to 5.7 l/s were included in the evaluation (29 out of 49 fractures). For variant Regio.10, with calculated inflows in the range of 2.1 to 4.4 l/s, fractures from all of the implementations (36 fractures) were included. The model fracture transmissivities are plotted in the graph in Fig. 34 and compared with the measured transmissivity values from the WPT performed on the borehole sections (27 measured values). The course of the curves shows a significantly lower dispersion of values for variant Regio.10, which is related to a lower random variability of transmissivities (specified deviation $\sigma_{\ln(T)}$ = 1.0). On the contrary, the higher specified variability and higher dispersion of values for variant Regio.9 correlates very well with the results of WPT.

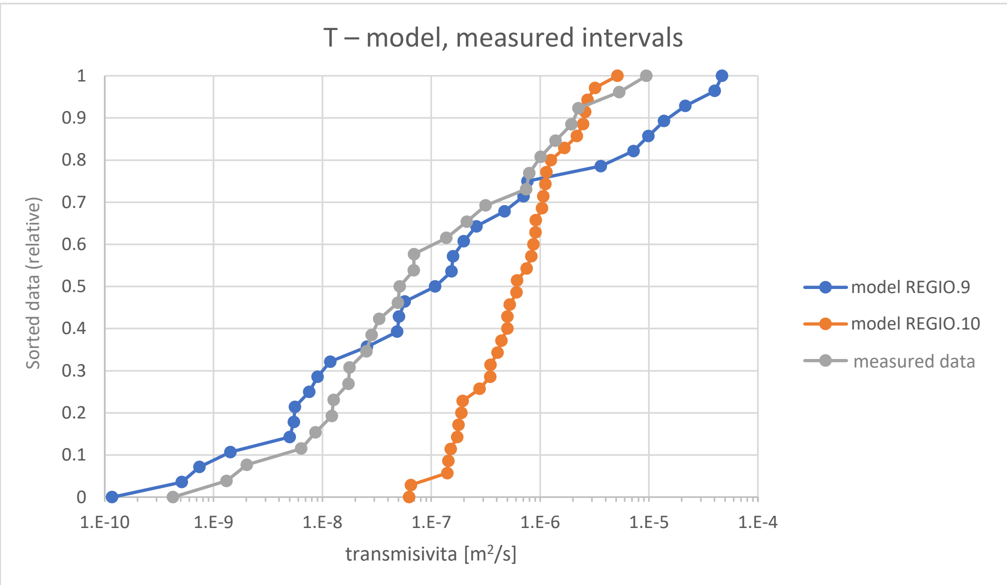

Fig. 34 Model transmissivities of fractures crossing boreholes S-8, S-27, S-31, and S-36 in the calibrated variants Regio.9 and Regio.10 and measured transmissivities in borehole sections evaluated from WPT

HydroDFN model of the rock block

The work on the basic detailed HydroDFN model of the rock block focused on importing and implementing data from the GeoDFN model, on the phase of generating the geometric model, and on the effective definition of the conditions on the boundary of the model block.

The geometry of the fracture network of the GeoDFN model is the basic input for creating the HydroDFN model, and the flow and transport model is then implemented on a modified geological model adapted for the needs of the hydrogeological modeling:

1) A stochastic sGeoDFN model generated in the DFRAM program. For the HydroDFN model, the fracture geometry is delivered in VTK format (which allows direct visualization in ParaView and is suitable for further processing. It also contains both geometry and fracture parameters). From the VTK file, the fracture geometry is converted using the prepared script in the form of an IFZ file (a special text format for importing/exporting fractures, which is further included in the calculation in ConnectFlow),
2) A deterministic dGeoDFN model created in the MOVE program, or a further refined (conditional) semi-deterministic dGeoDFN model. For the HydroDFN model, the fracture geometry is delivered in DXF format (directly exporting the deterministic model in MOVE) or VTK format (a processed semi-deterministic model). From the DXF or VTK files, the fracture geometry is converted using a prepared procedure into an IFZ file, which is used in the simulations in ConnectFlow.

During the preparation of the conceptual HydroDFN model, the conditions at the boundaries of the detailed model of the rock block were specified from the calculation of the flow model on a regional scale. The calculations of the regional model pointed to a relatively large dispersion of pressure values in the specified boreholes and the size of inflows into the mine. In addition, the time required to calculate the regional model is relatively small (minutes to the first tens of minutes, depending on the density of the fracture network). For these reasons, the concept of defining boundary conditions at the boundary of the detailed model was partially modified. The original concept assumed a procedure consisting of two consecutive steps, as follows:

1) Calculation of flow in the regional HydroDFN model (1.1 × 0.9 × 1.0 km) and evaluation of pressure ratios in intersecting “regional” fractures with surfaces delimiting the area of the detailed model (130 × 130 × 100 m),
2) Entering the obtained pressure values from the regional model as boundary conditions in the detailed HydroDFN model and performing calculations in the domain of the detailed model.

The modified concept of HydroDFN modeling (see Fig. 35), which was applied during the construction of the basic model, and which was used during the solution in subsequent stages, is more complex and more efficient from the point of view of “transferring” pressure/balance conditions between the regional and detailed models. The model combines the regional and detailed scale of the task, i.e., an inner detailed domain (130 × 130 × 100 m), which is surrounded by the outer regional domain (1.1 × 0.9 × 1.0 km), is entered into the joint model.

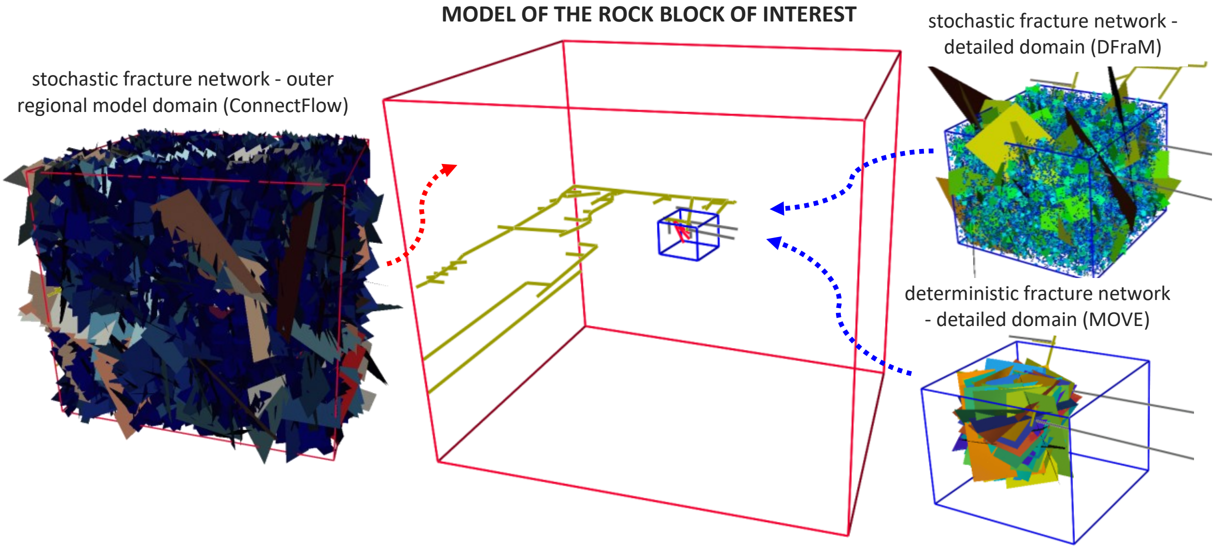

Fig. 35 Basic HydroDFN model of the rock block of interest in the ConnectFlow program – stochastic fracture network in the outer regional model domain (from the ConnectFlow program), detailed deterministic fracture network (from the MOVE program), and additional stochastic network (from the DFraM program) in the inner detailed domain

Stochastic sHydroDFN model

To generate the geometry of the fracture network of the basic model, the updated optimized parameters of the thickness distribution for populations 1–5 included in Tab. 8 (thickness distribution parameters for the number of fractures). These parameters were used to generate stochastic fractures in both the regional and detailed domains of the sHydroDFN model. The difference is in the generated size of the fractures in the individual domains:

- Fractures with a minimum area of 4 m^2 are generated in the internal detailed domain and the studied area of the rock mass, i.e., square fractures of 2 × 2 m and larger,
- Fractures with a minimum area of 2500 m^2 are generated in the outer domain, i.e., square fractures of 50 × 50 m and larger (variants with a minimum fracture size of 10 × 10 m and 30 × 30 m were also simulated).

In the phase of preparing the geometry of the hydrogeological sHydroDFN model, non-conductive (closed) fractures are removed from the geological sGeoDFN model. This process of reducing the number of fractures (see Fig. 36) consists of two consecutive steps, as follows:

A. Random selection of a share of the fractures from the input sGeoDFN, or a more computationally efficient method is used, where the P30 parameters of the fracture population are first reduced by the selected share and then a new, reduced input stochastic sDFN model is generated,
B. Analysis of the connectivity of the generated network, non-connective isolated fractures and fracture clusters that do not contribute to the flow are removed. This step is implemented as part of the generation of the model in the ConnectFlow program.

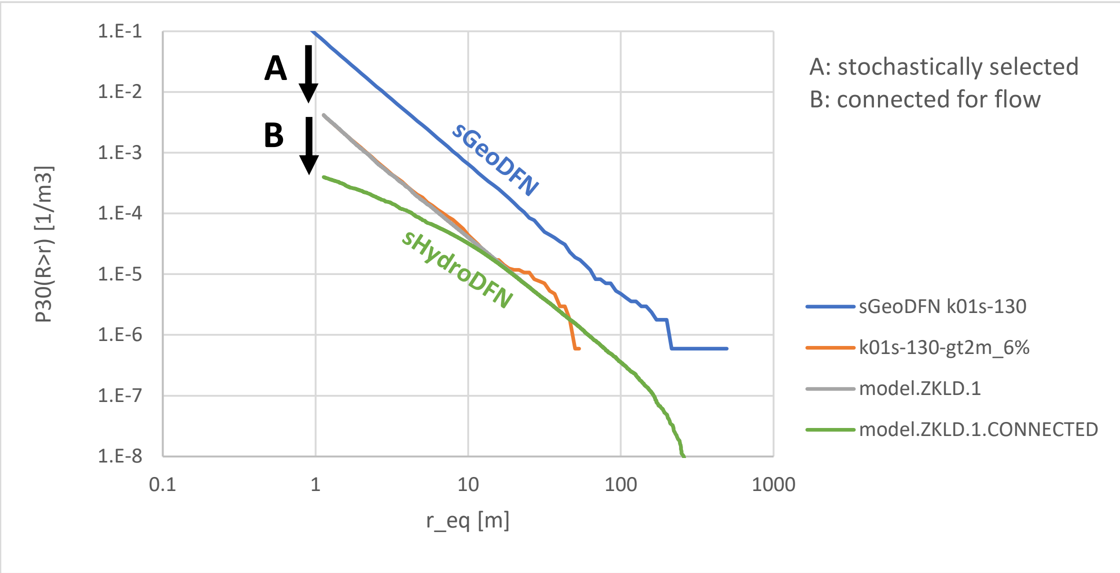

Fig. 36 Process of reducing the number of fractures during the preparation of the HydroDFN model, comparing the size and density of the fractures generated in the DFraM and ConnectFlow programs (parameter P_{30})

Based on the analysis of the variant implementations of the fracture network (generation and evaluation of the geometric DFN model), selected variants of the basic sHydroDFN model were prepared and a flow simulation was performed. An overview of the variants is given in Tab. 11.

A numerical calculation of groundwater flow and analysis of the results of the model were performed using the same procedure as in the case of the simulations of the regional HydroDFN model. The model variants were simulated on 10 and 20 implementations of the network, respectively. It takes 3-10 minutes to calculate the flow per each implementation of the fracture network.

Tab. 11 Overview of model variants of the basic sHydroDFN model

Model	Domain	L_{min} (m)	L_{max} (m)	r_{min} (m)	r_{max} (m)	Share of fractures in the connective HydroDFN	Number of implementations
ZKLD.0	reg+det	10.0	500.0	5.64	282.1	6%	10
ZKLD.1	regio	10.0	500.0	5.64	282.1	6%	10
	detail	2.0	500.0	1.13	282.1		
ZKLD.2	regio	30.0	500.0	16.93	282.1	6%	20
	detail	2.0	500.0	1.13	282.1		
ZKLD.3	regio	50.0	500.0	28.21	282.1	6%	20
	detail	2.0	500.0	1.13	282.1		
ZKLD.4	regio	50.0	500.0	28.21	282.1	3%	10
	detail	2.0	500.0	1.13	282.1	15%	
ZKLD.5	regio	50.0	500.0	28.21	282.1	8.5%	10
	detail	2.0	500.0	1.13	282.1		

The evaluation of the model results focused on the following:

- An analysis and comparison of pressure ratios in the newly drilled boreholes (the measured overpressure values in the boreholes with packers at the mouth are in the range of 5–10 m, i.e., measured pressure head of 27–32 m at a geodetic height of the borehole mouth of 22 m). The calculated pressure heads were processed in the packer intervals of boreholes S-27, S-31 and S-36 for individual model variants and fracture network implementations, see the overview of average model pressure values in Tab. 12, the complete set of calculated values is shown in Fig. 37,
- An analysis and comparison of the size of inflows to the Bukov URF (based on the operational monitoring data, the measured total inflow into the Bukov URF is approximately 3.3 l/s). The calculated outflows from the fractures crossing the boreholes and tunnels of the mine were processed for individual model variants and implementations of the fracture network .

The average measured overpressure in boreholes S-27, S-31, and S-36 (where the packers were only at the mouth) is in the range of 5–10 m. With the specified geodetic height of the boreholes of 22 m, the measured pressure head in the boreholes is therefore 27–32 m. For "optimal" model values the pressures were considered to be in the range of 24-35 m. Compared to the model results (Tab. 12), the variant ZKLD.4 with five suitable implementations of the network corresponds best to these values.

Tab. 12 Average modeled pressure heights in the packer intervals of boreholes S-27, S-31, and S-36 for the individual model variants and implementations of the fracture network (the values in the columns, i.e., the model variants, are sorted (using a color scale) according to the pressure measurements in the packed boreholes. The optimal values are up to approximately 2–13 m of overpressure at the mouth of the borehole, i.e., up to a pressure height of 24-35 m)

ID	ZKLD.0	ZKLD.1	ZKLD.2a	ZKLD.2b	ZKLD.3a	ZKLD.3b	ZKLD.4	ZKLD.5
1	19.8	19.8	22.6	21.5	23.9	22.4	3.1	31.2
2	20.8	20.2	26.0	22.5	25.0	22.4	17.9	37.6
3	22.5	22.9	28.7	22.7	31.1	24.3	22.6	41.6
4	31.2	30.9	29.2	25.5	33.9	28.8	26.4	45.5
5	46.6	46.4	59.5	25.9	35.4	38.8	28.5	46.2
6	47.8	47.8	74.8	26.4	40.3	49.6	30.5	51.1
7	53.6	53.5	87.1	40.3	63.0	51.5	31.3	76.6
8	62.6	62.0	90.1	46.6	66.9	58.5	33.6	107.4
9	63.7	63.5	135.9	49.0	84.5	72.7	66.6	129.1
10	#N	#N	136.8	106.9	177.8	84.8	67.7	187.7

mean model head in S27, S31, S36 — 24-35 m

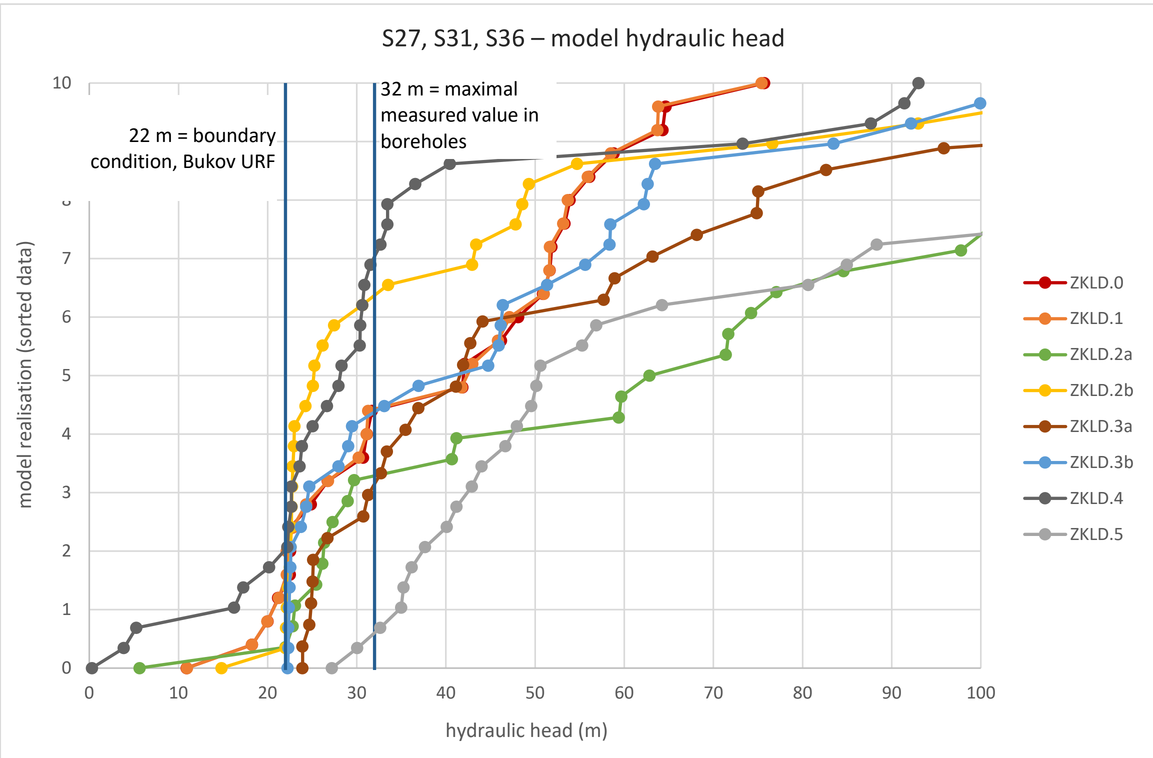

Fig. 37 Model pressure heights in boreholes S-27, S-31, and S-36 for the individual model variants ZAKLD.X. For each variant, the calculated values for all three boreholes and all 10 implementations of the network (i.e., 30 values) are sorted and plotted on the graph

For the five "optimal" implementations of the fracture network of the ZKLD.4 model, calibrated models were prepared with an inflow into the space of the Bukov URF of 3.3 l/s and the transmissivity values of the model fractures intersecting boreholes S-27, S-31, and S-36 were evaluated. The modeled transmissivity values of the fractures are plotted on the graph in Fig. 38 and are compared to the measured transmissivity values from the WPT performed on the borehole sections (27 measured values). All the curves have a very similar slope, but there is a relatively large difference in values between the individual implementations (horizontal shift of the curves) i.e., up to almost two orders of magnitude between implementation No. 2 and implementations No. 8 and 9. Implementation No. 5 best corresponds to the measured data from the WPT. This stochastic implementation of the sHydroDFN model ZKLD.4.r5 (the network "calibrated" to measured pressure values in boreholes, inflows to Bukov URF and measured transmissivity from WPT) was further used in the implementation of deterministic dHydroDFN and in upscaling to HydroECPM.

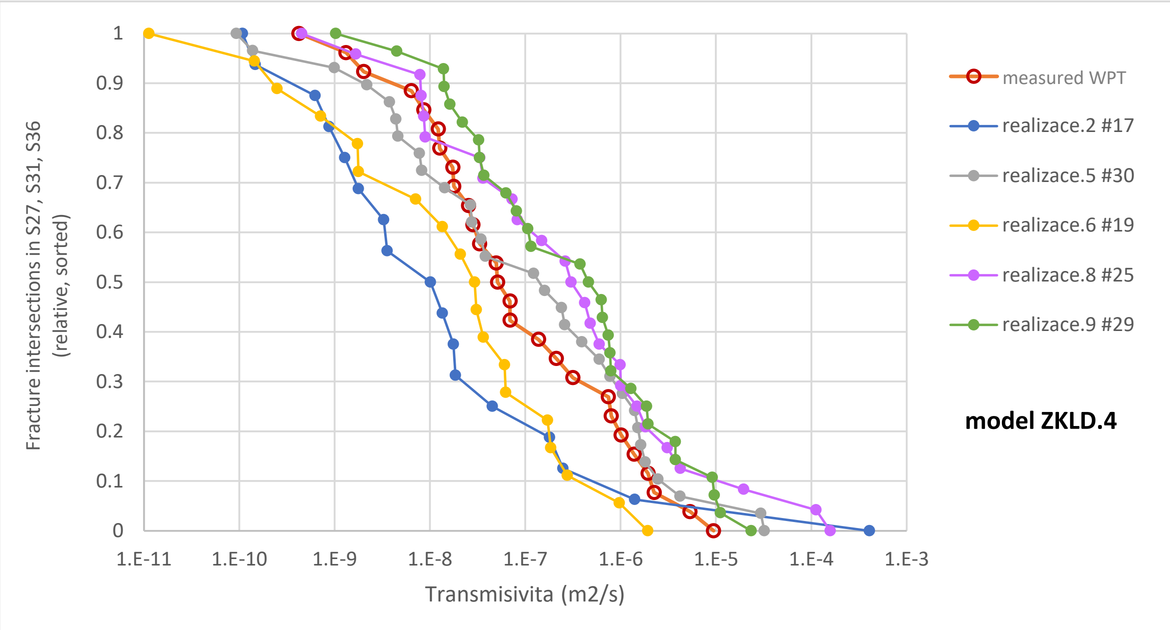

Fig. 38 Model transmissivities of fractures crossing boreholes S-8, S-27, S-31, and S-36 in calibrated outputs of model alterative ZKLD.4 and measured transmissivities in borehole sections evaluated from WPT

Semi-deterministic dHydroDFN model

The semi-deterministic dHydroDFN model is the same as the stochastic sHydroDFN model described above in terms of the size of the model domain and the specified boundary conditions. The designation "semi deterministic" refers to the input semi-deterministic dGeoDFN model, which geometrically refines the connection of the fracture network in the area of interest in the area of the newly drilled boreholes and borehole S-8. The semi-deterministic dHydroDFN model is a combined stochastic-deterministic model, where the fracture network consists of the following two inputs:

1) The basic stochastic sHydroDFN model described above (implementation ZKLD.4.r5), i.e., the input is the geometry of the fracture network including the basic version of the calibrated fracture transmissivity,
2) A semi-deterministic dGeoDFN model (version d01s_v06.rmin05, see Section 6.2.3). Transmissivities are randomly generated for the individual fractures (mesh) according to the same rule as for the stochastic fractures, i.e., a semi-correlated relationship is used

with a functional dependence on the size of the structure (equivalent radius) and with a log normal distribution. In the basic model, one transmissivity value is calculated for the entire structure.

To avoid duplication of the fractures crossing boreholes S-27, S-31, S-36, and S-8 in the model, all the randomly generated fractures crossing these boreholes are removed from the stochastic sHydroDFN model. The assumption for this procedure is that the prepared semi-deterministic dGeoDFN contains all the hydrogeological significant fractures that cross these boreholes. The "duplicate" stochastic fractures are removed in ConnectFlow, which has its own functions (commands) for this purpose.

The flow calculation was performed again on the prepared semi-deterministic dHydroDFN model, i.e., the outputs were analyzed and compared to the results of the stochastic sHydroDFN. From the point of view of the model balance, the total inflow to the Bukov URF in the semi-deterministic model was essentially identical to the inflow in the stochastic model. This is due to the small local reach of the fracture network of the semi-deterministic model within the Bukov URF, the minimal number of intersections with corridors, and the overall minimal influence.

However, the pressure conditions in the boreholes are significantly affected. The larger number of fractures in the semi-deterministic model and the overall better connection of the fracture network lead to a reduction of the model pressures in the boreholes almost to the level of the boundary condition specified in the corridors (22 m). The model overpressure in the boreholes is only 0.5–1.0 m depending on the generated transmissivity (in the stochastic sHydroDFN.ZKLD4.r5 the calculated average overpressure was 4.5 m).

In the next stage of processing and optimization of the HydroDFN model for the simulation of performed and proposed tests, the network generation procedure was slightly modified. The fractures were simplified to square fractures with a deterministically entered average dip and strike, which allows for better discretization of the fractures in the computational network and more efficient input of variable fracture parameters when calibrating the model.

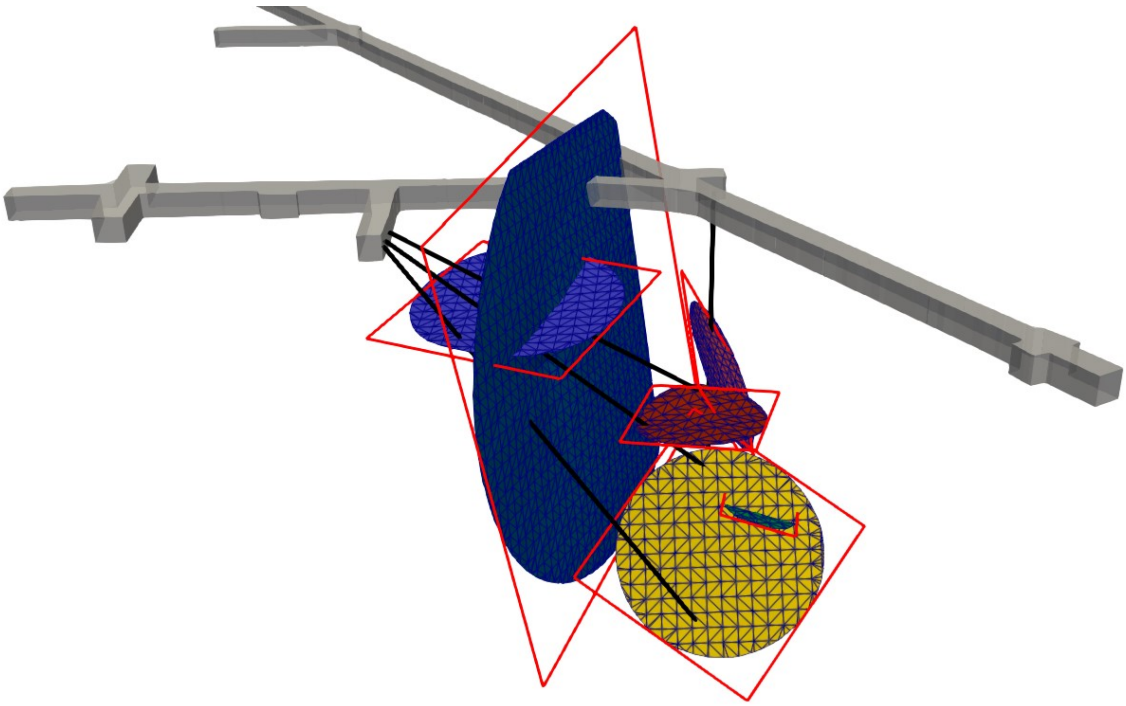

Fig. 39 Modified concept for the preparation of the dHydroDFN geometry in ConnectFlow - generating equivalent square deterministic fractures - sample for the selected meshes 12 to 17

6.2.5 HydroECPM model

The HydroECPM model, i.e., the equivalent porosity continuum hydrogeological model, is implemented in the following three steps:

1) Firstly, the selected area of the model is divided into a continuous 3D network of computational cells (e.g., in the shape of a cube), in which the simulation is to be performed by the ECPM concept and for which the equivalent hydraulic parameters are to be determined. The choice of the ECPM region and its discretization is a relatively important step and is related to the initial question: "What is the aim of the ECPM simulation, for what purpose is the overall simplification of the model performed?"
2) Secondly, the hydrogeological fracture network (HydroDFN) is converted into a defined network of cells by upscaling. For this purpose, the ConnectFlow program has a function, which for the individual cells of the continuum "cuts" the appropriate part of the fracture network from the HydroDFN (for a more precise determination of the parameters, it is advisable to define a certain "buffer"), in the individual directions *x, y, z* of the flow simulation and converts the fracture network in the given cell (interconnection and transmissivity of fractures) to the equivalent value of the hydraulic conductivity tensor of the given cell (the cell porosity is then calculated),
3) The third, last, step is a classic procedure for constructing and implementing the model, i.e., entering the boundary conditions and performing the simulation. The ConnectFlow program has a module for simulating the model based on the CPM concept used in the solution (alternatively, any software that can work with a prepared 3D cell network and the calculated equivalent parameters can be used, e.g., MODFLOW USG).

The main benefit of the ECPM concept, i.e., simplification of the complex fracture network DFN into the form of equivalent hydraulic parameters of CPM, is that it can be used in the space of a model without engineering objects, e.g., mine shafts, corridors, shafts, boreholes. These objects, if they are present in the model, usually represent one of the internal boundary conditions of the model, and around them it is necessary to adjust (refine) the ECPM discretization of the cell network, which returns complexity to the model and increases the level of complexity of the system. In this case, it is better to keep the original DFN concept around the objects and make use of the option to create a combined DFN ECPM model, which the ConnectFlow program also offers.

The following procedure was used in the processing of the HydroECPM model of the block of interest:

- The basis for the implementation of the HydroECPM model is the stochastic fracture network of the sHydroDFN.ZKLD4.r5 model (the basic calibrated version of sHydroDFN also used in processing dHydroDFN),
- Parameter upscaling was performed in two versions of 3D cell discretization, see Fig. 40. In a coarser grid of cells 100 × 100 × 100 m (HydroECPM.100) and in a finer grid of 25 × 25 × 25 m, which is further condensed to a size of 5 × 5 × 5 m in the detailed area of interest (HydroECPM.25),
- Combined DFN-ECPM models were compiled. The outer domain was simulated by the ECPM concept, the inner detailed domain with the corridors and boreholes was solved as a DFN model with a reduced mine extent (Bukov URF and the connecting corridors of the 12th floor exceed the detailed area in terms of extent and were therefore trimmed at this stage of the modeling so as not to interfere with the ECPM region)
- A flow calculation was performed, and the results were compared.

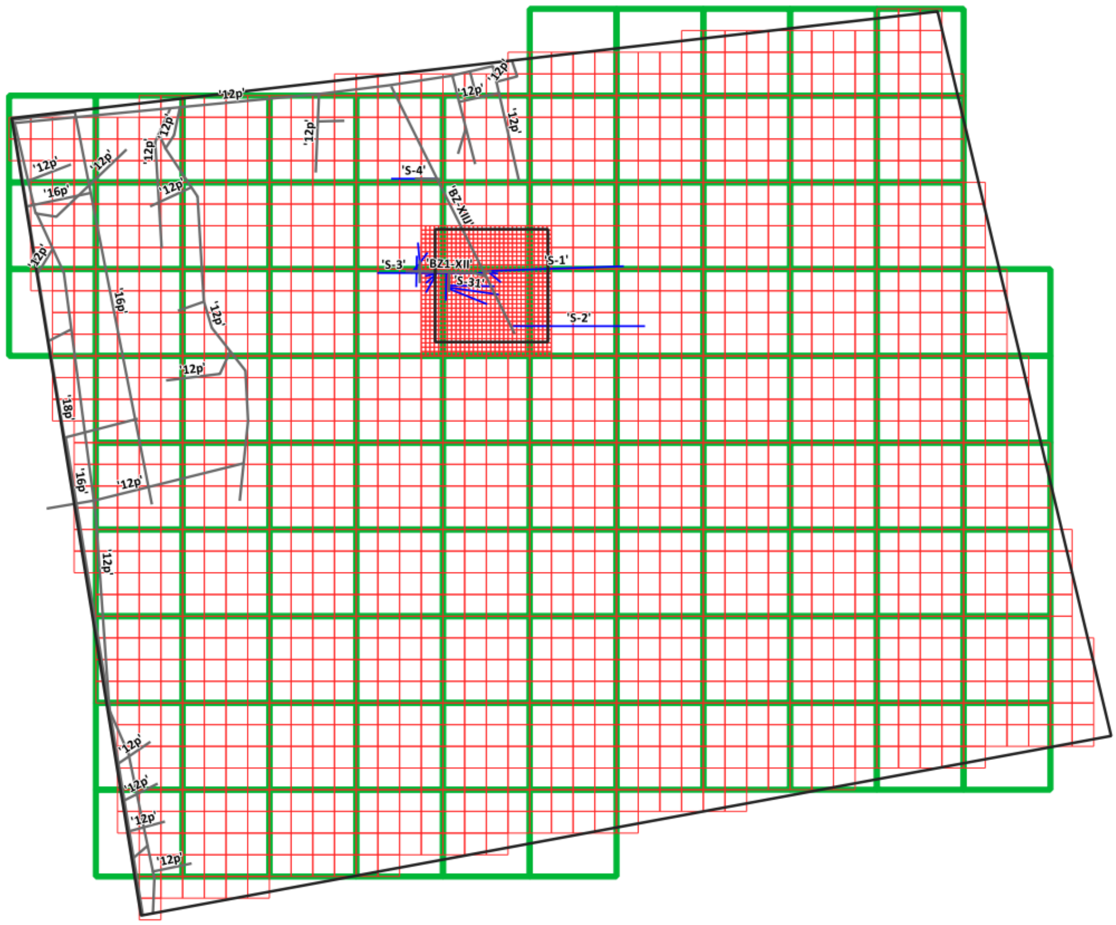

Fig. 40 Used discretization of HydroECPM model cells – green regular grid of cells 100 × 100 × 100 m (HydroECPM.100), red regular grid of cells 25 × 25 × 25 m, in the detailed part condensed to 5 × 5 × 5 m (HydroECPM.25)

Fig. 41 documents the calculated hydraulic conductivities in both HydroECPM models with a cell network of 100 and 25 m. The effect of discretization is particularly evident in areas with small fracture connections. In the 100 × 100 m network, a higher conductivity value is calculated in the ECPM model, better hydraulic communication is achieved between neighboring cells and the model is overall more homogeneous.

These differences are further prescribed in the flow simulation and the calculated pressure fields of both HydroECPM models differ quite significantly, see Fig. 42. In the central part in the area of the boreholes, the maximum pressure differences are approximately 20 m. In the wider area at the level of the 12th floor, the pressure difference is already approximately 100 m. The differences are also reflected in the overall balance of inflows to the specified part of the mine. In the HydroECPM.100 model the inflow is approximately double that of HydroECPM.25. A summary of the differences in the flow simulation results is presented together for the input HydroDFN model and both "equivalent" HydroECPM models in Tab. 13. Significantly better agreement of both approaches (DFN and equivalent ECPM) was expected in the simulation results.

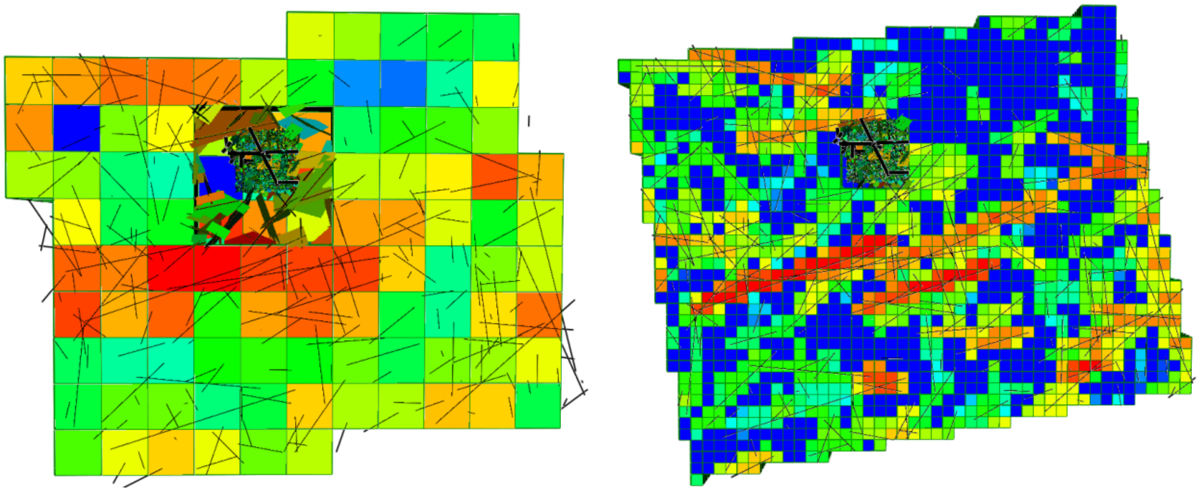

Fig. 41 Comparison of the calculated parameters of hydraulic conductivity (Kxx) -- on the left for the HydroECPM.100 model, on the right the HydroECPM.25 model (the black lines indicate the input HydroDFN fractures)

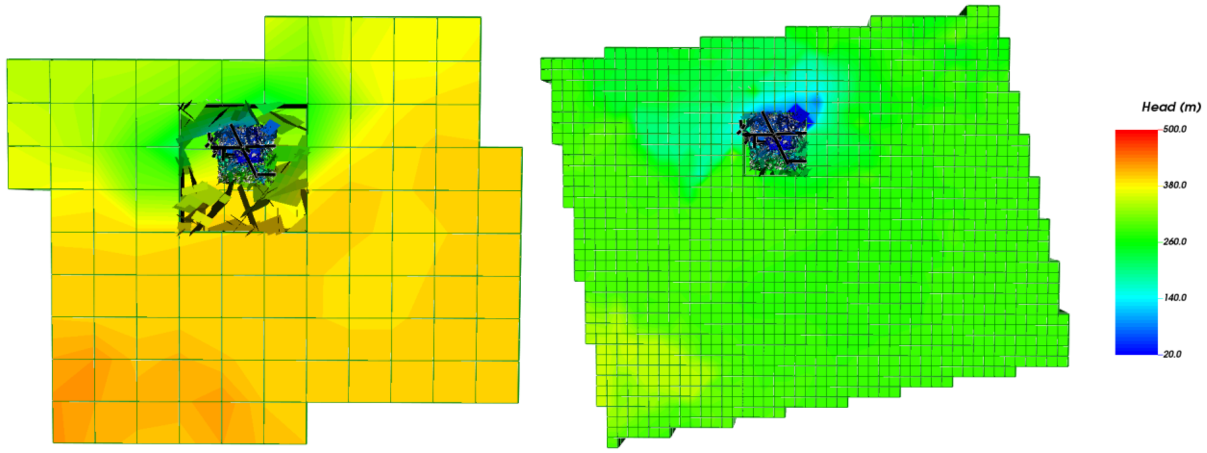

Fig. 42 Comparison of the calculated hydraulic pressure heads (Head) - on the left for the HydroECPM.100 model, on the right for the HydroECPM.25 model

Tab. 13 Summary of flow simulation results in the HydroDFN and equivalent HydroECPM models

Model output	HydroDFN	HydroECPM.25	HydroECPM.100
Pressure in S-27 (m)	22.6	23.0	23.7
Pressure in S-31 (m)	26.2	27.5	30.4
Pressure in S-36 (m)	50.2	61.2	82.2
Inflow to the specified mine works (up to the boundary condition) (l/s)	9.2	21.2	39.3
Length of the simulation (s)	118	63	15

6.3 Optimization of the Numerical Model

The model optimization stage (Stage 24) followed on from the processed basic numerical model and is described in detail in the interim report TR 702/2023 (Zuna et al. 2023). According to the proposed concept, a combined stochastic deterministic dHydroDFN model was further developed and calibrated:

- In the area of interest around boreholes S-27, S-31, S-36, and S-8, the basic semi-deterministic fractures network model dGeoDFN (conditional on measured data from boreholes) version d01s_06 was optimized with a minimum radius of generated fractures r_min 5 m. There are 43 semi-deterministically entered fractures, and the average dip and strike and the stochastically generated center and size are shown in Tab. 14 and Fig. 43 shows the schematic connection of semi-deterministic fractures between intersections with boreholes,
- On a wider scale in the area, i.e., outside the area of the described intersections of fractures with boreholes, a stochastic network of fractures sHydroDFN implementation ZKLD.4.r5 was used (the stochastic network of fractures is generated in the entire model domain, but the fractures crossing the four boreholes of interest are removed from it).

The created meshes of semi-deterministic fractures (in the MOVE program they are curved surfaces according to the actual coordinates of the intersections and the orientation of the fractures) are fitted in the model with a plane with an average strike and dip. The model intersections of the fractures with boreholes are not always exactly identical to the measured coordinates, but may be slightly shifted. At the same time, the order of some of the fracture intersections is reversed, but it is important to preserve data continuity and to ensure that a given intersection intersects a given packer borehole interval. In total, there are 82 intersections of semi-deterministic fractures with the boreholes S-27, S-31, S-36, and S-8 in the model.

Optimization of the numerical model focused on modifying the geometry of the semi-deterministic dHydroDFN model and calibrating the hydraulic parameters of the semi-deterministic fractures. The dHydroDFN model and fracture transmissivity were optimized using selected measured data and system states and in several model variants. Hydraulic conductivity K on borehole sections of length L from the WPT, evaluated according to the formula of Moye (1967), was used to enter the input value of fracture transmissivity (transmissivity of the section is $T = K*L$).

Tab. 14 Geometric parameters of dGeoDFN fractures of the d01s_06_rmin5m model and parameters for the model in ConnectFlow with square fractures (displacement of fracture center coordinates [x,y] by [-622900, -1129700])

Mesh ID	Dip	Strike	Azimuth	r (m)	L=2r (m)	Xc	Yc	Zc
0	39.1	122.6	212.6	34.8	69.5	628.19	749.50	4.15
1	17.0	96.0	186.0	7.4	14.9	612.44	757.75	4.66
2	65.9	118.3	208.3	7.9	15.9	627.81	775.13	16.77
3	72.2	47.4	137.4	6.1	12.3	632.06	774.50	-25.65
4	36.2	113.7	203.7	14.4	28.9	581.06	757.38	19.62
5	88.7	8.0	98.0	45.4	90.9	592.06	753.38	14.44
6	57.2	258.3	348.3	35.8	71.7	622.19	767.88	-19.79
7	9.0	69.0	159.0	9.9	19.8	614.63	756.63	9.63
8	28.8	125.2	215.2	48.9	97.7	594.94	746.75	11.49
9	36.1	123.0	213.0	7.5	15.1	596.06	750.75	10.67
10	47.1	108.2	198.2	54.6	109.1	599.75	737.13	-5.81
11	33.5	107.0	197.0	41.3	82.5	605.81	750.63	11.44
12	8.5	124.5	214.5	14.2	28.4	599.63	756.25	12.99
13	84.0	27.7	117.7	33.4	66.7	609.63	761.63	4.43
14	16.6	337.9	67.9	5.2	10.3	630.81	743.75	-13.64
15	52.9	96.6	186.6	14.0	28.1	624.94	740.75	-17.63
16	3.3	206.7	296.7	9.0	17.9	623.31	748.25	-0.94
17	66.3	11.4	101.4	11.6	23.2	628.44	764.88	-3.03
18	21.9	95.8	185.8	6.6	13.1	626.50	750.38	-5.65
19	86.4	41.6	131.6	84.2	168.4	617.00	736.25	-32.19
20	62.2	16.7	106.7	14.1	28.2	602.50	745.88	1.67
21	74.9	229.2	319.2	13.4	26.8	603.56	743.50	-6.62
22	31.8	109.4	199.4	7.1	14.2	608.88	746.63	-3.16
23	41.7	244.0	334.0	9.6	19.2	609.88	748.00	-4.95
24	44.8	88.2	178.2	9.0	18.0	609.69	749.00	-1.05
25	86.7	18.2	108.2	11.9	23.8	623.81	743.38	-19.04
26	69.7	229.4	319.4	15.4	30.8	619.75	741.88	-2.96
27	72.4	271.1	1.1	19.3	38.7	619.81	743.88	-5.57
28	27.4	258.3	348.3	14.8	29.7	625.63	743.25	-16.56
29	82.8	219.7	309.7	17.6	35.1	634.56	747.63	-29.20
30	84.6	45.3	135.3	7.3	14.6	634.81	744.75	-16.42
31	46.6	86.6	176.6	13.5	27.0	610.13	743.38	-10.28
32	80.0	360.0	90.0	5.1	10.2	606.88	769.13	20.93
33	67.1	30.6	120.6	8.4	16.8	582.38	763.50	25.99
34	60.2	9.7	99.7	12.1	24.1	584.81	762.88	25.48
35	87.4	222.6	312.6	17.6	35.1	623.31	734.00	-19.07
36	73.0	22.9	112.9	6.7	13.3	598.94	746.88	6.59
37	81.4	191.7	281.7	5.5	11.0	600.63	740.63	2.38
38	85.1	174.9	264.9	5.6	11.3	619.38	740.00	-26.85
39	16.8	42.1	132.1	5.3	10.6	623.94	774.75	-15.15
40	43.5	204.6	294.6	6.5	12.9	626.63	774.38	-22.38
41	54.4	182.1	272.1	5.0	10.0	627.63	771.50	-24.76
42	75.4	84.0	174.0	7.0	13.9	633.19	772.75	-26.58

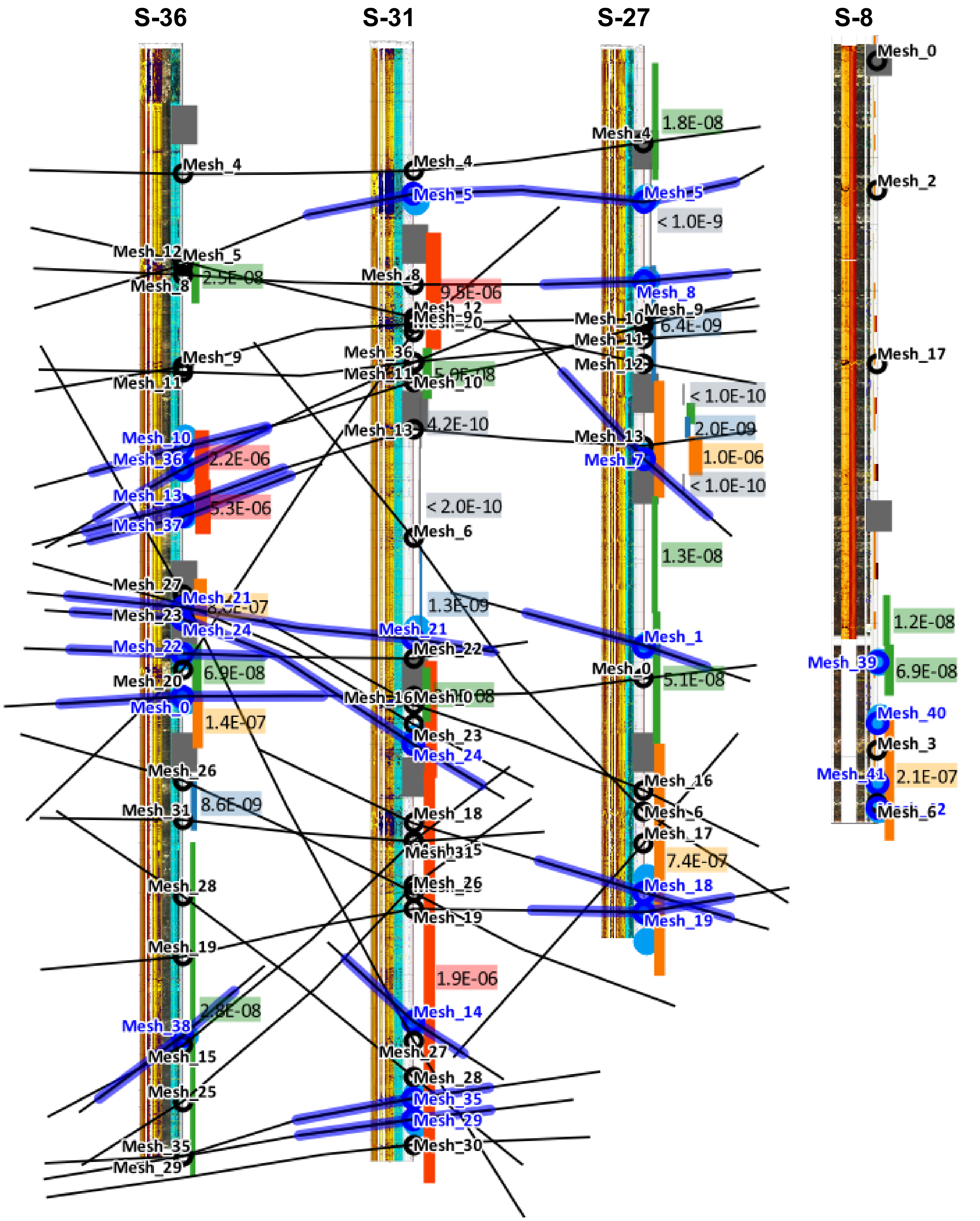

Fig. 43 dGeoDFN model – schematic connection of fractures between intersections with boreholes. Intersections with identified borehole inflows are highlighted in blue, the values indicate transmissivity from WPT evaluated according to Moy (1967)

Three selected system states were simulated on the assembled model, and the model and measured results were compared, and the next optimization procedure was evaluated:

1) The state with unaffected pressure ratios with a system of boreholes with packers. Pressures H_i in the individual boreholes intervals were evaluated and compared with the measurements,
2) The state with open taps and water outflowing from all intervals. The size of the outflow Q_i and the total outflow were evaluated and compared with the measurements,
3) The state with open taps only in the selected conductive interval S36_3ab. The outflow from the open interval and the pressures H_i in the other packer intervals of the boreholes were evaluated.

As part of the optimization process, i.e., model calibration, simulations were run with the aim of identifying which model parameters significantly contribute to model inaccuracies and need to be modified:

- The transmissivities of fractures crossing the upper shallow intervals of boreholes S-31 and S-27 (mesh 34, 4, and 5) were modified and increased. The measured pressure values in these intervals are significantly lower than the model ones and there is an important connection of the fractures to the drainage effect of the corridors, which was not identified. WPT was not performed in the shallow fractured part of S-31, which would possibly confirm a higher permeability, there is a possible influence of the excavation influenced zone (EIZ), etc. The transmissivity of the sections with the EIZ was gradually increased to 6.7 10^{-6} m^2/s during the optimization,
- A significantly better agreement of the model results with the measured pressures was achieved when entering the measured WPT value into only one selected fracture. The transmissivity from the WPT was primarily assigned to a fracture with an identified inflow, in the case of multiple inflows in a section or, conversely, in a section without an inflow, it was entered into a fracture that seemed to be more appropriate according to the connection diagram. The result is a heterogeneous pressure field that approaches the measured values in the intervals. Locally, however, significant differences may be observed, e.g., a low model pressure value in the deep interval S27_1, or conversely a high value in the shallow intervals S31_3 and S36_4,
- A better agreement between the measured and model data was achieved when the transmissivity values of semi-deterministic fractures were increased (compared to the values evaluated from the WPT),
- A graphical comparison of the measured values and model results for the selected optimized variants and three simulated system states is shown in Fig. 44,
- Tab. 15 shows an overview of the measured and model transmissivities and fracture parameters in the final optimized model variant var10.

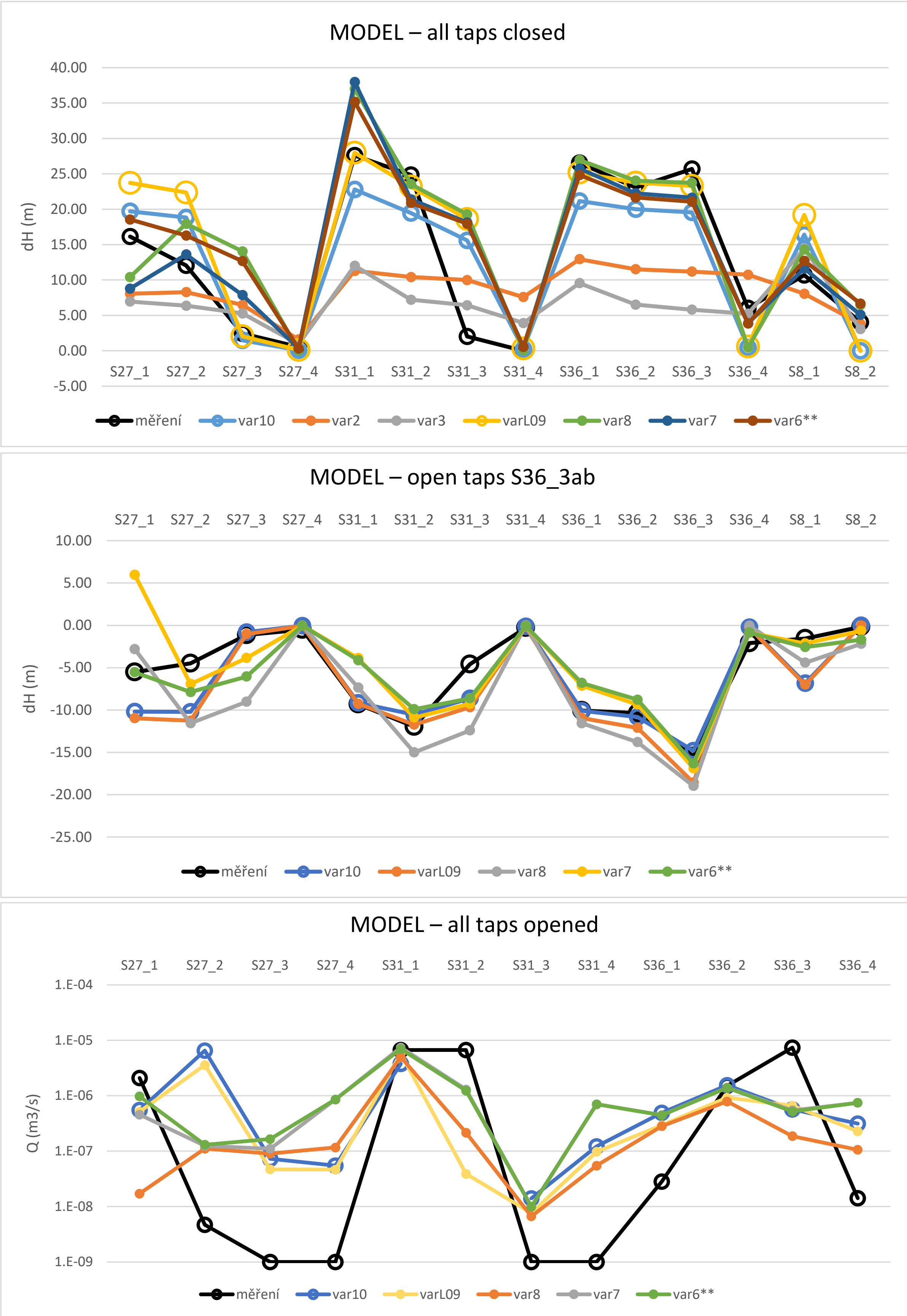

Fig. 44 Comparison of measurements and model results of selected optimized variants

Tab. 15 Overview of transmissivities and fracture parameters in the optimized model variant var10

Borehole	Interval	Mesh ID	X	Y	Z	WPT_T	VTZname	Hydro	WPT_ID	T_MODEL	maxR
S-27	o	34	585.261	756.071	22.702	1.0E-05	EIZ	0	32	6.7E-06	15.00
S-27	o	4	588.346	756.018	20.849	1.0E-05	EIZ	0	32	6.7E-06	15.00
S-27	4	5	592.332	755.944	18.452	1.0E-05	EIZ	1	32	6.7E-06	15.00
S-27	4	8	596.358	755.876	16.033	6.4E-09	VTZ3	1	3	1.3E-08	15.00
S-27	4	9	598.486	755.840	14.754	fix_5E-10	disabled	0	36	1.0E-10	3.00
S-27	4	11	600.315	755.809	13.655	fix_5E-10	disabled	0	36	1.0E-10	3.00
S-27	4	10	600.475	755.806	13.559	fix_5E-10	disabled	0	36	1.0E-10	0.00
S-27	4	12	601.277	755.793	13.077	fix_5E-10	disabled	0	36	1.0E-10	3.00
S-27	3	13	605.812	755.708	10.351	fix_5E-10	disabled	0	36	1.0E-10	3.00
S-27	3	7	606.468	755.696	9.957	3.2E-07	VTZ4	1	4	6.4E-07	20.00
S-27	2	1	616.209	755.530	4.105	fix_5E-10	disabled	1	36	1.0E-10	0.00
S-27	2	0	617.259	755.511	3.474	5.1E-08	VTZ6	0	6	1.0E-07	12.00
S-27	1	6	623.669	755.403	-0.380	fix_5E-10	disabled	0	36	1.0E-10	3.00
S-27	1	16	624.782	755.383	-1.049	fix_5E-10	disabled	0	36	1.0E-10	0.00
S-27	1	17	625.948	755.363	-1.749	fix_5E-10	disabled	0	36	1.0E-10	0.00
S-27	1	18	628.987	755.308	-3.575	fix_5E-10	disabled	1	36	1.0E-10	0.00
S-27	1	19	631.587	755.262	-5.137	7.4E-07	VTZ7	1	7	1.5E-06	6.00
S-31	o	34	585.277	753.308	21.861	1.0E-05	EIZ	0	33	6.7E-06	15.00
S-31	o	4	589.046	752.779	18.886	1.0E-05	EIZ	0	33	6.7E-06	15.00
S-31	o	5	591.871	752.382	16.656	1.0E-05	EIZ	1	33	6.7E-06	15.00
S-31	4	8	595.333	751.895	13.921	fix_5E-10	disabled	0	37	1.0E-10	3.00
S-31	4	12	597.470	751.596	12.236	9.5E-06	VTZ1	0	8	1.9E-05	15.00
S-31	4	9	597.911	751.534	11.889	fix_5E-10	disabled	0	37	1.0E-10	3.00
S-31	4	20	598.999	751.381	11.031	fix_5E-10	disabled	0	37	1.0E-10	0.00
S-31	4	36	599.468	751.315	10.660	fix_5E-10	disabled	0	37	1.0E-10	0.00
S-31	4	11	599.486	751.313	10.647	5.0E-08	VTZ2	0	9	1.0E-07	10.00
S-31	4	10	601.547	751.024	9.022	fix_5E-10	disabled	0	37	1.0E-10	0.00
S-31	3	13	603.541	750.739	7.446	4.2E-10	VTZ3	0	10	8.4E-10	10.00
S-31	3	6	608.899	749.988	3.220	< 2.0E-10	VTZ5	0	12	2.0E-10	15.00
S-31	3	21	613.098	749.399	-0.093	1.3E-09	VTZ6	1	13	2.6E-09	8.00
S-31	3	22	613.732	749.310	-0.593	fix_5E-10	disabled	0	37	1.0E-10	3.00
S-31	2	16	614.753	749.162	-1.401	fix_5E-10	disabled	0	37	1.0E-10	0.00
S-31	2	0	615.253	749.092	-1.796	fix_5E-10	disabled	0	37	1.0E-10	3.00
S-31	2	24	616.093	748.975	-2.460	1.4E-06	VTZ7	1	14	2.8E-06	12.00
S-31	2	23	616.738	748.884	-2.970	fix_5E-10	disabled	0	37	1.0E-10	0.00
S-31	1	31	620.049	748.420	-5.579	fix_5E-10	disabled	0	37	1.0E-10	3.00
S-31	1	18	621.489	748.218	-6.715	fix_5E-10	disabled	0	37	1.0E-10	0.00
S-31	1	15	623.635	747.917	-8.408	fix_5E-10	disabled	0	37	1.0E-10	6.00
S-31	1	26	623.680	747.911	-8.443	fix_5E-10	disabled	0	37	1.0E-10	0.00
S-31	1	25	624.663	747.773	-9.219	fix_5E-10	disabled	0	37	1.0E-10	0.00
S-31	1	19	625.246	747.691	-9.679	fix_5E-10	disabled	0	37	1.0E-10	3.00
S-31	1	14	630.668	746.930	-13.957	1.9E-06	VTZ9	1	16	1.9E-06	15.00
S-31	1	27	632.300	746.701	-15.244	fix_5E-10	disabled	0	37	1.0E-10	0.00
S-31	1	28	634.748	746.357	-17.175	fix_5E-10	disabled	0	37	1.0E-10	0.00
S-31	1	35	634.771	746.354	-17.194	1.9E-06	VTZ9	1	16	1.9E-06	15.00
S-31	1	29	635.345	746.273	-17.647	fix_5E-10	disabled	1	37	1.0E-10	0.00
S-31	1	30	636.476	746.115	-18.539	fix_5E-10	disabled	0	37	1.0E-10	0.00
S-36	4	4	588.335	749.789	16.677	not measured	noVTZ	0	30	2.0E-10	3.00
S-36	4	5	591.421	748.542	12.711	2.5E-08	VTZ1	0	17	5.0E-08	10.00
S-36	4	12	592.455	748.124	11.382	fix_5E-10	disabled	0	38	1.0E-10	3.00

S-36	4	8	592.502	748.104	11.321	fix_5E-10	disabled	0	38	1.0E-10	3.00
S-36	4	9	595.069	747.067	8.022	2.2E-06	VTZ2	0	18	4.4E-06	6.00
S-36	4	11	595.821	746.763	7.055	5.3E-06	VTZ3	0	19	1.1E-05	6.00
S-36	4	10	599.400	745.316	2.456	fix_5E-10	disabled	1	38	1.0E-10	0.00
S-36	4	36	599.732	745.181	2.028	fix_5E-10	disabled	1	38	1.0E-10	0.00
S-36	4	37	601.122	744.620	0.242	fix_5E-10	disabled	1	38	1.0E-10	0.00
S-36	4	13	601.172	744.599	0.178	fix_5E-10	disabled	1	38	1.0E-10	3.00
S-36	3	27	603.930	743.484	-3.377	fix_5E-10	disabled	0	38	1.0E-10	0.00
S-36	3	23	604.068	743.428	-3.555	fix_5E-10	disabled	0	38	1.0E-10	0.00
S-36	3	21	604.407	743.292	-3.990	fix_5E-10	disabled	1	38	1.0E-10	0.00
S-36	3	24	605.133	743.001	-4.921	8.0E-07	VTZ4	1	20	1.6E-06	16.00
S-36	2	20	605.452	742.871	-5.327	fix_5E-10	disabled	0	38	1.0E-10	0.00
S-36	2	22	606.034	742.636	-6.077	6.9E-08	VTZ5	1	21	1.4E-07	10.00
S-36	2	0	608.912	741.475	-9.785	1.4E-07	VTZ6	1	22	2.8E-07	15.00
S-36	1	26	611.871	740.282	-13.578	fix_5E-10	disabled	0	38	1.0E-10	0.00
S-36	1	31	611.961	740.245	-13.694	8.6E-09	VTZ7	0	23	1.7E-08	10.00
S-36	1	28	613.701	739.542	-15.931	fix_5E-10	disabled	0	38	1.0E-10	0.00
S-36	1	19	617.573	737.977	-20.908	fix_5E-10	disabled	0	38	1.0E-10	3.00
S-36	1	15	619.225	737.309	-23.033	2.8E-08	VTZ8	0	24	5.6E-08	15.00
S-36	1	38	619.890	737.041	-23.887	fix_5E-10	disabled	1	38	1.0E-10	0.00
S-36	1	25	621.913	736.223	-26.488	fix_5E-10	disabled	0	38	1.0E-10	0.00
S-36	1	35	623.964	735.394	-29.125	fix_5E-10	disabled	0	38	1.0E-10	3.00
S-36	1	29	624.253	735.278	-29.496	fix_5E-10	disabled	0	38	1.0E-10	0.00
S-8	2	0	628.200	772.500	19.888	not measured	noVTZ	0	31	2.0E-10	5.00
S-8	2	2	628.200	772.500	12.011	not measured	noVTZ	0	31	2.0E-10	0.00
S-8	2	17	628.200	772.500	0.930	not measured	noVTZ	0	31	2.0E-10	0.00
S-8	1	39	628.200	772.500	-16.559	6.9E-08	VTZ7	1	26	1.4E-07	10.00
S-8	1	40	628.200	772.500	-20.285	2.1E-07	VTZ8	1	27	2.1E-07	15.00
S-8	1	3	628.200	772.500	-22.098	fix_5E-10	disabled	0	39	1.0E-10	0.00
S-8	1	41	628.200	772.500	-24.006	fix_5E-10	disabled	1	39	1.0E-10	0.00
S-8	1	6	628.200	772.500	-24.930	2.1E-07	VTZ8	0	27	2.1E-07	20.00
S-8	1	42	628.200	772.500	-25.541	fix_5E-10	disabled	1	39	1.0E-10	0.00

Modifications and optimization of the model achieved significantly better agreement in the pressure field, but larger differences remained in the balance and distribution of outflows from the intervals (see the comparison in the model with open taps in all intervals), where the values differ by several orders of magnitude. These are mainly shallow intervals of boreholes, where the model values are significantly higher. This may be related to the connection of semi-deterministic fractures in the shallower part to some of the fractures from the outer stochastic part, which may drain through these fractures in the model. However, there are also differences in deeper intervals, e.g., in the interval S31_2 and S36_3, the model outflow in all variants is approximately one order of magnitude lower. These differences are related to the connection of fractures in the detailed and regional domains and may be solved by optimizing the regional stochastic network of fractures by multiple implementations.

From the implementation of the variant models, in which the hydraulic parameters of semi-deterministic fractures were optimized, it is possible to make the following conclusions:

- By modifying the distribution of transmissivity values on the fractures, the given model may be optimized only partially and to a limited extent. The optimization and reverse adjustment of the geometric model and semi-deterministic fractures, i.e. changing the size and above all the connection of the fractures, is also very important,
- Optimization of parameters showed that most of the semi-deterministic fractures from the prepared geometric model were not relevant for the hydraulic model, the flow probably concentrates in a limited amount or in parts of the fractures and thereby creates a very heterogeneous pressure field,
- Better agreement of the model and measurement was achieved when transmissivity was entered from the WPT for a specific fracture. This is also related to the creation of the geometric model, which cannot be done only based on the geological data, but it is also necessary to ensure the relevant input hydrogeological data, i.e., transmissivity measurement at the level of the individual fractures, when the WPT measurements on sections of several meters are not sufficient for detailed processing of the fracture network,
- The size of the outflow from borehole intervals, or individual fractures, is not only a local matter of the semi-deterministic network, but also the optimization of inflows through fractures from the rock mass is necessary (optimization of the connection to the fracture network of the external domain using multiple implementations of stochastic networks).

7 Special Analysis of the Drill Core – Laboratory Tests

Laboratory analysis of representative rock types was performed on selected parts of the boreholes in order to determine the petrology, mineralogy, and geomechanical parameters of the rock matrix, and fillings of the studied fracture zones, etc. Transport laboratory experiments focused on testing tracers, their sorption, and diffusion parameters. Migration laboratory experiments were performed on rock samples with natural fractures and on a physical model (rock block). The methods provided a realistic range of model input parameter values, which were subsequently used in modeling and were validated by subsequent tests in boreholes under in-situ conditions.

7.1 Geological and Petrographic Analysis

Along the orientation of the drill cores, a structural geological and petrological analysis of the drill cores was performed. Individual planar structural elements (fractures, shear fractures, longitudinal fractures, fracture zones, tectonic faults and reactivated foliation) were described on the drill cores. Structural and lithological data are summarized in a borehole log processed in LogPlot7 software.

On selected parts of the drill core, samples were taken for the production of polished cuttings, which were subjected to microscopic analysis. Samples of contrasting lithologies, e.g., amphibolite, and samples of the predominant rock type (biotite-amphibolic paragneiss in various stages of migmatitization) were taken. A total of 54 samples were collected, 14 from borehole S-27, 24 from borehole S-31 and 16 from borehole S-36. A detailed description of the cutting material for individual boreholes is part of the appendix to Technical Report 521/2020 (Zuna et al. 2020), and for boreholes S-27 and S-31 (Appendix 3) and borehole S-36 (Appendix 6) it is part of TR 551/2021 (Zuna et al. 2021).

7.2 Study of the Fracture Fillings

A total of 74 samples of vein and fracture mineral filling were taken from boreholes S-27, S-31, and S-36. A total of 23 samples were selected for analysis. The samples were divided based on mineralization types according to the methodology used in earlier studies at the Bukov URF (Bukovská et al. 2017):

- Carbonate, or quartz-carbonate veins over 1 cm – 9 samples – analyses include major elements, trace elements, fluid inclusions, C and O isotopes, Sr isotopes in carbonates,
- Carbonate, or quartz-carbonate thin veins – 4 samples – fluid inclusions, C and O isotopes in carbonates,
- Quartz-feldspar and quartz veins – 4 samples – fluid inclusions,
- Sulfide mineralization – 6 samples – S isotopes in pyrites.

7.2.1 Interpretation of the Results

Quartz-feldspar and quartz veins:

These veins are probably the oldest vein type in the area.

The high temperatures of homogenization (up to 330 °C) and the presence of CO_2 in the inclusions indicate that the veins were formed at the end of the metamorphic processes in the area.

Carbonate and quartz-carbonate veins:

These are mainly composed of calcite, with rare occurrences of dolomite-ankerite carbonate.

Based on the isotopic composition of C and O and the character of the fluid inclusions, three generations of veins were distinguished:

Generation 1:

- Two veins from borehole S-31 (5.0 m and 16.25 m) with inclusions with homogenization temperatures of up to 180 °C.
- Fluid d18O values indicate source brines of sedimentary pools with a proportion of waters of a metamorphic origin.
- These veins correspond to the veins of the ore stage of development at the Rožná deposit.

Generations 2 and 3:

- Veins with minerals and inclusions with homogenization temperatures of 50 to 80 °C, or 100 to 150 °C.
- Fluid d18O values between -1.5 and -14.4 ‰ (SMOW) indicate source waters of a meteoric origin.
- The salinity of the aqueous solution in the inclusions is variable (0.7 to 21.5 wt.% NaCl eq.).
- These veins probably correspond to the vein mineralizations of the late to early late stage of development at the Rožná deposit.

Detailed information and results are included in Technical Report No. 5 (Zuna et al. 2023)

7.3 Transport Experiments

The study of transport parameters focused on the testing of tracers, their sorption, and diffusion parameters, as well as a study of the transport behavior on natural fractures. Sorption experiments were performed on samples from drill cores (boreholes S-27, S-31 and S-36) for selected tracers, both for the rock matrix and for samples with fracture fillings (chlorites, clay minerals). The interaction of tracers with rock was studied using static batch experiments. As the output of the static batch experiments, the value of the distribution coefficient R_d was calculated. Since in-situ tracer experiments with fluorescent dyes were expected to last for several hours, kinetic sorption experiments were performed in the laboratory study. In order to evaluate the experiments and understand the sorption and diffusion processes, the performed rock characterization included determination of petrological and mineralogical composition, and physical-mechanical properties (porosity, density, specific surface area, SSA, CEC, etc.).

For transport experiments on a larger scale, a granite block with an induced fracture and drill core samples with a natural fracture (from borehole S-36) were used. The following tracers were tested for the fracture experiments: NaCl, KI, KBr, fluorescein and Rhodamine WT. On-line recordings were taken using ISE ion-selective electrodes (I^-, Br^-) and UV Vis detectors. A programmable fraction collector was used for sampling and subsequent analysis of tracer concentrations (Cl^-, fluorescein, Rhodamine WT). Breakthrough curves were also tested depending on different flow rates and pressure gradients.

Descriptions of the tests and the results of the experiments are included in TR 551/2021 (Zuna et al. 2021)

7.4 Geotechnical Tests

The geotechnical properties of the tested rocks were described in relation to their petrographic, structural composition, and textural anisotropy. The parameters studied were as follows: indirect tensile strength, uniaxial compressive strength, triaxial compressive strength, deformability modulus, rock abrasiveness, coefficient of thermal conductivity, and specific heat capacity, specific gravity, bulk density, total porosity, open porosity, velocity of passage of longitudinal ultrasonic waves, coefficient of hydraulic conductivity of the rock. The laboratory tests and analyses were based on common technical standards (ČSN, EN, ISO), a set of methods recommended by the International Society for Rock Mechanics, or other regulations and recommendations.

The results of the laboratory tests are shown in the following table (Tab. 16).

The rock samples were tested in the direction of the borehole axis, which is oblique to the foliation. Foliation oriented in this way adversely affected the magnitude of strength values in simple compression, when several bodies “slipped” on the surface predisposed in this way.

The determined values of the parameter *m* from the triaxial tests are in the interval 13.3–18.5. According to the results, higher values could be expected for the migmatitic gneiss (m ~ 23–33). The determined lower values indicate that there is a violation in the plane of the foliation, which in the measured samples is suitably oriented with respect to the direction of loading. As a result, breakage occurs parallel to the biotite grains, and these values correspond more to mica schist.

The anisotropy of seismic wave speeds is up to 10%. Waves traveling in the plane of the foliation propagate faster than across it.

Tab. 16 Mechanical-physical properties of the rocks

Borehole	Indirect tensile strength (MPa)	Unixial compression strength (MPa)	Triaxial compression strength (-)	Elasticity modulus (GPa)*	Deformation modulus (GPa)*	Poisson number (-)*	Abrasiveness CAI (-)	Thermal conductivity ($W \cdot m^{-1} \cdot K^{-1}$)	Thermal capacity ($MJ \cdot m^{-3} \cdot K^{-1}$)	Open porosity (%)	Total porosity (%)	Bulk density ($kg \cdot m^{-3}$)	P-wave velocity ($km \cdot s^{-1}$) min/max	S-wave velocity ($km \cdot s^{-1}$) min/max	Coefficient of hydraulic conductivity ($m \cdot s^{-1}$)
S-27	8.4	77.0	13.8	**	**	**	4.3	2.32	2.14	0.20	***	2810	6.752/ 6.345	3.898/ 3.645	$< 10^{-14}$
S-31	6.2	91.0	18.5	88.0	87.0	0.27	3.7	2.29	1.97	0.39	1.77	2848	6.401/ 6.270	3.893/ 3.617	$< 10^{-14}$
S-36	8.1	95.0	13.3	83.0	87.0	0.27	3.8	2.18	1.95	0.18	3.93	2774	6.655/ 6.152	3.899/ 3.589	$< 10^{-14}$

* Evaluated in the stress field 20–40 % UCS.

** Not possible to evaluate. The sample disintegrated along the foliation surfaces.

*** Not possible to evaluate. The specific density value is lower than the dry bulk value.

8 Hydraulic Tests

Hydraulic tests focused on the study of the hydraulic parameters using interval WPT after drilling the boreholes, and the most conductive and connected intervals of boreholes S-27, S-31, and S-36 were determined. After the installation of multipacker systems and the stabilization of pressure ratios, outflows from individual intervals were studied and pressure changes were monitored using the installed piezometers. Hydraulic dipole tests were performed to optimize the input parameters of the tests. Before the tracer test, a hydraulic test was performed to verify the hydraulic conditions in the studied intervals, pressure reactions in the intervals, and flow balances were measured to calculate the tracer concentration and balance. The results were subsequently used for the predictive model and optimization of test parameter settings. A detailed description and test results are included in Interim Report No. 5 (Zuna et al. 2023). On the basis of the performed tests, the test instrumentation was optimized, the measurement system was modified, and the input parameters of the tracer tests were modified.

8.1 Hydraulic Tests in the Boreholes – Water Pressure Tests

A mobile device was designed and subsequently manufactured for the WPT. This involved both the development of the conceptual design of a newly developed device and its subsequent physical production, testing, and use in the WPT and tracer experiments (Stage 6).

The aim of the hydraulic tests in the boreholes was to determine the hydraulic parameters of the rock environment in the individual sections of the boreholes, in which multipacker systems were subsequently installed, and in which transport experiments were performed. The obtained data also served as an input for the creation of the hydraulic transport models.

Between 2020 and 2021, interval WPT were performed in boreholes S-27, S-31, S-36, and S-8. A total of 32 intervals were tested in these boreholes. Details and the results of the WPT measurements are described in detail in the technical reports (borehole S-27, Zuna et al. 2020), boreholes S-31, S-36 in TR No. 3 (Zuna et al. 2021)

The tested sections in the boreholes were defined by a pair of GeoPro Bimbar 1 hydraulic packers with a diameter of 72 mm, which were inflated with water using a manual pressure pump. The exception was the deepest intervals, which were defined only by the end packer and the sections from the packer “to the bottom” were tested. The length of the sealing element of the packer was 0.5 m. The packers were inflated as required, usually to a pressure of 20 to 25 bar, which ensured a completely sealed delimitation of the test interval. The WPT were performed using equipment consisting of a high-pressure pump, a pressure sensor, a flow meter, and a data logger.

Each of the tested intervals was tested with the following set of tests (unless otherwise stated):

1) The initial WPT test consisted of a pulse test, where a pressure pulse of 5-6 bar was rapidly applied to a defined section of the borehole. The borehole was then hydraulically closed, and the pressure drop was monitored over time until the natural hydraulic pressure stabilized. Based on the pressure drop rate during the pulse test, it was possible to qualitatively estimate the permeability of the given section of the borehole and prepare a suitable configuration of the device for the WPT.

2) The pulse test was followed by an injection pressure test in a constant injection pressure or constant injection flow configuration. For sections with lower permeability, the variant of the pressure test with constant injection flow rate was selected and the increase in pressure was monitored in the tested interval until a constant pressure value stabilized. For intervals with higher permeability, an injection pressure test was performed with a constant injection pressure and the test lasted as required until the constant flow rate was established. For tests with a constant injection pressure, a pressure was chosen to “over pressurize” the natural hydraulic pressure in the tested floors. A high-pressure pump or Grundfos MP1 was used as a source of pressurized water. The length of individual injection tests in both variants ranged in the order of a few units of hours, depending on the permeability of the specific tested interval and the speed of establishing the measured parameters.

3) The third type of hydraulic tests performed on the borehole floors were pressure drop tests. These were usually performed after the completion of the previous injection pressure test (see above). The pressure drop test began by closing the borehole and then the pressure drop was monitored until it stabilized. Depending on the permeability of the tested section and the amount of injected water in the previous test, the pressure in the tested section of the borehole stabilized within a few minutes to hours. The stabilization of the pressure after the drop test did not always correspond to the stabilization of the pressure after the pulse test at the beginning of the test, which is caused by the violation of the hydraulic balance of the environment during the injection tests.

In several cases, when the pressure practically did not decrease at all during the pulse test, or decreased very slowly (1bar/15 minutes), only a time-limited pulse test was performed, and the interval was assigned a limit permeability ($< 5 \cdot 10^{-10}$ m · s^{-1}).

8.1.1 Evaluation of the WPT

The primary data obtained during the measurement had to first be cleaned of erroneous data and measurement artifacts during the evaluation. Cleaned primary data from hydraulic tests were subsequently evaluated using the formula for steady flow according to Moye (1967). The evaluated hydraulic parameters are shown in Tab. 17.

Tab. 17 Evaluation of WPT in boreholes S-27, S-31, S-36, and S-8

	Measurement from	Measurement to	Natural hydrostatic pressure, height above mouth	Test type	Test / steady flow Q	Pressure increase (dP)	Hydraulic conductivity k	Comment
	m	m	m		$m^3 \cdot s^{-1}$	m	$m \cdot s^{-1}$	
S-27_VTZ1	2.7	9.7	4.28	const. Q	$1.67 \cdot 10^{-7}$	8.7	$2.54 \cdot 10^{-9}$	
S-27_VTZ2	8.7	15.7	-	pulse only	0		$<5 \cdot 10^{-10}$	Very impermeable zone. Not measured due to time

								limitations. K estimate
S-27_VTZ3	15	22	5.2	const. Q	$1.67\cdot10^{-7}$	22.8	$9.13\cdot10^{-10}$	
S-27_VTZ4	22	29	0.82	const. P	$1.02\cdot10^{-5}$	29.2	$4.51\cdot10^{-8}$	
S-27_VTZ5	29	36	2.6	const. Q	$1.67\cdot10^{-7}$	11.6	$1.86\cdot10^{-9}$	
				const. P	$7.67\cdot10^{-7}$	57.4	$1.76\cdot10^{-9}$	
S-27_VTZ6	36	44	13.0	const. P	$2.35\cdot10^{-6}$	47.0	$6.40\cdot10^{-9}$	
S-27_VTZ7	44	58.02	11.4	const. P	$3.93\cdot10^{-5}$	48.7	$5.30\cdot10^{-8}$	
S-31_VTZ1	13	20	3.6	const. P	$4.88\cdot10^{-5}$	4.41	$1.35\cdot10^{-6}$	
S-31_VTZ2	20	23	1.4	const. P	$4.33\cdot10^{-6}$	61.34	$1.65\cdot10^{-8}$	
S-31_VTZ3	23	26	16.51	const. Q	$1.00\cdot10^{-7}$	*165*	$1.41\cdot10^{-10}$	dP estimate
S-31_VTZ4	26	33	19.8	const. Q	$1.67\cdot10^{-7}$	*230*	$<8.81\cdot10^{-11}$	dP estimate
S-31_VTZ5	28	31	<17.3	const. Q	$8.33\cdot10^{-9}$	*15*	$<1.30\cdot10^{-10}$	dP estimate
S-31_VTZ6	32	39	12.77	const. Q	$1.67\cdot10^{-7}$	*108*	$1.88\cdot10^{-10}$	dP estimate
S-31_VTZ7	39	46	22.11	const. P	$1.27\cdot10^{-5}$	7.78	$1.98\cdot10^{-7}$	
S-31_VTZ8	39.4	42.6	17.38	const. P	$6.97\cdot10^{-7}$	15.64	$1.04\cdot10^{-8}$	
S-31_VTZ9_a	45.7	71	11.06	const. P	$6.91\cdot10^{-5}$	37.27	$7.93\cdot10^{-8}$	
S-31_VTZ9_b	45.7	71	11.06	const. P	$6.69\cdot10^{-5}$	37.49	$7.64\cdot10^{-8}$	
S-36_VTZ1	14	17	0.83	const. P	$2.04\cdot10^{-6}$	60.6	$7.92\cdot10^{-9}$	
S-36_VTZ2	25	28	6.02	const. P	$5.08\cdot10^{-5}$	17.0	$7.03\cdot10^{-7}$	Direct communication with int. 28–31 m
S-36_VTZ3_a	28	31	0.07	const. P	$4.05\cdot10^{-5}$	4.8	$1.98\cdot10^{-6}$	Direct communication with int. 25–28 m
S-36_VTZ3_b	28	31	0.15	const. P	$6.70\cdot10^{-5}$	11.6	$1.36\cdot10^{-6}$	
S-36_VTZ4	34	37	21.07	const. P	$3.87\cdot10^{-5}$	36.5	$2.49\cdot10^{-7}$	
S-36_VTZ5	38	41	6.10	const. P	$6.14\cdot10^{-6}$	66.8	$2.16\cdot10^{-8}$	
S-36_VTZ6	41	44	6.83	const. P	$9.93\cdot10^{-6}$	54.3	$4.30\cdot10^{-8}$	
S-36_VTZ7	46	49	6.45	const. P	$6.45\cdot10^{-7}$	56.1	$2.70\cdot10^{-9}$	
S-36_VTZ8	50	70.2 (bottom)	11.50	const. P	$1.33\cdot10^{-6}$	49.6	$1.40\cdot10^{-9}$	
S-8_VTZ1	2	5	-	pulse only	-	-	$<5\cdot10^{-10}$	Very impermeable zone. Not measured due to time
S-8_VTZ2	5	8	-	pulse only	-	-	$<5\cdot10^{-10}$	
S-8_VTZ3	9	12	-	pulse only	-	-	$<5\cdot10^{-10}$	
S-8_VTZ4	19.5	22.5	-	pulse only	-	-	$<5\cdot10^{-10}$	
S-8_VTZ5	26.8	29.8	-	pulse only	-	-	$<5\cdot10^{-10}$	

								limitations. K estimate
S-8_VTZ6	35	38	9.89	const. P	$8.23 \cdot 10^{-7}$	50.2	$4.07 \cdot 10^{-9}$	
S-8_VTZ7	38	41	6.32	const. P	$5.34 \cdot 10^{-6}$	57.4	$2.31 \cdot 10^{-8}$	
S-8_VTZ8	42	49.8	3.21	const. P	$2.03 \cdot 10^{-5}$	57.6	$4.05 \cdot 10^{-8}$	

An overview of the evaluated hydraulic conductivities from the WPT in boreholes S-27, S-31, S-36, and S 8 is included in Fig. 45.

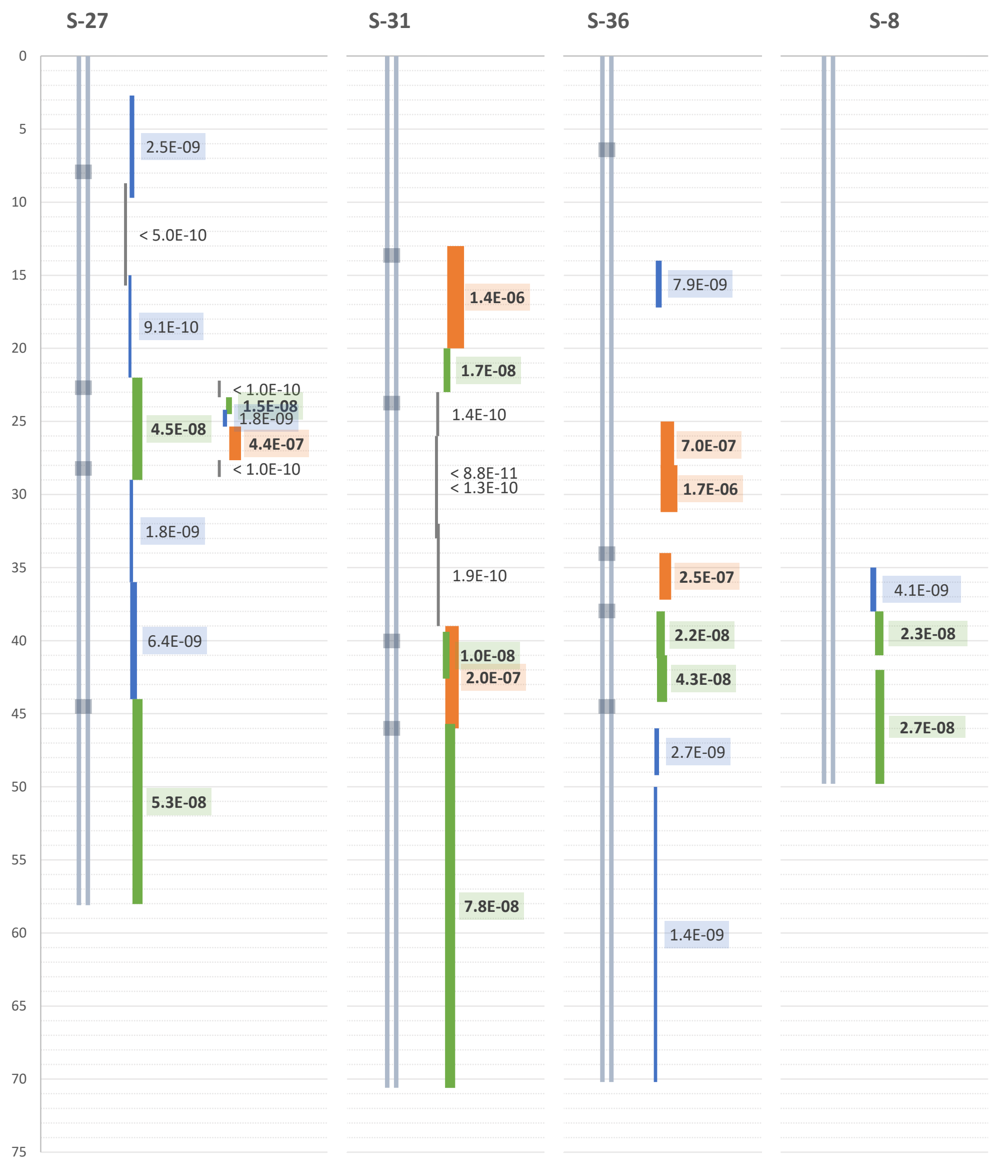

Fig. 45 Overview of the evaluated hydraulic conductivities from the WPT in boreholes S-27, S-31, S-36, and S-8

8.2 Hydraulic Tests Between the Boreholes

8.2.1 Pressure Changes - Flow Rates

After installation of all multipacker systems in boreholes S-27, S-31, S-36, and S-8, the boreholes were closed to stabilize the pressure conditions. After stabilization of the pressures in the rock environment of the individual boreholes, hydraulic connection tests were performed by opening/closing the studied intervals. On the basis of the obtained results, pulse tests were subsequently performed.

Fig. 46 shows the steady flow values from the open section of the borehole and the pressure drip values at the end of the performed tests (the pressure drop values are given for the maximum decrease in the tested open section and pressure responses in the other closed intervals of the multipackers).

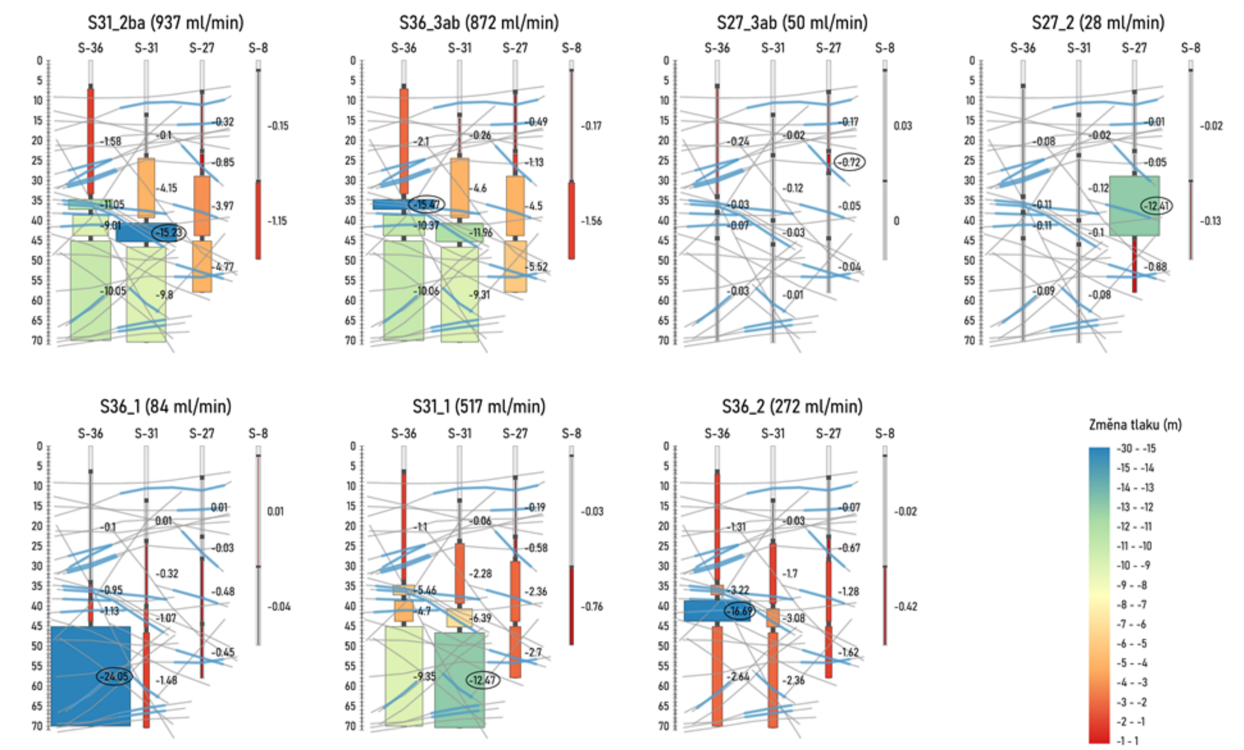

Fig. 46 Interval opening tests - pressure responses and hydraulic communication between borehole intervals

The greatest pressure responses in the closed sections were detected after the opening of the interval S36_3, i.e., in the order of tens of meters in the neighboring sections to units of meters in the more distant sections. Changes in the order of decimeters in the shallow sections of boreholes S-27, S-31, and S-8 are related to a very small natural overpressure in these sections. On the contrary, the smallest pressure response to a relatively high pressure drop in the tested interval and low outflow values were found in tests S27_2 and S36_1. These sections of the borehole are very poorly conductive with low transmissivity of intersecting fractures. Small pressure changes (0.72 m) and a very small outflow (50 ml/min) in the section S27_3 are related to the small natural overpressure in the section, i.e., a larger pressure reduction in this interval cannot be achieved.

Based on the evaluated "steady" outflow values and pressure changes in the open sections, the hydraulic conductivity of the tested interval was calculated according to Moy (1967). For most intervals, a very good agreement of the values with the results of previously performed WPT (before the installation of the multipackers) was observed.

Subsequently, pulse tests were performed based on the obtained results. After their evaluation, the instrumentation was optimized, and a series of longer hydraulic tests ensued. The test results are included in interim report No. 4 (Zuna et al. 2022).

8.2.2 Implementation of Hydraulic Pulse Tests

Hydraulic pulse tests were designed based on the results of flow tests and interval tests. A precise HPLC pump (ECP201L) was used for the application of a constant flow, taking into account the parameters of the environment. Pressure measurements were taken with pressure sensors (JSP) with data recording (Comet MS6). The pressure sensors were connected to the input of the measured interval and to the mouth of the multipacker. Groundwater from borehole S-1 was used for the hydraulic tests due to the high volumes required.

Fig. 47 Pulse test instrumentation

Based on previous tests, a flow rate of 1.0 l/min was applied for 10 min at the tested intervals S27_3, S31_2, S36_3 (both inputs) and a flow rate of 1.0 l/min was applied for 5 minutes at the intervals S27_1, S31_3, S36_2, injection of 1.5 l/min into interval S36_3.

During the pulse tests, the change in the pressure field affected the "close" surroundings of the tested section (up to a distance of units to tens of meters), there was no significant influence of the pressure conditions at a greater distance in the investigated environment. The entire system returned to its original state in a relatively short time, which made it possible to perform a larger number of tests with the aim of analyzing mutual hydraulic communication between the individual intervals of the boreholes than in classic longer-term tests with a steady flow. However, they are more suitable for the evaluation of hydraulic parameters and for the implementation of tracer tests.

Fig. 48 shows the maximum pressure values in the intervals during the pulse tests:

- The tests confirmed very good mutual communication between intervals S31_2 and S36_3,
- Interval S27_3 is in hydraulic connection with the “shallow” interval S36_4. The much smaller pressure response in the neighboring borehole S-31 was rather surprising,
- The deep interval S27_1 has a very low hydraulic communication with the deep intervals of boreholes S-31 and S-36, but it communicates more with the shallower intervals S31_3 and S36_4.

Detailed information on the test instrumentation, measured parameters, and the test results are provided in technical report 630/2022 (Zuna et al. 2022).

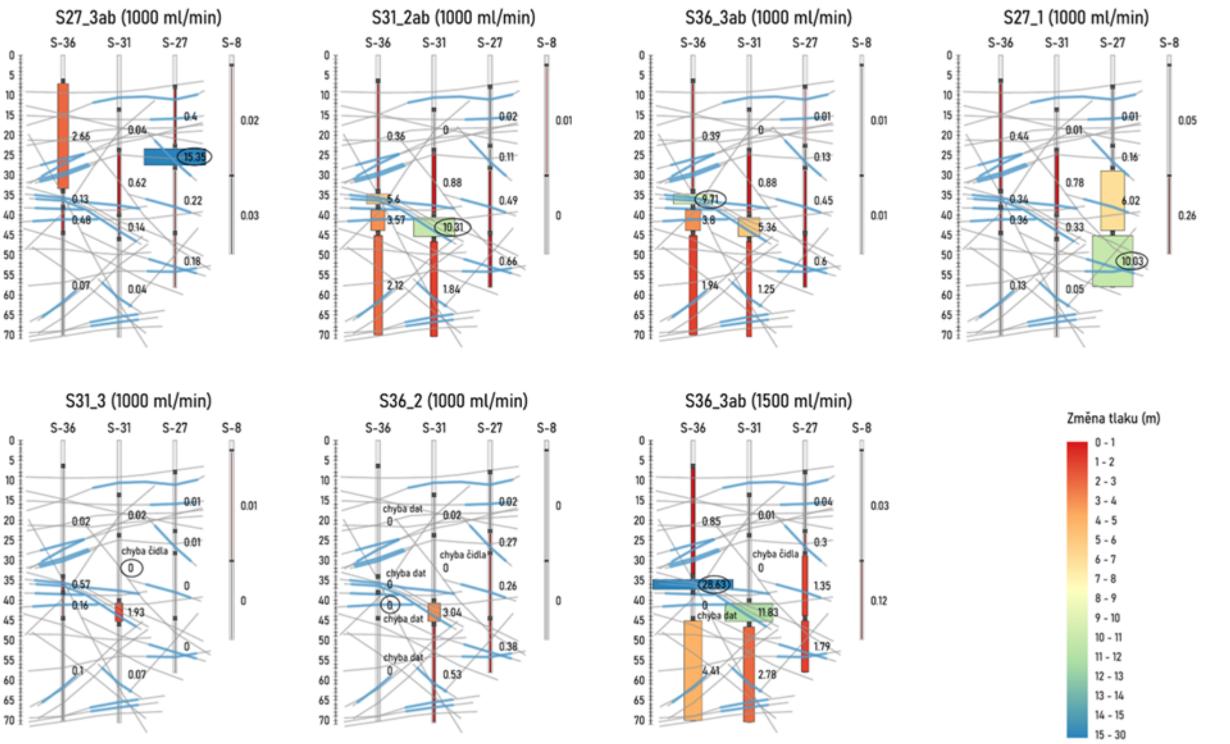

Fig. 48 Pulse tests - pressure responses and hydraulic communication between borehole intervals

8.2.3 Injection Dipole Tests

Based on the evaluated interval opening/closing tests and pulse tests, test intervals were selected, and flow rates (1-1.7 l/min) were determined for the injection dipole tests. The same instrumentation was used for the dipole tests as for the pulse tests. For flow rates higher than 1 l/min, a G13 pump with a frequency converter was used.

Due to the injection of water into the interval of interest, there is an increase in pressure in the entire interconnected system of fractures. The largest pressure changes were achieved, as expected, in the injected section S31_2. The small diameter of the supply pipes caused significant pressure losses not only in the injection (S31_2) but also in the outflow branch (S36_3). This resulted in an increase in pressure in these intervals, even though a constant level was maintained at the outlet of the pipe. At measured outflows greater than approximately 450 ml/min, the flow in the piping was turbulent and pressure losses were more significant. This insight is important for other projects, especially for zones with high flow rates/drainage.

Fig. 49 shows the results of the maximum pressure changes at the end of the dipole injection tests, i.e., approximately when the pressure ratios stabilize, and the main findings are as follows:

- Tests S31_2ab → S36_3ab (between very well-connected intervals in the deeper part of the rock mas) verified the sizes of outflows and pressure changes important for the design of the tracer tests,
- The connection in the deeper part of the rock mass between neighboring S31 and S27 is not so significant, better hydraulic connection of the fractures is found in the deeper interval S27_1,
- In the shallower part of the rock mass between S27_3 and S36_4, even at high pressures in the injected interval, relatively small pressure responses were measured in the other sections, and the pressure field here is apparently significantly influenced by the connection of fractures with the corridors of the mine, although no significant outflows from the walls are observed.

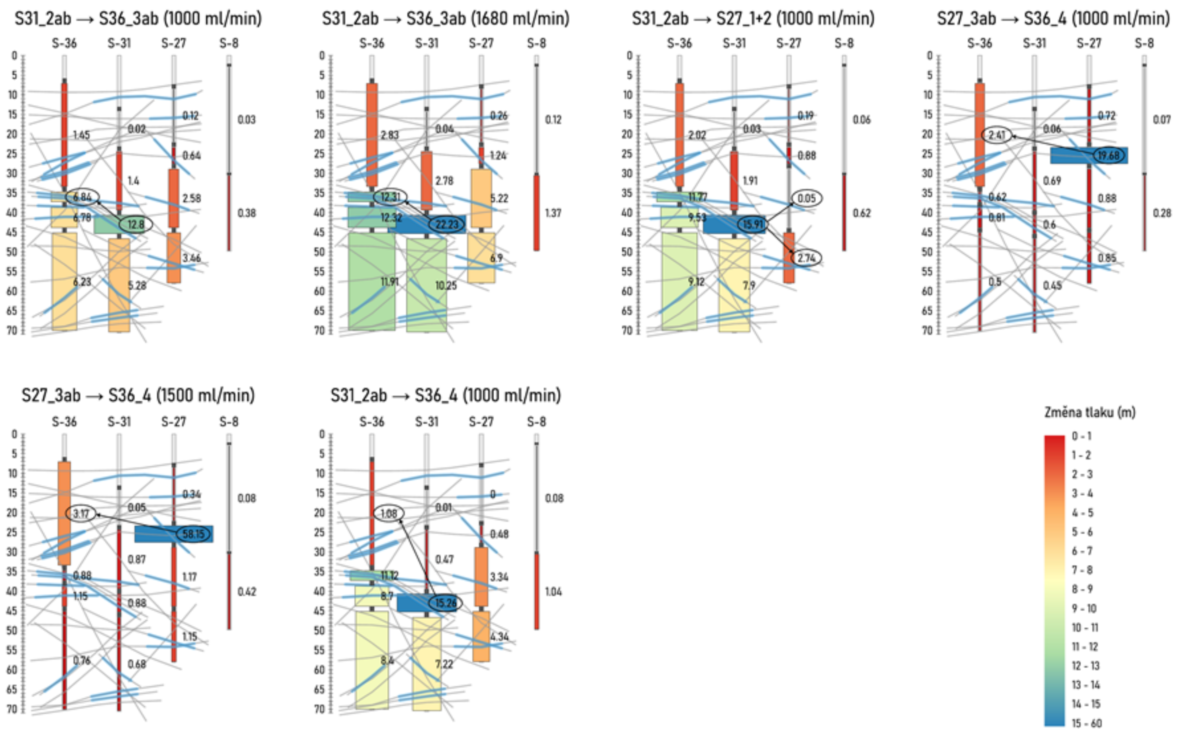

Fig. 49 Dipole injection tests - pressure responses and hydraulic communication between borehole intervals

9 Implementation and Evaluation of Tracer Tests

9.1 Laboratory Tests – Test Preparation

Laboratory tests in Stage 25 were focused on the additional study of the sorption properties of selected tracers on rock material (rock, fracture fillings) and diffusion experiments on the rock matrix. Transport experiments were also performed on natural fractures taken from drill cores. The transport experiments were performed on natural fractures with both inactive tracers (KI, Fluorescein, Rhodamine) and active tracers (HTO, ^{22}Na, ^{134}Cs, ^{133}Ba). Visualization of the transport was performed using µCT analysis and subsequent measurements on GeoPET tomography (^{18}F). To visualize the 3D distribution of activity after fracture experiments with radionuclides (Cs, Ba), non-destructive analysis using gamma emission computed tomography (SPECT) was used. The aim of the tests was the study of transport on a real fracture, the development and testing of the proposed instrumentation. In Stage 25, additional tests and trials were also performed for the use of a “cocktail” of multiple tracers (e.g., Fluorescein x Rhodamine WT), development and optimization of the measuring system, and testing the system for in-situ tests. For in situ experiments, the use of salts (KCl and KI) was verified in the laboratory with the possible use of iodide concentration measurements using ISE and conductivity (EC). During the transport experiments, fluorescein did not sorb when applied alone, but in a cocktail with Rhodamine it showed a slight increase in sorption, and a shift of the maximum peak on natural fractures (effect of fracture filling) was also observed.

9.2 In Situ Tracer Tests

The aim of the tracer tests was to obtain a better understanding of the transport of selected tracers in the fracture system, improve its prediction ability and thereby provide input data for transport modeling. It is necessary to select a suitable methodology with a good knowledge of the rock environment, hydraulic conditions, and the behavior of the given tracer in the rock environment. Due to the wide range of processes that take place in the rock environment, either due to the properties of the rocks or the composition of the groundwater, it is appropriate to use a wider range of tracers. The individual breakthrough curves then describe the influence of the aforementioned parameters on the migration of the tracers (Zuna et al. 2023).

Based on the results of the monitoring and hydraulic tests performed in the previous stages of the project, the most suitable communicating intervals were selected, and in Stage 26, activities focused on the in-situ tracer tests. For the tracer tests, instrumentation was developed, tested and used both for the experiment itself and its monitoring. During laboratory tests and tracer tests, a detection systems for measuring flow, iodide concentrations, dyes, e.g., fluorescein, and conductivity were tested. Based on the evaluation of the hydraulic tests and predictive models, tests focusing mainly on the active zones were performed at selected intervals.

Before the tracer tests, a hydraulic test was performed to verify the hydraulic conditions in the selected intervals (S31_2 and S36_3). Both the intervals are equipped with two inputs and the “dead” volume is filled with silicone padding. Based on the geometric model, the transport distance between the intervals is approximately 13.5 m (Fig. 50).

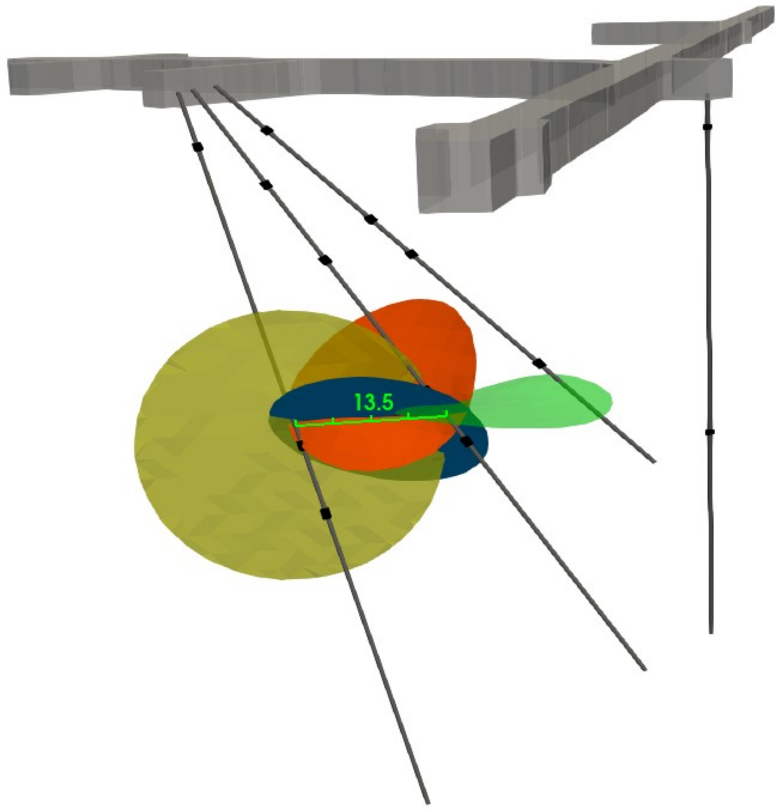

Fig. 50 Example – transport distance model S36_3 and S31_2 (13.5 m)

The pressure changes in the intervals and the measured flow balances were used to calculate the tracer concentrations and balance, and the results were then applied to the predictive model and the optimization of the test parameters (Zuna et al. 2023).

During Stage 26, three tracer tests were performed and evaluated using the conservative tracers KCl, KI, and fluorescein at concentrations of 0.01 M KCl to 0.1 M KI. Laboratory experiments on a natural fracture demonstrated the conservative nature of these tracers (Zuna et al. 2022). Conductive (S31_ 2 to S36_3) and less conductive fracture (S31_1 to S36_3ab) intervals were tested. The distance between the intersections of the fractures with boreholes was approximately 28 m, i.e., twice as long as the distance of the intersections in the test (S31_2 to S36_3).

For the injection of water into the intervals, the device (Fig. 51) developed in the previous stages of the project and the optimized measuring systems including flow cells (Zuna et al. 2020; Zuna et al. 2021), based on the laboratory tests, were used. A precise HPLC pump (ECP201L) was used for constant flow injection, taking into account the parameters of the environment. Flow rates higher than 1 l/min were achieved by the injection system, which consisted of a VERDER G13 (AxFlow) piston-diaphragm pump, controlled by a Danfoss frequency converter using a magnetic-inductive flow sensor and a safety valve. Pressure measurements were performed using pressure sensors (JSP) with data recording (Comet MS6). The pressure sensors were connected to the input of the measured interval and to the mouth of the multipacker. Developed and optimized flow cells for the given flow rates were used at the inlet and outlet. Flow measurements were provided by precise flow meters MIM 12 (Kobold) and ES Flow (Bronkhors), which were tested and calibrated in the laboratory before the measurements. The method of detection depended on the selected tracer or their mixtures (conductometry/EC, ISE electrodes I^-, Br^-, UV spectrometry or solution sampling (measured ex situ). Hydrochemical measurements were conducted using a WTW 3630IDS device with the following conductivity probes: WTW TetraCon925_P, ORP: WTW ORP T_900P, pH: WTW SenTix94X_P, O2: WTW FDO925_P.

Fig. 51 Workstation in ZK-2 during the tracer test

Based on the evaluation of the hydraulic tests and predictive models, in the first stage of the tests, attention focused on the active zones in the studied boreholes and selected intervals.

Based on the hydraulic tests, the tests were designed as follows:

- The outlet interval (OUT) was opened before the test – min. 3 days in advance to stabilize the pressure conditions (recording of steady flow – OUT) + sampling of groundwater from the studied interval for the test (sufficient volume depending on flow and test time);
- Connection of control and measuring systems and onset of water injection within the interval IN – min. 24 hours in advance (stabilization of flow conditions and pressures) – influence of instrumentation, etc. (recording of Q values, pressure, concentration/conductivity – background concentration);
- Injection of tracer (same Q as for the water injection). The injection time and tracer concentration were chosen based on previous tests and the transport model;
- Flushing after the test (i.e., injection of water into the inlet interval-IN and with the outlet interval-OUT open) min. 48 hours and then the end of the test (according to the course of the penetration curve). The ideal time was until the concentration drops to the background value (sufficient storage water);
- Natural flushing – leaving the output interval open – measurement;
- Opening the injection/or all intervals for flushing the entire system - min. 1 week (until the concentration of the tracer reaches the background level - groundwater).

Considering the significant interconnectedness of the entire system, and the large volumes of water in the intervals, etc., it was necessary to consider the risk of contamination of the boreholes by the tracers. For this reason, the use of radioactive tracers was not possible (N.B. the use of radioactive tracers was not in the description of the project according to the works contract). With regard to interval lengths and "dead volumes", the cleaning/flushing of the intervals from the tracers is problematic. Interval flushing was time consuming for most of the tests. After testing the transport of the least conductive structure (S31_1 – S36_3), flushing took place for more than 1.5 months, and subsequently all intervals were opened to "clean" the entire system.

Attention was also focused on the differences in hydrochemical parameters in the studied intervals, especially on the EC and pH values, which have an effect on the behavior of the tracer and the balance of the tracer in the case of using salts (conductivity measurements). During the measurements, the flow rates from the individual intervals were monitored and the hydrochemical parameters (EC, pH, Eh, LDO) were measured in the flow cell.

9.3 Evaluation of the Tracer Tests

Basic evaluation of the tracer tests mainly includes a calculation of the balance of the tracer and the analysis and control of the measured data, which further serve as a basis for a detailed evaluation using a mathematical model and the determination of fracture transport parameters (described in the following Section). The detailed evaluation of the tests is given in Technical Report No. 5 (Zuna et al. 2023).

9.3.1 Evaluation of Tests 1 and 2

In both tests 1 and 2 (with the same configuration of the input and output interval), the same arrival time of the tracer in the output measuring cell was determined approximately 100 minutes from the start of tracer injection, see the Breakthrough curves of both tests in Fig. 52. The maximum conductivity of the tracer was reached in approximately 300 min, the doubled value in test 2 corresponds to the doubled input concentration of the tracer used.

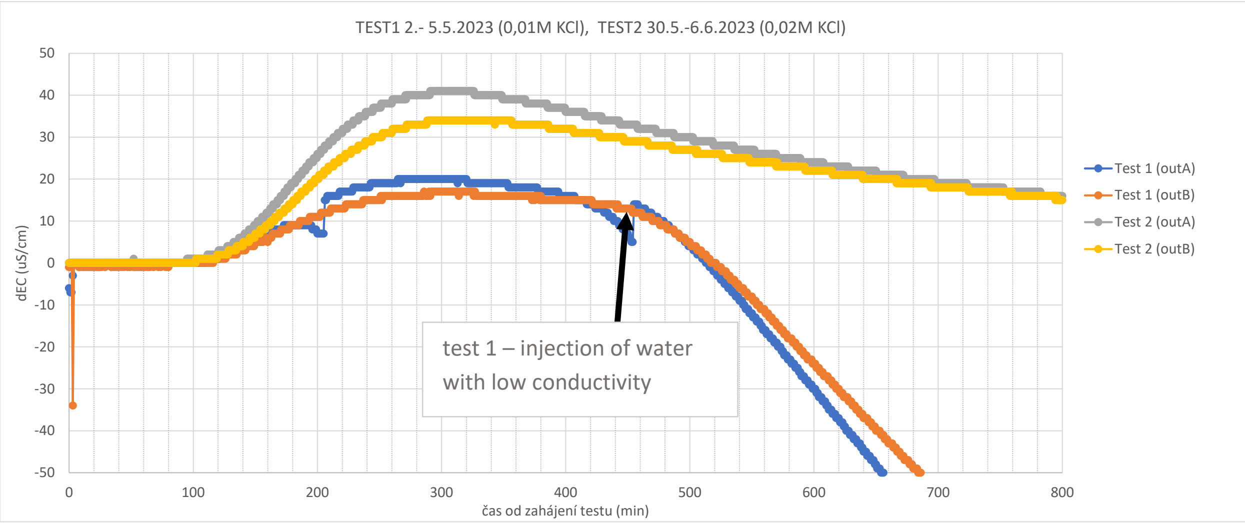

Fig. 52 Breakthrough curve - tests 1 and 2 between intervals S31_2ab and S36_3ab

In the predictive simulation in the optimized model (transport was calculated simply by the particle tracking method), the mean inflow time corresponding to the maximum conductivity was calculated to be 150 min, i.e., half the time, and the measured transport of the tracer is slower, apparently due to a higher transport opening (porosity of the fractures). A more detailed model evaluation was performed as part of the finalization of the numerical model (Section 10).

Calculation of the total balance of the tracer (recovery) from the breakthrough curve is important for the evaluation of the areal extent of the experiment and as a calibration parameter for the verification of the fracture connectivity in the given area of the solution. An important condition for the correct interpretation of the results of the tracer test is clearly defined and constant boundary conditions. For example, the calculation of the overall balance of test 1 was complicated by the small volume of the water supply and the use of completely different water with low conductivity for injection from time 450 min. The calculation of the overall balance of both tests was further complicated by the different conductivity of the groundwater flowing out from the individual intervals. Based on the performed measurements, this is a natural “property” of the investigated rock block, when water with a different (in some intervals, significantly different) background conductivity value flows out of each interval of the borehole. In the evaluation of test 2, it was necessary to include in the balance calculation the higher conductivity of the injected “pure” water from the time of approximately 1400 minutes (see Fig. 53). Based on experience, the test was modified (higher volumes of water, use of iodide, etc.).

The calculated total amount of tracer that flowed out of the outlet interval S36_3ab over the entire measurement period was roughly 75% of the input value. However, the calculation of the balance from the conductivity values just above the background (units of µS/cm) is not accurate, as it is affected by the sensitivity and stability of the measuring probes and is burdened by an error that may reach several units to tens of a percent. Roughly speaking, approximately 30-40% of the tracer could not be “tracked down” on the balance and remained partially in the system of interconnected fractures in the rock environment (in minimal concentrations) or partially drained into the drainage system (in the area of the access corridors).

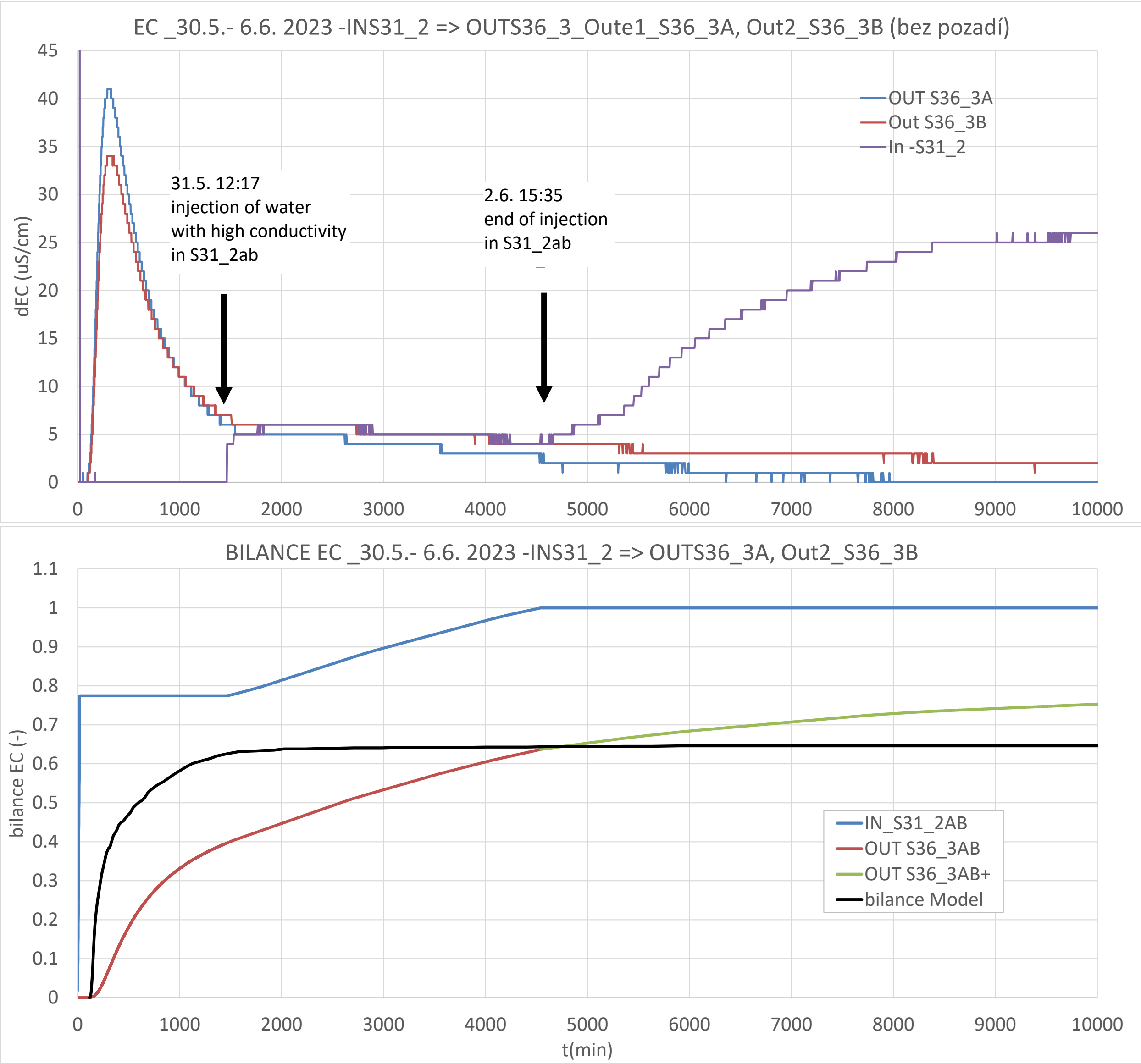

Fig. 53 Balance of the tracer during test 2 – at the top, the breakthrough curve in the IN and OUT intervals, at the bottom, a graph of the total balance (in relative units)

9.3.2 Evaluation of Test 3

In test 3, in addition to conductivity, the iodide concentration was also directly measured between intervals S31_1 and S36_3ab using more accurate and sensitive ISE probes, allowing minimum values to be measured two orders of magnitude lower than the WTW probes measuring conductivity (EC), see the breakthrough curve in Fig. 54. The influence of different water conductivity in the individual intervals (fracture systems) was also minimized. According to the ISE records, the arrival time of the tracer in the output measuring cell was approximately 3.5 hours from the start of the injection. The increase in conductivity values in the output was recorded only after approximately 7 hours. Nevertheless, the course of the EC penetration curve corresponds to the course of the ISE. The maximum tracer concentration was reached at 5:00 p.m., i.e., approximately three times longer than in test 2 (see the comparison in Fig. 55). At the same time, 3-4 times lower conductivity values than in test 2 were measured.

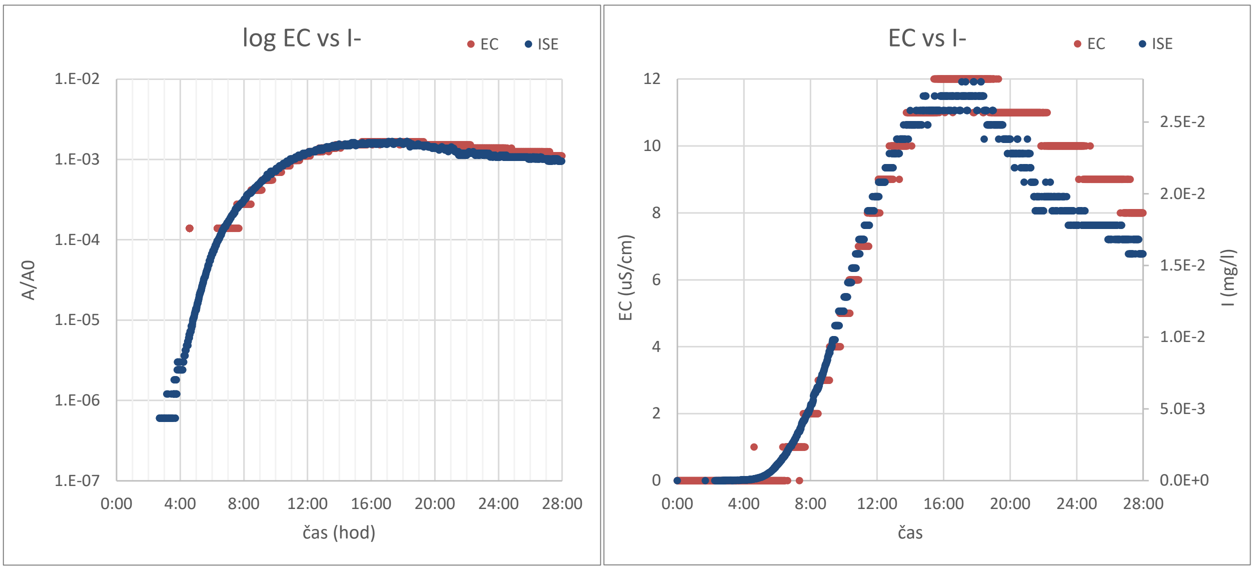

Fig. 54 Breakthrough curve – test 3 between intervals S31_1 and S36_3ab (on the left relative concentration and logarithmic scale, on the right absolute values)

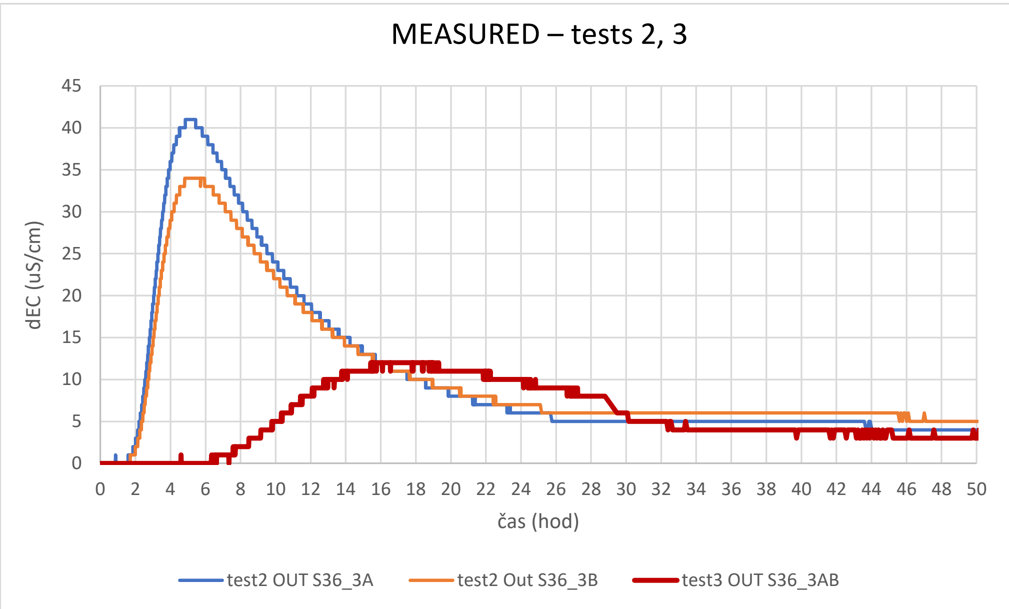

Fig. 55 Breakthrough curves – tests 2 and 3

The time of maximum concentration of the tracer according to the predictive simulation of the transport on the optimized model was roughly half again, i.e., 8 hours. A more detailed model evaluation was processed as part of the finalization of the numerical model.

The total injected amount of iodide in test 3 was 332 g. The calculation of the balance (recovery) in the graph in Fig. 56 includes a period of 22 days from the start of the experiment. During the first 7 days, the tracer flowed out of outlet S36_3ab in a total amount of 60 g, i.e., 18%. A significantly larger amount of tracer remained in the fracture system, and also possibly in the free volume of the injection borehole.

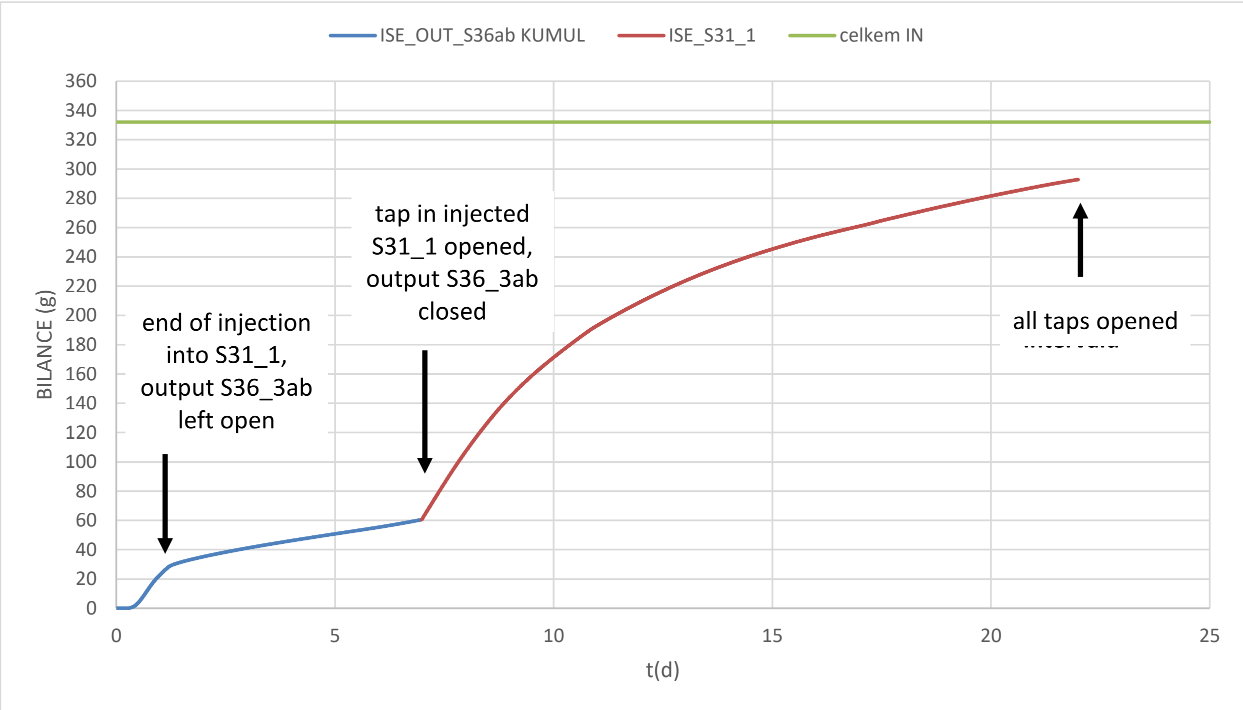

Fig. 56 Balance of the tracer during test 3 – graph of the total balance of the I^- tracer (in grams)

10 Finalization of the Numerical Model

The finalization stage of the numerical model (E27) follows on from the modeling work performed in the previous Stages 12, 21, and 24, which focused on the preparation of the fracture network geometry and flow simulation. The aim of the work in Stage 27 was to complete the numerical model, verify and update the hydraulic parameters, and determine the transport parameters of specific semi-deterministic fracture based on the tracer tests. A description and evaluation of the tracer tests are included in report TR 702/2023. For the model evaluation of the transport parameters of fractures, the outputs of tracer tests 2 and 3 were used, in both tests the KI solution was used as a conservative tracer:

- Tracer test 2 between the intervals IN S31_2ab → OUT S36_3a+3b (0.02M KI). The EC breakthrough curve was used for the model, i.e., the values of conductivity measured by the WTW probes. KI concentrations were also measured by the ISE probe, but the KI breakthrough curve showed a time shift with regard to the EC curve, which was not clarified.
- Tracer test 3 between the intervals IN S31_1 → OUT S36_3a+3b (0.1M KI). Considering the large free volume of the interval S31_1, a five-fold higher tracer concentration was used based on the predictive model. The breakthrough curve of the KI concentration measured by the new ISE probes, which have a significantly higher sensitivity (by two orders of magnitude) than the WTW probes for measuring EC conductivity, was used for the model.

In the constructed DFN model, intervals S31_2 and S36_3 (tracer test 2) are interconnected by one semi-deterministic fracture labelled “mesh24”. The distance between the intersections of both intervals with the fracture is 13.5 m, see Fig. 57 (left). The connection of intervals S31_1 and S36_3 (tracer test 3) is more complicated. The main connection between the intervals is through a pair of fractures “mesh14” and “mesh24” (the same fracture that connects the intervals in tracer test 2), see Fig. 57 (right). However, the geometry of the actual connection will be more complicated with regard to the length of the interval and the large number of interpreted fractures (e.g., based on the well-logging, two more inflows from fractures were found in the lower part of the interval, i.e., “mesh29” and “mesh35”, according to the ABI record there is a series of more significant disturbances, but no inflow in the upper part of the interval). The shortest distance between the intersections of the fractures with boreholes is approximately 28 m, i.e., twice as long as the distance of intersections in tracer test 2.

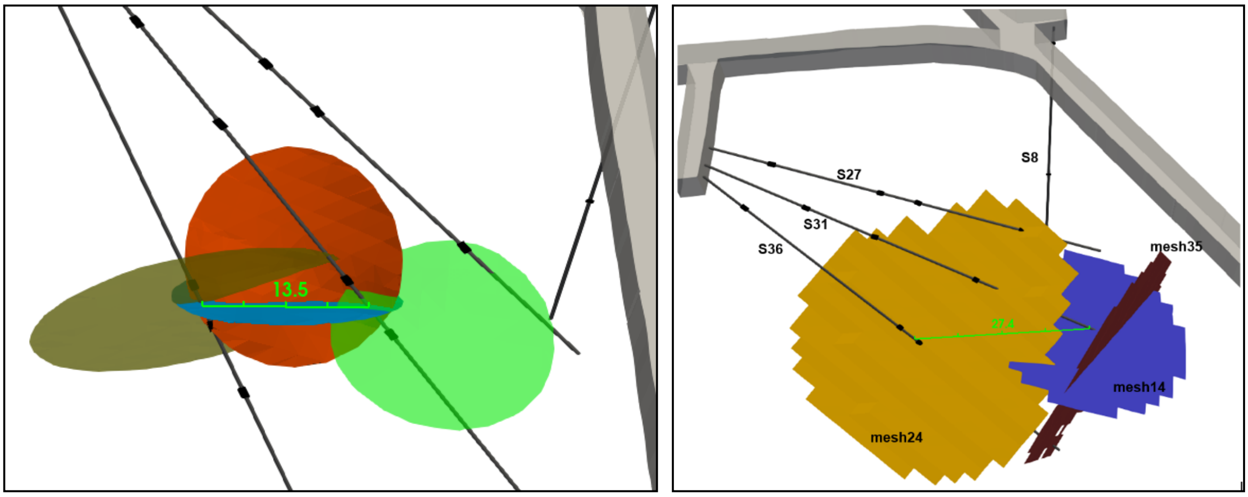

Fig. 57 Interconnection of the tested intervals with the semi-deterministic fractures – on the left for tracer test 2 (IN_S31_2ab OUT_S36_3ab), on the right for tracer test 3 (IN_S31_1 - OUT_S36_3ab)

For the selected fractures mesh14 and mesh24, based on the results of the tracer tests, the parameters of transmissivity and transport divergence and the value of longitudinal dispersivity (transverse dispersivity is 10% of the longitudinal) were evaluated and calibrated by the model. For the conservative KI tracer, other transport processes (sorption, diffusion into the rock matrix) were not considered and modeled. The input values of the parameters entered into the transport model are based on previous works, i.e., WPT measurements and construction of the optimized model, and are summarized in Tab. 18. The transport divergence a_T was calculated from the transmissivity value T according to the equation:

$$a_T = c \cdot T^{0,5} \ ,$$

where the value of the parameter c is usually determined from experimental work. The value of 0.5 used in the expansion calculation was derived from Crawford (2008).

Tab. 18 Input parameters of transmissivity and transport divergence of the fractures of interest

Source	Fracture transmissivity (m^2/s)		Transport divergence (m)	
	mesh14	mesh24	mesh14	mesh24
WPT of interval in S31	$1.9 \cdot 10^{-6}$	$1.4 \cdot 10^{-6}$	0.00069	0.00059
WPT of interval in S36	x	$8.0 \cdot 10^{-7}$	x	0.00045
Optimized model in S31	$1.9 \cdot 10^{-6}$	$2.8 \cdot 10^{-6}$	0.00069	0.00084
Optimized model in S36	x	$1.6 \cdot 10^{-6}$	x	0.00063

The procedure for modeling the tracer tests and calibration of transport parameters is as follows:

1. Construction of the hydraulic model for tracer test 2, i.e., with one fracture of interest mesh24 and input parameters from the optimized model according to Tab. 18,

2. Calculation of flow in the fracture and evaluation of pressures, or outflow for three steady states: unaffected mode with closed taps in intervals, affected mode with open interval S36_3ab, and affected mode during tracer test 2, i.e., injection into S31_2ab, outflow from S36_3ab,
3. Calibration of fracture transmissivity to water table and balance criteria. Transmissivity is fine-tuned for all three simulated states,
4. Construction of the transport model and simulation of tracer test 2. The entered transport divergence values are calculated from the calibrated transmissivity values from point 3,
5. Calibration of the transport divergence, or the coefficient c, and the dispersivity. A comparison and fitting of the progress of the measured and model breakthrough curves of the tracer,
6. Variant simulation of tracer test 2 with a different spatial distribution of transmissivity and transport divergence. The procedure from constructing the model (point 1) to calibrating the model and fine-tuning the parameters (point 5) is repeated,
7. Construction of the hydraulic model for tracer test 3, i.e., with two fractures mesh14 and mesh24. In fracture mesh24, the calibrated values from point 3 were entered, whereas in fracture mesh14, the transmissivity parameters from the optimized model according to Tab. 18 were used,
8. Calculation of flow in the fracture and evaluation of pressures, or outflow for three steady states: unaffected mode with closed taps in intervals, affected mode with open interval S36_3ab, and affected mode during tracer test 3, i.e., injection into S31_1, outflow from S36_3ab,
9. Calibration of fracture transmissivity to the water table and balance criteria. Fine-tuning of transmissivity to all three simulated states,
10. Construction of the transport model and simulation of tracer test 3. The transport parameters i.e., coefficient c and dispersivity, are entered from the calibrated model of the previous test 2 (point 5),
11. Evaluation of the progress of the measured and model breakthrough curve of the tracer and recalibration of the transport divergence, or the coefficient c, and dispersivity,
12. Evaluation of the model results.

10.1 Simulation of Tracer Test 2

10.1.1 Construction of the Hydraulic Model

The model of tracer test 2 was based on the fracture geometry of the optimized model and is conceptually solved as a section from this model. It t includes a semi-deterministic fracture mesh24 of size 30 × 30 m discretized into 0.3 × 0.3 m or 1 × 1 m elements depending on the model variant.

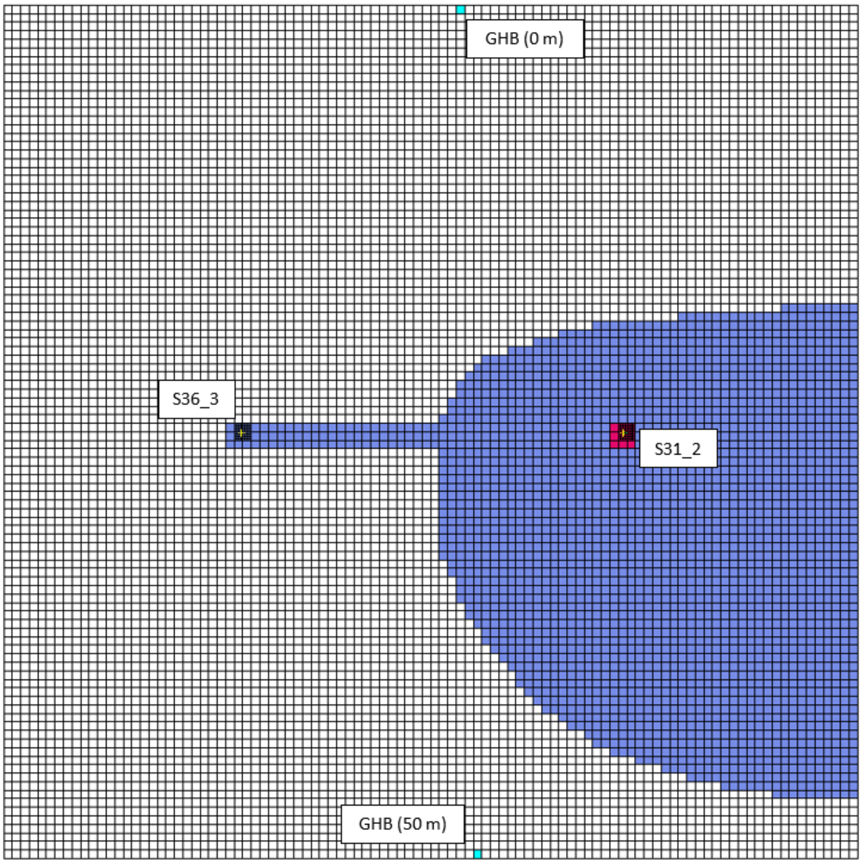

Fig. 58 Discretization of the model fracture mesh24 into 0.3 × 0.3 m elements – variant with three transmissivity zones and a simplified preferential connection between the tested boreholes

An example of the discretization of model fracture mesh24 into 0.3 × 0.3 m elements in the variant with two transmissivity zones and a simplified preferential connection between the tested boreholes S31 and S36 is shown in Fig. 58. The figure also shows the specified general head boundary (GHB) conditions representing the connection of the fracture to the surrounding fracture network.

10.1.2 Variants with Spatial Input of Parameters

For the fracture of interest mesh24, two transmissivity values evaluated from the WPT in boreholes S31 and S36 are available from the measurements. The real spatial variability of the hydraulic and transport parameters on the fracture is a very current theme and is addressed, for example, by the international project GWFTS Task 10. Therefore, during the model evaluation of the tracer test we also focused on several variants of the special input of transmissivity and transport expansion values into the calculation elements forming the fracture:

A) A simple homogeneous model with one constant value throughout the fracture,
B) A simple heterogeneous model with two values throughout the fracture,
C) A simple heterogeneous model with three values throughout the fracture and a preferential path between intersections with the boreholes,
D) A homogeneous model with one constant value throughout the fracture, but with a share of impermeable NOFLOW elements randomly generated in space (representing sealed areas),

E) A heterogeneous model with variability generated geostatistically in the GSTools program,
F) A heterogeneous model with variability generated geostatistically in the ConnectFlow program.

A graphic overview of the variants of the special input of parameters is given in Fig. 59.

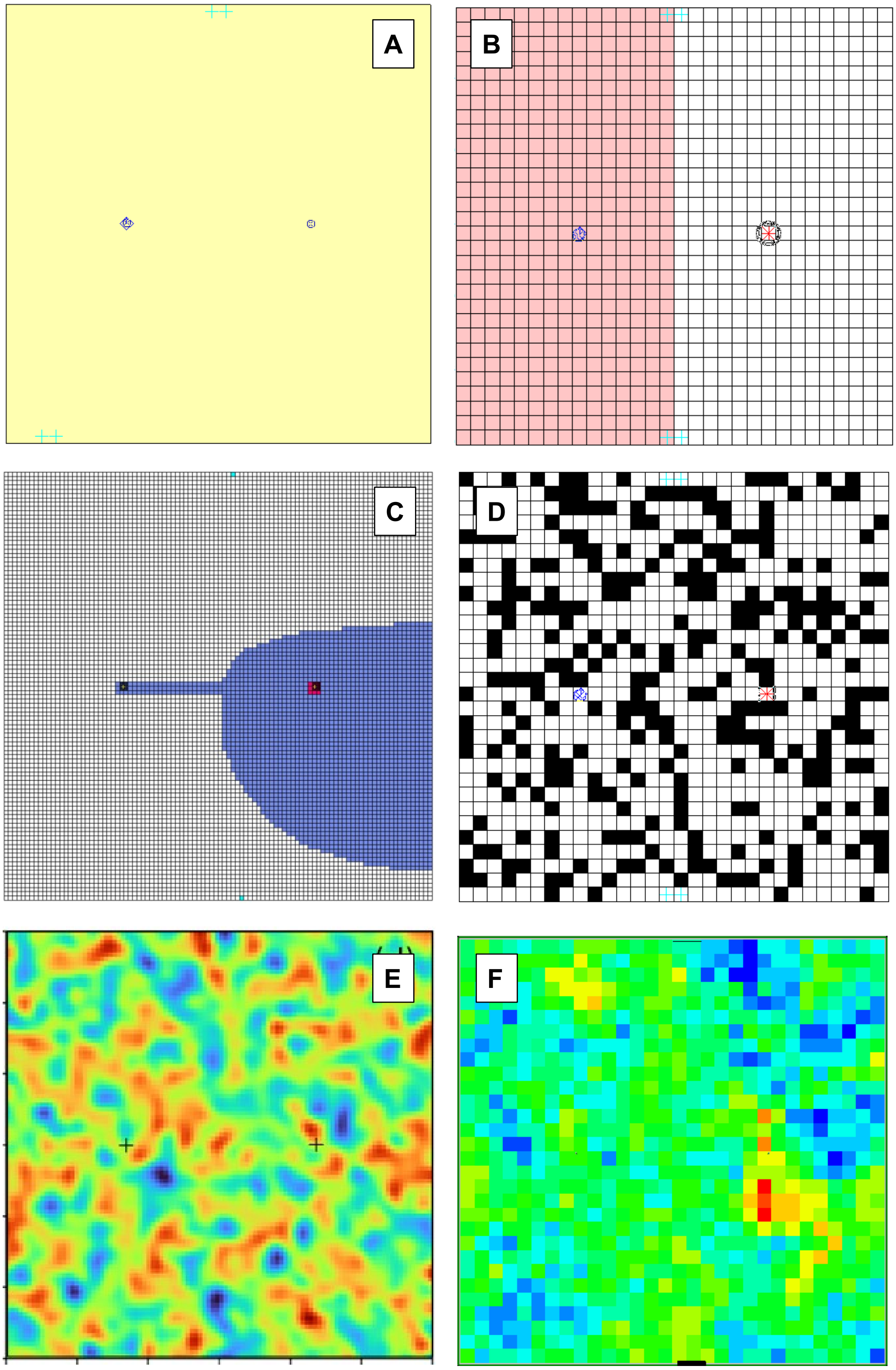

Fig. 59 Overview of the variants of the special input of parameters in the fracture

10.1.3 Flow Simulation and Model Calibration

Simulations of flow and subsequent transport were implemented in several software programs:

- Flow and transport in MODFLOW USG,
- Flow in MODFLOW2005, transport in MT3D USGS, transport using the particle tracking method in MODPATH7,
- Flow and transport using the particle tracking method in the ConnectFlow DFN module.

One of the “secondary” reasons why the test was simulated in several software packages, was to verify the capabilities of these tools during tasks for which specific and detailed measured data are available (i.e., not only, often incomplete, data taken from the literature). Tasks with a similar content are currently being solved for SÚRAO (e.g., validation of a flow and transport model in a fracture in GWFTS Task 10) and the experience gained from this project has an overlap and application in other projects and contracts with the client.

Calibration of fracture parameters is one of the most important points in the entire modeling process. The calibrated parameter values (or range of values) are subsequently extrapolated to the entire fracture network and provide a relevant basis for the preparation of the transport model (transport divergence is calculated from the transmissivity).

The flow model was calibrated for thee steady states: unaffected mode with taps closed at all intervals (A), affected mode with S36_3ab interval open (B) and affected mode in tracer test 2, i.e., injection into S31_2ab, outflow from S36_3ab (C) . An overview of the measured and modeled pressure and flow values in sections S36_3 and S31_2 for the final calibrated state of the variant with three transmissivity zones and the specified preferential connection between the tested boreholes is presented in Tab. 19. Fig. 60 shows the calibrated transmissivity values for this variant.

Tab. 19 Calibration of the flow model in the variant with three transmissivity zones and the specified preferential connection between the tested boreholes. Measured and modeled values of pressure and flow in sections S36_3 and S31_2 during the three phases of the experiment, the values highlighted in bold were used as the boundary conditions of the groundwater flow model (the measured absolute pressure at the pressure head is shown in parentheses)

System status	S36_3 measured	S36_3 modeled	S31_2 measured	S31_2 modeled
A) Unaffected (taps closed)	H = 25.0 m (504 kPa)	H = 24.97 m (difference −0.12%)	H = 25.4 m (510 kPa)	H = 25.33 m (difference −0.28%)
	Q = 0 m^3/s	Q = 0 m^3/s	Q = 0 m^3/s	Q = 0 m^3/s
B) Open S36_3	H = 8.2 m (336 kPa)	**H = 8.20 m**	H = 11.7 m (373 kPa)	H = 11.57 m (difference −1.11%)
	$Q = -1.42 \cdot 10^{-5}$ m^3/s	$Q = -1.65 \cdot 10^{-5}$ m^3/s (difference 16.20%)	Q = 0 m^3/s	Q = 0 m^3/s

C) Open S36_3, injection to S31_2	*H* = 17.7 m (431 kPa)	***H* = 17.70 m**	*H* = 26.8 m (524 kPa)	*H* = 26.82 m (difference 0.07%)
	Q = −2.02 · 10^{-5} m^3/s	*Q* = −2.12 · 10^{-5} m^3/s (difference 4.95%)	*Q* = 1.67 · 10^{-5} m^3/s	***Q* = 1.67 · 10^{-5} m^3/s**

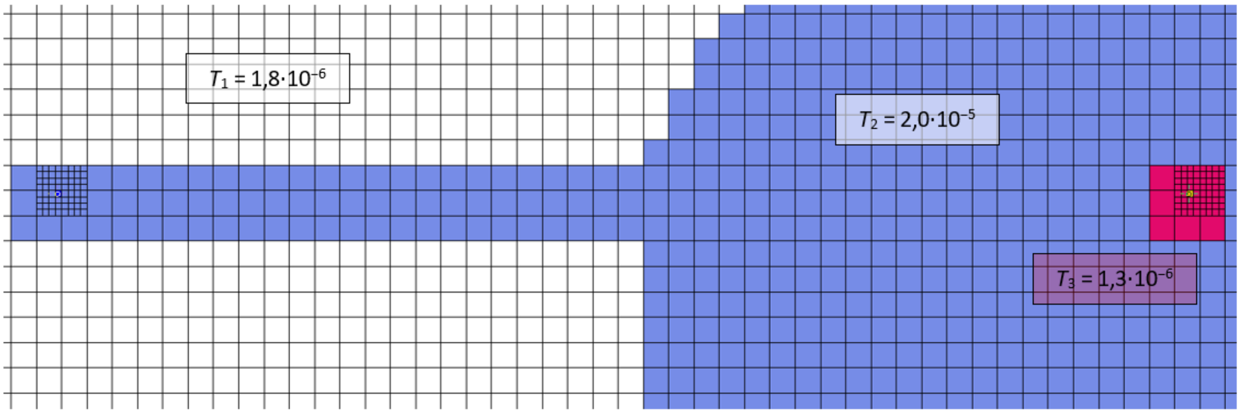

Fig. 60 Calibrated transmissivity values – variant with three transmissivity zones and specified preferential connection between the tested boreholes

10.1.4 Transport Simulation and Model Calibration

The basic method of simulating transport in fracture networks is particle tracking, which is implemented in all the used software programs, in the case of DFN models (in ConnectFlow) it is practically the only method used and only includes transport affected by advection. The inclusion of other transport processes requires the use of software based on the CPM/ECPM concept (MT3D) or other highly specialized tools.

The implementation of transport using the particle tracking method in the DFN model is computationally significantly less demanding than the complete transport solved in the CPM model. For example, the ConnectFlow makes it possible to very quickly and efficiently implement a large number of stochastic simulations (see Fig. 61), which are the basis for statistical evaluations.

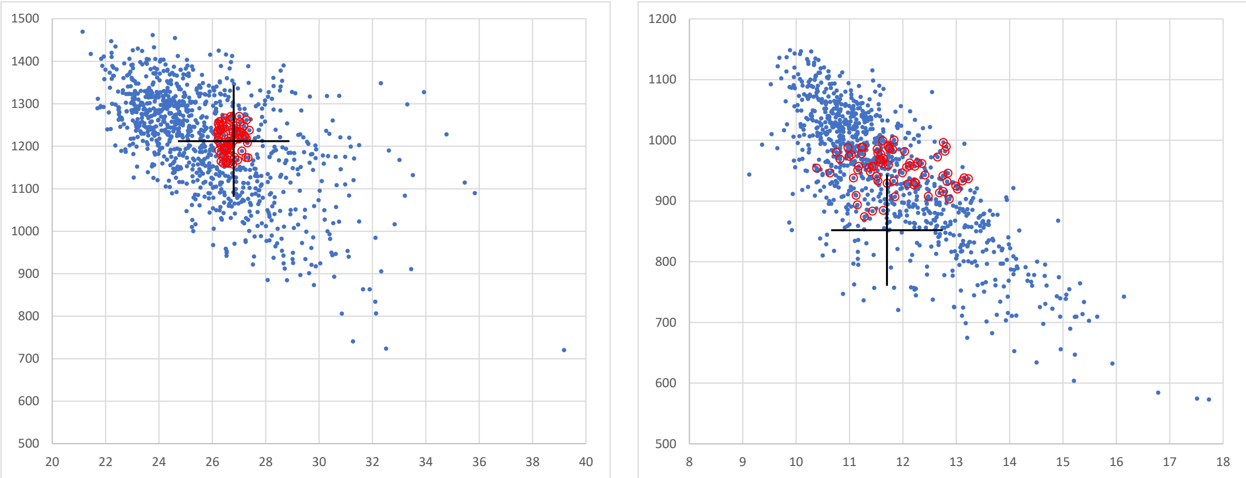

Fig. 61 Outputs from 1000 implementations of the flow model (variant F) in tracer test 2 (left) and opening S36_3ab (right). Selected implementations are highlighted in red, which in the chosen "small" range of values correspond to the measurement (black cross)

The breakthrough curve from the particle tracking (if it includes only the influence of advection) may be compared with the calculation using full transport (with the inclusion of other processes, in particular dispersion in the case of conservative tracers) on the timeline in reaching the peak concentrations. From the comparisons made using different software programs and on different variants of the surface distribution of parameters, it was verified that both methods provide the same results, see Fig. 62, whereby the peak concentrations for both models are reached in 240 minutes. The measured value of the peak in 300 minutes (see the orange breakthrough curve) may be achieved by calibrating the model. Specifically, the transport divergence, or coefficient *c*, which may be calibrated by both calculation methods (more efficiently and quickly by the particle tracking method). The difference in the values of the maximum concentrations is caused by the dispersion of the tracer in the fracture, which is not included in ConnectFlow or MODFPATH particle tracking, and must be calibrated by calculating the full transport in another program, i.e., MT3D.

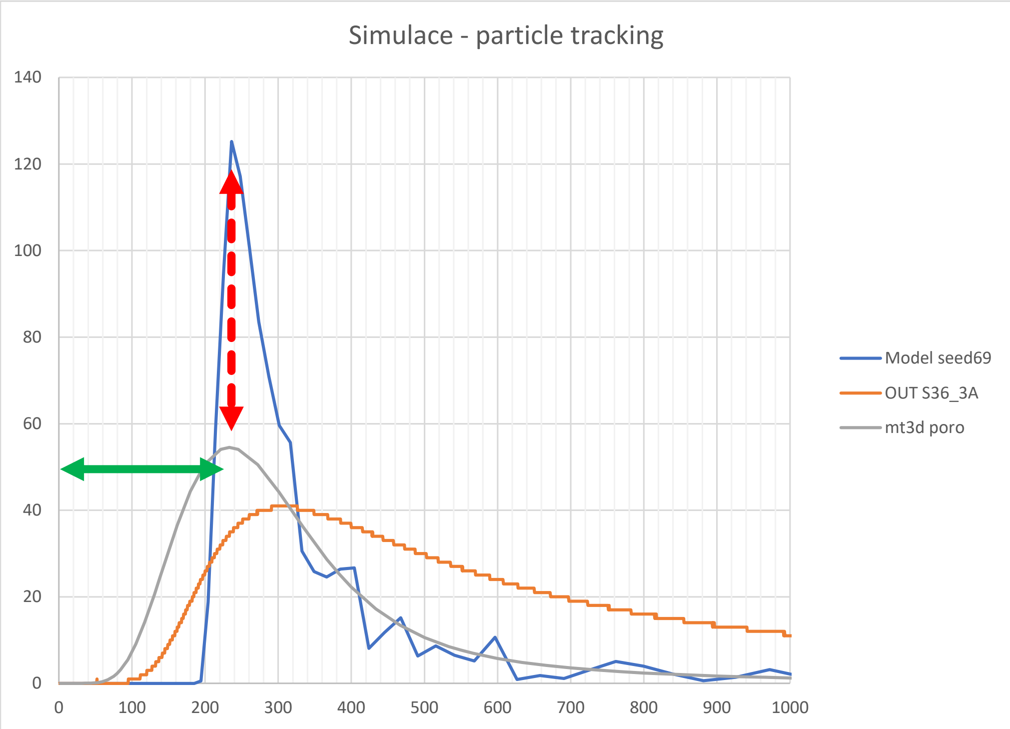

Fig. 62 Comparison of breakthrough curves - uncalibrated implementation with geostatistically generated variability (F, seed69) - calculation of transport using the particle tracking method in ConnectFlow and full transport in MT3D. The green arrow highlights the same time to reach "peak" concentrations, the red arrow highlights the difference in maximums due to tracer dispersion in the fracture

An important output of the modeling (also in connection with other solved projects) is the finding that the measured breakthrough curve of tracer test 2 could be calibrated in all simulated variants of the areal distribution of parameters A to F, i.e., from the simplest homogeneous variant to the most complex geostatistically generated parameters in more implementations. As a result, this would mean (if it is confirmed by further experiments) that the heterogeneity of parameters at the level of the fracture (its research is very complicated) is not so important for modeling flow and transport in fracture networks and may be replaced by simpler parameters. Tab. 20 summarizes the calibrated values of the fracture parameters for the individual model variants. For dispersivity values, the effect of numerical dispersion, which is half the size of the calculation element, is taken into account. A graphical comparison of the measured and model breakthrough curves is given in Fig. 63 to Fig. 66.

Tab. 20 Overview of calibrated mesh24 fracture parameter values for the individual model variants

Variant	Transmissivity (m²/s)	Coefficient c	Dispersivity* (m)
A	$4.6 \cdot 10^{-6}$	1.1	1.5
B	$3.2 \cdot 10^{-6}$–$5.6 \cdot 10^{-6}$		
C	$1.3 \cdot 10^{-6}$–$2.0 \cdot 10^{-5}$	0.9	0.6
D	$3.0 \cdot 10^{-5}$	1.1	1.0
E	$2.0 \cdot 10^{-6}$ (mean value)	0.7	1.6
F	$4.7 \cdot 10^{-6}$ (mean value)	0.5 (seed139)	

* *total dispersion, i.e., the sum of the entered value and the numerical dispersion*

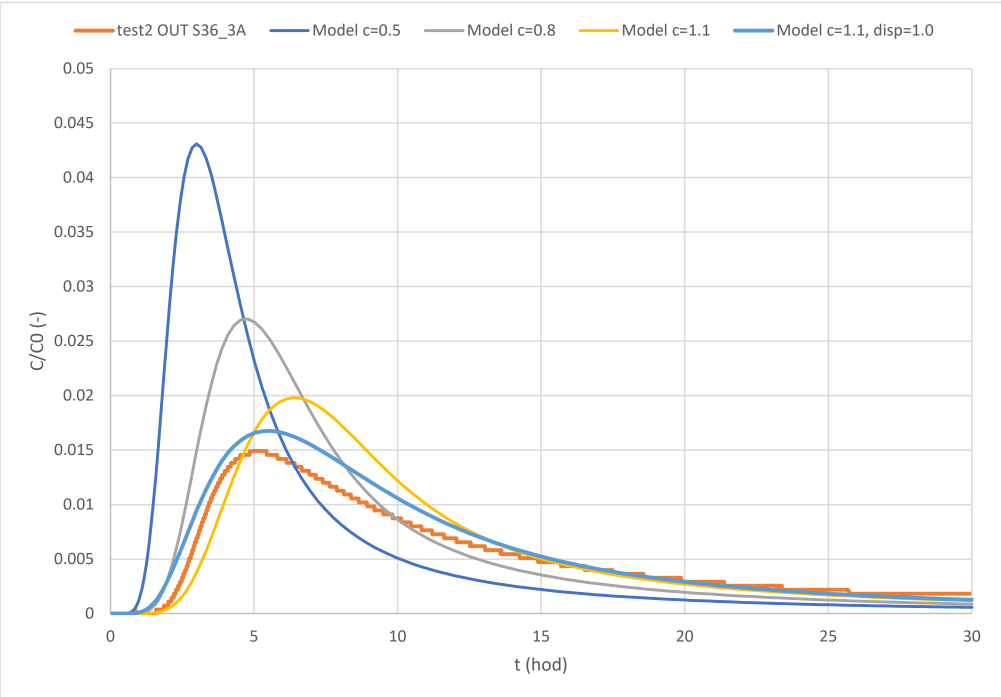

Fig. 63 Comparison of breakthrough curves - homogeneous model with one value (variant A) - calculation of full transport in MT3D for different c and dispersivity coefficient parameters

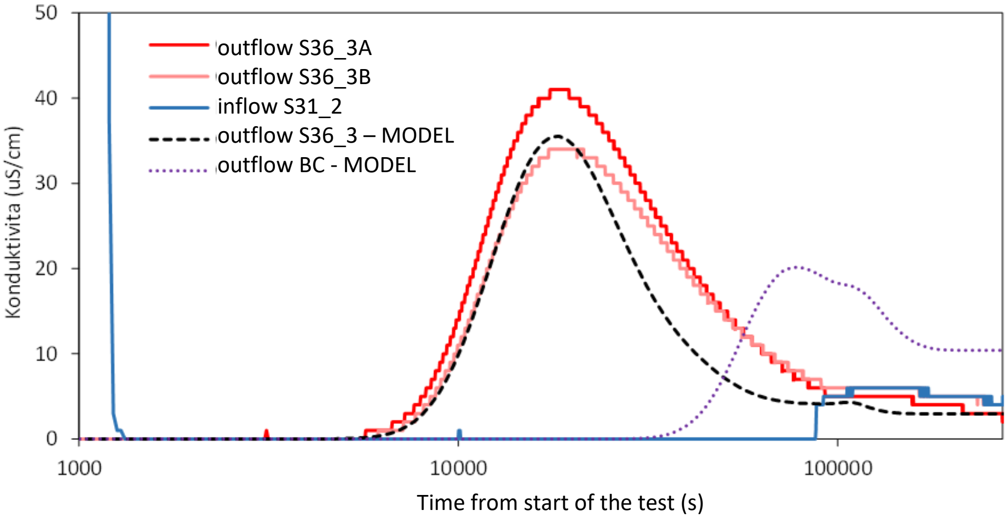

Fig. 64 Comparison of breakthrough curves - calibrated heterogeneous model with three values (variant C) - calculation of full transport in MODFLOW USG

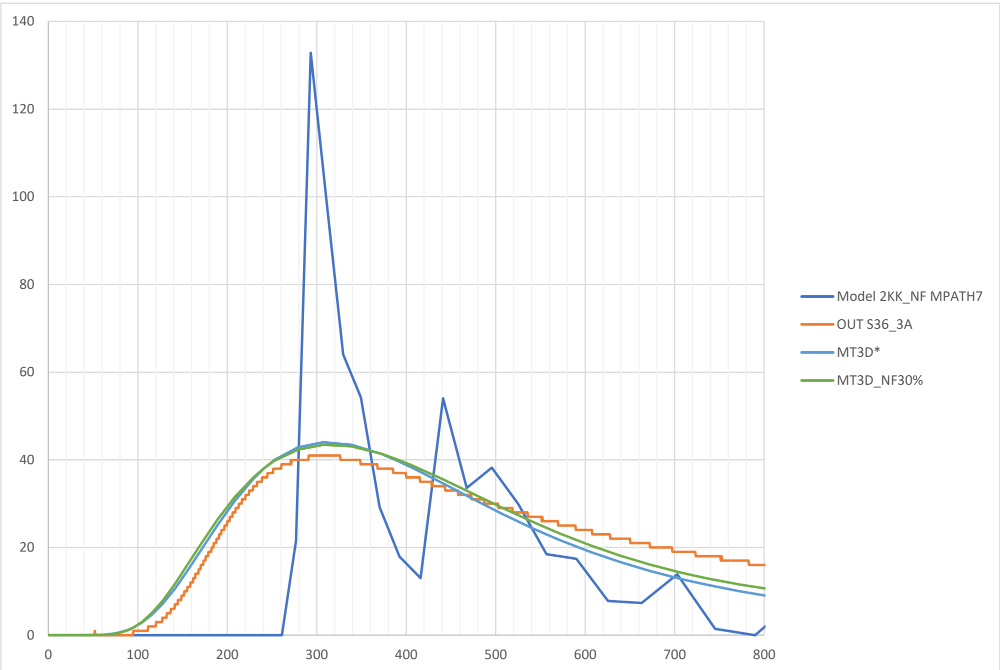

Fig. 65 Comparison of breakthrough curves - calibrated homogeneous model with a share of impermeable NOFLOW elements (variant D) - calculation of transport using the particle tracking method in MODPATH and full transport in MT3D

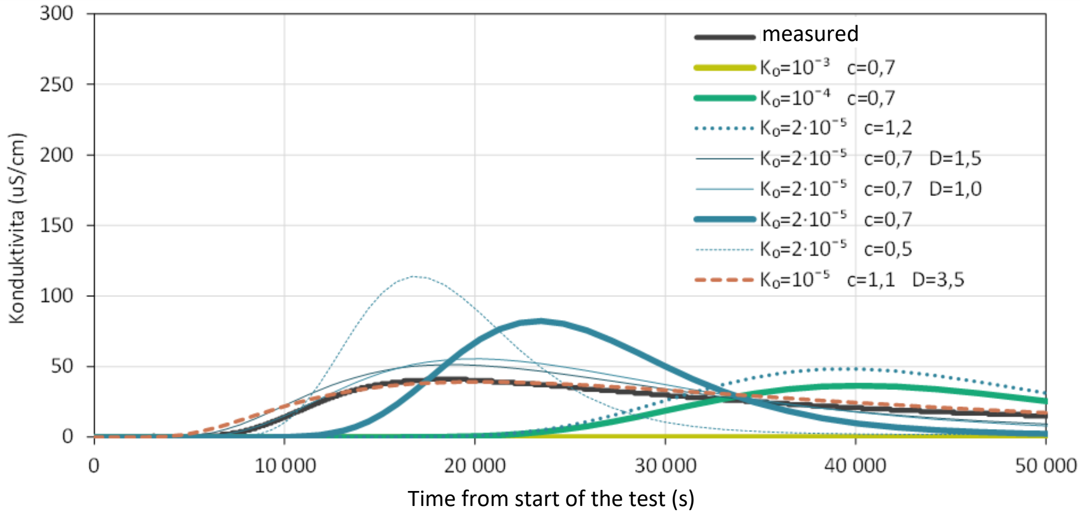

Fig. 66 Comparison of breakthrough curves - heterogeneous model with geostatistically generated parameters in GSTools (variant F) - calculation of full transport in MT3D for different c and dispersivity coefficient parameters

10.2 Simulation of Tracer Test 3

Conceptually, the model of tracer test 3 is solved analogously to the previous model of tracer test 2. The geometry of the fractures is based on the optimized model and is assembled as a cross-section from this model. It includes semi-deterministic fractures mesh24 and mesh14 discretized into 1 × 1 m elements, see Fig. 68. The figure also shows the intersections with boreholes S-31 and S-36, the mutual intersection of the fractures and the general head boundary conditions (GHB) representing the connection of the fracture to the surrounding network of fractures.

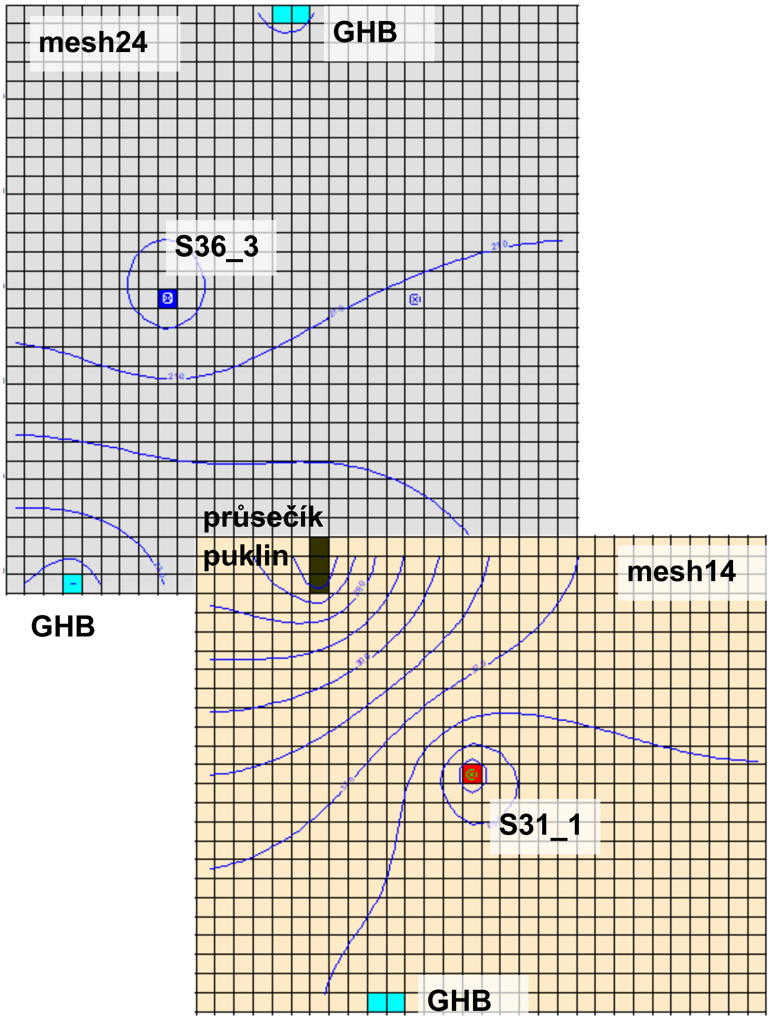

Fig. 67 Discretization of model fractures mesh14 and mesh24 into 1 × 1 m elements, indication of boreholes, intersection of fractures and general head boundary conditions (GHB). Model isolines of hydraulic head are also plotted

Fig. 68 shows a diagram of the injection section S31_1 with the intersections of fractures from the geometric model. The input section for tracer test 3 is more complicated than for test 2 and more significantly affects the input of the initial tracer pulse and the evaluation of transport parameters, and model calibration, etc.:

- The free volume in the borehole (109 l) is roughly 5x larger than the injected tracer volume (20 l). Therefore, the tracer is significantly diluted and slowed down even before entering the fracture,
- Based on the well-logging results, there are three fractures with inflows in the section (no detailed WPT were performed on the corresponding smaller sections of the borehole, which would specify the permeable fractures/zones). In the model, we assume that during the test the injected amount of tracer will be distributed to these three fractures in the same proportions as the measured inflows into the borehole, i.e. 22% into the fracture mesh14.

Using the 1D model of the borehole section S31_1, the injection of a 20 min tracer pulse was simulated and the course of the pulse (breakthrough curve) at the point of intersection with the fracture mesh14 was evaluated, see Fig. 69. Modification of the pulse was simulated for dispersivity values in the range of 0-0.5 m. Delay of the entry of the tracer into the fracture mesh14 is approximately 40 min, the maximum pulse decreases to less than 40% of the injected value, and the pulse length extends to approximately 100 min.

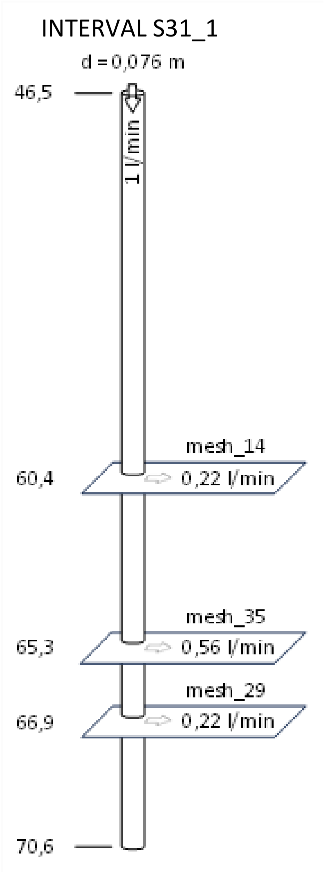

Fig. 68 Diagram of the injection section S31_1 with delineation of the expected conductive fractures based on well-logging

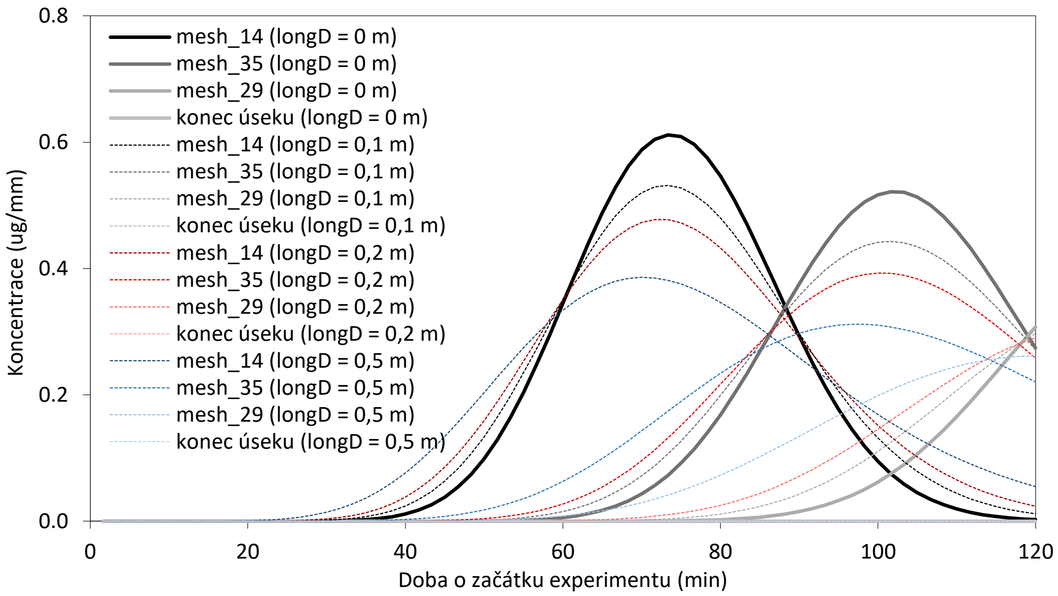

Fig. 69 Modeled breakthrough curves in section S31_1 at the level of individual fracture intersections – for different values of longitudinal dispersivity

10.2.1 Calibration of the Model

Based on the above assumptions, a flow model was first built and calibrated for all three states of the system (unaffected state, open section S36_3ab and injection in tracer test 3). The simulation of tracer test 3 was performed for a homogeneous variant of transmissivity in the surface of the fracture. The parameters for the fracture mesh24 were entered from the calibrated model of tracer test 2. The simulations were performed in the MODFLOW/MT3D program.

After calibrating the hydraulic model, the transport of the tracer was simulated with the setting of the coefficient *c* and the dispersivity from the simulation of tracer test 2. The results were evaluated by comparing the measured and model breakthrough curves, and the model was modified in order to calibrate the parameters of the fracture mesh14:

- The breakthrough curves for selected models are plotted in the graph in Fig. 70,
- For the basic model "in22%" with the fracture mesh14 injection setting at the assumed level of 22% (according to the well-logging) tracer transport is significantly slower. In the interval S36_3 it appears only after 14 hours, i.e., more than 10 hours later than it was measured, and in overall lower concentrations,
- It was not possible to successfully calibrate this model (in22%) by adjusting the dispersion or transport expansion parameters,
- Faster transport and an increase in the tracer balance at the exit may be achieved in the model by increasing the amount of water injected into the fracture mesh14, i.e., by further redistribution of the inflow between the three fractures (which will not correspond to the values from the well-logging),
- The values of inflow into the fracture mesh14 were tested by model when injecting 50% (i.e., 500 ml), 60% (600 ml) and 100% (i.e., a hypothetical variant with only permeable mesh14). All these models were first calibrated hydraulically (flow model) and the transport was subsequently simulated with dispersivity values of 1.0 m and coefficient *c* = 1.1

(calibrated as part of the simulation of tracer test 2), further partial modifications of the model were also performed,

- For the model with a specified proportion of 50% of the injected quantity into mesh14, the model with a higher dispersivity of 2 m corresponded better to the measured breakthrough curve. A greater dispersion effect in this case does not necessarily mean a higher dispersion in the fracture, but due to relatively large input uncertainties, it may also mean a greater dispersion, or dilution in the volume of the borehole,
- For the model with the specified proportion of 60%, the measured breakthrough curve also matched the specified dispersivity of 1 m quite well, a better match was further achieved by reducing the concentration of the tracer at the entrance to the fracture to 30% of the original value (see model "in60%(a)" in the graph) , which would correspond to a higher dispersion when the tracer passes through the interval S31_1.

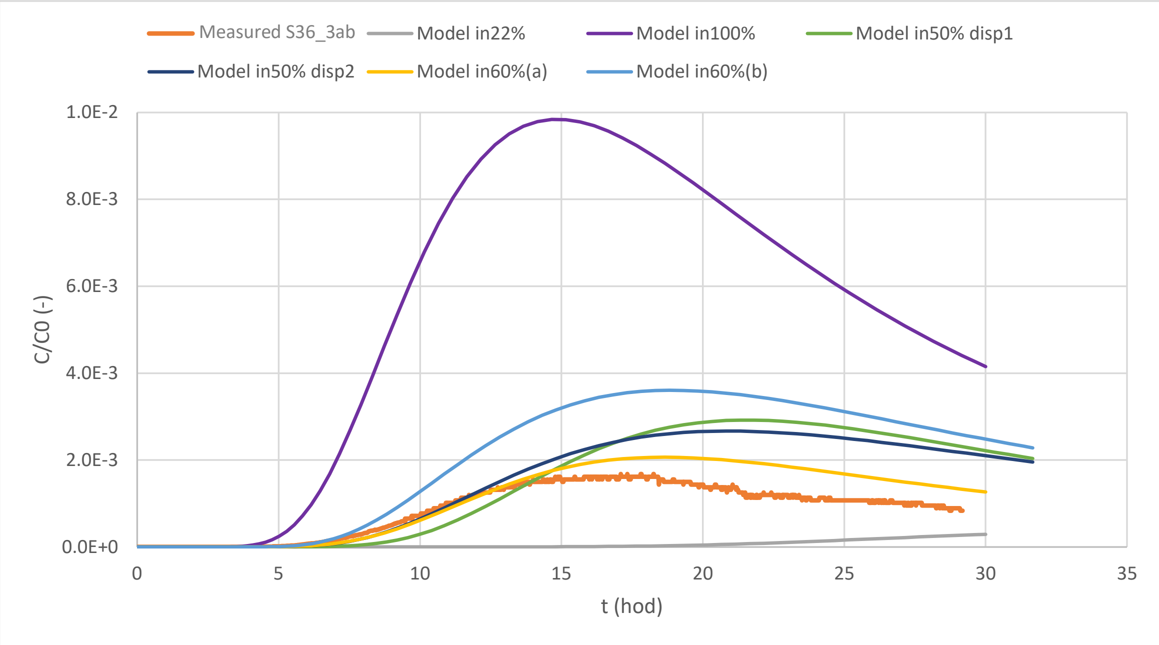

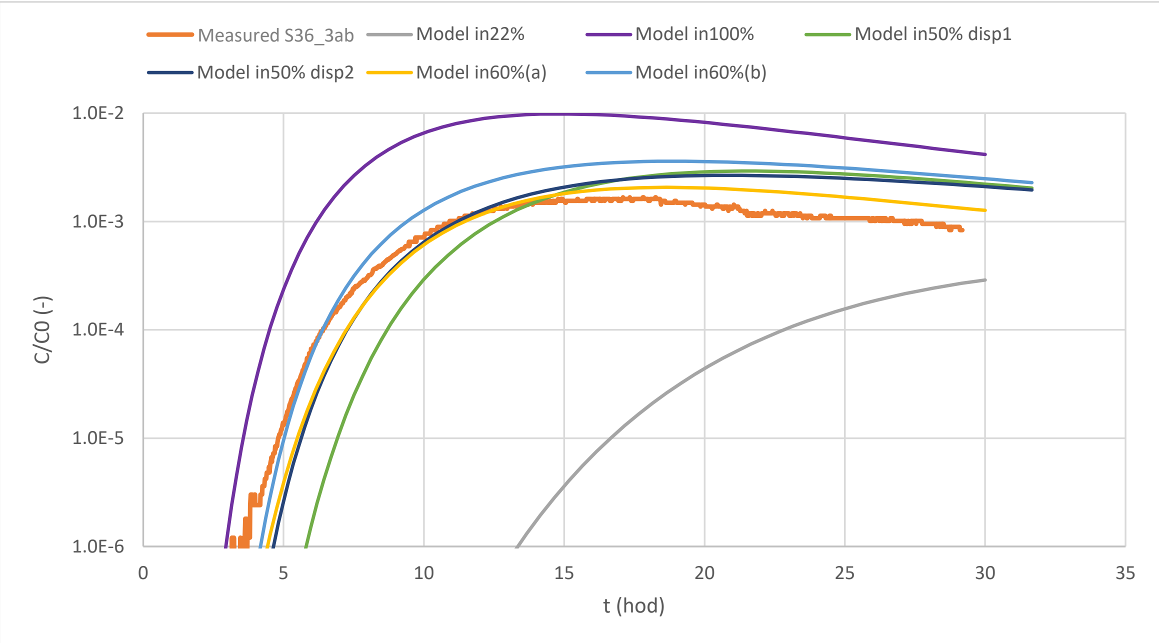

Fig. 70 Tracer test 3 - model breakthrough curves for different settings of the source pulse (linear concentration scale in the upper graph, logarithmic in the lower)

10.3 Summary of the Results

During the finalization stage of the numerical model (Stage 27), the modeling work focused on a simulation of the tracer tests and evaluation of the transport parameters of specific fractures of the semi-deterministic HydroDFN model prepared in the previous stages. A summary of the knowledge gained is summarized in the following points:

- The evaluation of the transport experiment is affected by uncertainties in the geometry of the task, the hydraulic description (boundary conditions) and the instrumentation of the experiment. The aim of the work in the previous stages of the project (laboratory, monitoring, modeling, etc.) was to minimize these input uncertainties. This was achieved quite well in tracer test 2. One of the problems in the performance of the test was a shorter injection time, during which steady conditions were ensured, and therefore it was not possible to evaluate the overall balance of the tracer. In tracer test 3, there were more input uncertainties, although they were known in advance, but unfortunately another test configuration was not possible, i.e., injection section of the borehole was too long (and without filling to reduce the free volume) with a larger number of fractures, detailed pilot WPT, and therefore only unverified conductive fractures/ zones. A larger number of input uncertainties of different types represent many degrees of freedom in the phase of constructing the model, the evaluation of transport parameters is then more complicated, and the outputs are distorted by inaccuracies in the input itself,
- The tracer test models included only the fractures of interest between the tested intervals, i.e., they represented a section of the HydroDFN model. The connection to the surrounding fractures was entered conceptually as a GHB condition (with specified hydraulic height and resistance coefficient). The results of the hydraulic simulations and successful calibration with the measured values confirmed the possibility of using this simplified specification to solve the parameters of specific fractures,
- Detailed measurements of fracture openings on small samples using surface scanning point to a large variability of opening values (e.g., GWFTS Task 10). The question is the extrapolation of this heterogeneity to the scale of a real fracture and its effect on the results of tracer flow and transport between two boreholes at a distance of several units up to tens of meters. Various approaches to generating transmissivity and transport divergence in the fracture area were therefore simulated with homogeneous (one value) and highly heterogeneous distribution (geostatistically generated range of values), while the simulation results of tracer test 2 showed that it is possible to calibrate the model parameters for all the selected approaches,
- Calibrated fracture transmissivity values (mesh24 for tracer test 2) vary slightly depending on the area distribution variant and are in the range of 2.0 to 4.7 10^{-6} m^2/s. For the variant of homogeneous distribution with heterogeneity generated by NOFLOW elements (the approach used in the models of the Finnish company Posiva), the calibrated transmissivity is almost an order of magnitude higher, 3.0 10^{-5} m^2/s. In all the model variants, the calibrated values are therefore higher than the measured values from the WPT (more precisely calculated from the WPT), which should be used very carefully as inputs in the uncalibrated ones,
- Incorrectly entered fracture transmissivity values in the model subsequently affects the calculation of transport, because the transport divergence of fractures is usually calculated using a power function precisely from the transmissivity value. Another parameter that enters into the calculation of transport divergence is the proportionality coefficient *c*, which is usually considered to be 0.5. During multiple implementations (1000x) in the ConnectFlow program, an optimal transport solution (corresponding to the measured breakthrough curve) was found even for this value of 0.5. For homogeneous variants or with less heterogeneity, the value of coefficient *c* was calibrated in the range of 0.9 to 1.1,

- A combination of higher calibrated transmissivity values and coefficient *c* means an overall higher transport divergence and therefore a larger volume of water that is found in the fractures and in which the tracer is diluted. For a fracture size of 30 × 30 m, transmissivity according to WPT and $c = 0.5$, the volume of water in the fracture is 0.5 m^3. For the calibrated transmissivity four times greater and the coefficient $c = 1.1$, the volume of water in the fracture is 2.1 m^3,
- A relatively important finding is that in all models it was necessary to enter a non-zero value of dispersion, i.e., even in models with a large area heterogeneity, in which we assumed that the generated preferential zones would replace the effect of dispersion, but there is a lot of room for testing the transport model, there are a greater number of geostatistical generation methods,
- Comparison of the breakthrough curves from the calculation of transport using the particle tracking method (only advection, 1D trajectory) and full transport (advection and dispersion in a 2D network) showed comparability of the results, i.e., the same mean tracer inflow times (time of maximum concentration) were calculated. The particle tracking method is therefore a very effective tool for basic evaluation of transport due to its calculation speed.

11 Conclusion

During the project implementation, the set objectives (Section 1.1) were fulfilled and a whole range of knowledge and experience was gained, which may be used for further study or subsequent experiments. The main experiences, recommendations, and suggestions are presented below (Sections 11.1 –11.2).

11.1 Summary of Experience and Recommendations

Methods of measuring the orientation and evaluation of the properties of fractures and their limitations:

Measurements on the walls of the URF

This method focuses on the mapping of fractures on the exposed walls of underground spaces (corridors). The advantage is direct access to the rock mass and the possibility of detailed observation of the fractures. The disadvantage is the inability to measure subhorizontal fractures and fractures parallel to the corridor.

Measurements on drill cores

This method focuses on the analysis of fractures in rock samples taken by drilling the boreholes. It allows us to measure the orientation and properties of the fractures at depth. The disadvantage is the neglect of fractures that are parallel to the axis of the borehole. Measuring the inclination and azimuth of fractures is only possible on an oriented drill core, the reverse reorientation of the drill core is highly imprecise even with the use of well-logging data and their scanning. Nevertheless, the structural characterization of the drill core, including the filling, thickness, and nature of the fractures, is necessary for a comprehensive analysis of the rock mass, including follow-up laboratory tests of the fillings and determination of the character of mineralization, e.g. tectonic faults.

Acoustic (ABI) and optical (OBI) television

This well-logging method, which uses acoustic waves to map the internal structure of the borehole, allows us to obtain a detailed image of the fractures and other structures in the borehole. Thanks to the possibility of measuring the opening of fractures, indications of their potential opening or, on the contrary, closing may be obtained. The disadvantage is the inability to distinguish subparallel fractures from foliations and the difficult interpretation of data caused by the high frequency of foliations (typical for metamorphic rocks). The data from the acoustic television also do not show the real appearance of the rock mass and need to be combined with the optical television. The OBI (developed television image) method enables a more detailed evaluation of tectonic faults compared to the ABI40 method. The use of the acoustic television is particularly suitable in turbid water, where poor visibility does not allow a high-quality image of the borehole wall using the optical television to be obtained. Both methods complement each other well.

Borehole azimuth and inclination

Accurate knowledge of the borehole orientation (azimuth and inclination) is crucial for the correct evaluation of well-logging data, including acoustic television data. At a borehole inclination of less than 50° from the horizontal, the ABI40 probe may be unintentionally rotated, which leads to inaccurate fracture orientation data (correction).

Data comparison and output in the form of a borehole log

To compare data from different methods, it is necessary for the data to have a similar format and output. This may be achieved, for example, by using specialized software tools such as MOVE, WellCAD, LogPlot, CoreBase, etc. The borehole log summarizes and integrates the results of structural and petrological analysis of drill cores and boreholes, thereby providing a comprehensive overview of the rock environment. In the optimal case, it is necessary to combine software tools in which well-logging data are processed with macroscopic description tools, such as WellCAD.

Generating a sGeoDFN model:

Population of fractures

Statistical tests showed that the population of fractures in the rock mass do not meet the criterion for uniform distribution, but rather show the character of a belt (equatorial) distribution with a weak directional concentration.

Populations 1–5, defined on the basis of dominant fracture orientations, show a bipolar character with moderate concentrations and are well described by the Fisher distribution, which has proven to be a suitable method for generating a stochastic DFN network from field data.

The analysis did not demonstrate the hierarchical nature of the populations in terms of fracture termination. This means that in this case it was not possible to establish a clear dependence between older and younger generations of fractures. This also implies the (im)possibility of systematically processing the termination of all fractures across individual populations. This may only be reliably achieved for larger stochastically generated and/or deterministic structures in the sGeoDFN model.

Correlation of structural and well-logging measurements with the model:

Limitations of field measurements

Field measurements of fractures are limited to the exposed surfaces of the rock mass in underground spaces, which may lead to an underestimation of the total number and frequency of fractures.

Limitations of the well-logging

Well-logging methods, such as acoustic television, provide detailed information about fractures at borehole depth, but their interpretation may be challenging and influenced by technical factors. In the case of subhorizontal boreholes, this is, for example, imperfect centering of the probe in the borehole.

Combination of methods and modification of the DFN model

For optimal results, it is advisable to combine data from field measurements, well-logging records, and modeling. Oriented drill cores in combination with the acoustic camera represents an alternative method for detailed analysis of fractures in depth, and according to experience from other projects, their combination is required for a comprehensive description of the rock environment. To achieve agreement between the sGeoDFN model and data from field measurements and well-logging records, it may be necessary to adjust the frequencies of individual fractures populations in the model to match the field measurements more closely.

Use of 3D models for designing the drilling works:

The photogrammetric models of the corridors in combination with the structural-geological model surrounding the experimental rock block proved to be a very suitable tool for planning subsequent technical works. Not only do they provide the possibility of displaying the working space on a scale of 1:1 at any time, but the possibility of projecting geological structures even into the depth of the rock mass proved to be essential when planning the course and depth range of individual boreholes. It makes it possible to prevent collisions with significant structural elements or minimizes the mutual influence of boreholes. Visualization of inflow locations, fault zones, fractures from well-logging measurements and individual floors of multipacker systems is then key to their design and evaluation.

Instrumentation – measuring the pressure in the intervals:

Before the actual implementation of the measurements, the following factors must be taken into account as part of its project preparation and proceed according to the points listed below. The aim of these recommendations is to select a suitable borehole diameter and instrumentation for the expected measured pressures and flows.

- Based on hydrogeological monitoring, determine the expected water flow in the rock mass.
- Based on the water flow, design the inner diameter of the piping so that there is no influence (“braking”) of the flow and pressure losses in the system.
- Based on the hydrogeological monitoring, determine the expected water pressure in the rock mass.
- Based on the water pressure, design sensors with a suitable range.
- Have the option to duplicate the measurements in individual intervals with multiple sensors (i.e., different ranges, backup sensor - validation option).
- Based on the structural-geological mapping, well-logging methods (mainly ABI, OBI, resistivity measurement) and water pressure tests, estimate the number of test floors and choose the appropriate intervals.
- Choose a suitable packer diameter based on the number of floors and the diameters of the piping.
- Based on the diameter of the packer, choose a suitable drilling diameter. Choose the packers so that they may be removed and reinstalled (e.g., changing the measurement interval).
- Choose test intervals as short as possible and fill them with filler to reduce dead volumes.
- Online data monitoring is necessary so as to react flexibly to the borehole collapsing or change the reading settings.

Water pressure tests:

- Performing WPT in inclined boreholes is technically more demanding and there is a higher risk of the packer jamming than performing WPT in vertical boreholes.
- Conducting well-logging methods prior to WPT has proven to be very helpful in designing the extent and length of intervals in which WPTs are to be conducted. Resistivity methods

often revealed a prominent fracture or fracture zone communicating over a greater distance. In turn, ABI/OBI methods identified fractures and fracture zones with potentially higher permeability.

- WPTs are time consuming. A pulse test is sufficient to identify an impermeable zone. For a project that focusses on fracture connectivity, the tests may not be aimed at determining the hydraulic parameters of relatively impermeable floors.
- In order to identify mutual hydraulic communication between separate sections of the borehole, around packers, etc., it is also advisable during WPT to monitor the pressure below the tested interval and the discharge from the borehole before and during the test (at the mouth of the borehole).
- In similarly focused projects, it is advisable to perform WPT in two stages, i.e., after evaluating summary accelerated WPT in the first stage focused on the complete length of the investigated boreholes (floors of a larger extent, e.g. 5-7 m each), count on performing WPT focusing on the identification and measurement of individual fractures (floors of a shorter extent of 1–3 m) in the second stage WPT measurement on the given borehole.
- When performing WPT on another borehole, when the neighboring borehole is already fitted with a multipacker system, it is advisable to consistently verify the hydraulic communication with the floors of the borehole with the packer by monitoring the increase in pressure/inflow to the individual floors. It proved beneficial to use an online system for monitoring the pressure increase in the floors of the installed borehole.
- In the event that the layout of the floors in the installed borehole is found not to be optimal, modify the layout of the floors of the multipacker system so that it better captures the inflows to the monitored floors. For this purpose, the multipacker system should be designed in advance and should be taken into account in the work time schedule.

Tracer tests:

- For the tracer tests, it is good to understand the behavior of the fracture system using hydraulic tests (pulse, dipole) and based on the results of the predictive transport model.
- Based on the modified predictive model and laboratory tests, the experiment and input parameters were designed, e.g. selection of suitable intervals, flow rate, pressure gradient, tracer concentration, tracer injection time, test time, frequency of recording and sampling, etc. The suitable test parameters must be specified for the successful performance of the test (e.g., sufficiently large maximum and minimum concentration responses, suitable pressure field, flushing time of the system for further tests, etc.).
- The stability of the measuring system without the need for frequent calibration (before the test/verification after the test) is important for the performed tests.
- For the tests, it is good to minimize both the “dead volume” of intervals and auxiliary instrumentation (e.g., piping, flow cells, “padding” of intervals, pipe diameters). For the selected flow rates, optimization of the flow measuring cells is also recommended (depending on the dead volume, speed of response to measured parameters, etc.).
- For long-term tracer experiments, it is necessary to ensure accurate and stable instrumentation and a backup source of electricity (e.g., no power outages).
- For the tracer tests, use groundwater directly from the studied interval (e.g., due to the variability of the geochemical composition of groundwater in fracture systems).
- For tests in the conductive zone with high flow rates from the interval, a large amount of water is required for the tracer test. It is therefore necessary to take water from the

selected interval sufficiently in advance to ensure the necessary volume of water for the flushing phase of the test.

- During the tests, problems were solved at high flow rates (up to approximately 1.2 l/min), when some measuring systems do not react quickly enough and the measurement signal is subsequently delayed (e.g., UV Vis measurement in a flow cell). Pressure losses (“throttling”) may also occur in the measuring cells, which affects pressure changes in the system.
- At high flow rates, the system may be pressurized, and the increased pressure may subsequently affect the detection system (e.g., influencing the measuring electrodes)
- At high flow rates, the use of standard automatic sampling systems (e.g., programmable autosamplers) is limited, because during the sampling (switching of the sampling valve) the system is choked/pressurized and therefore the flow rate is affected.
- When using groundwater from a fracture system, it is useful to filter the groundwater (during sampling) in order to remove possible colloidal particles, turbidity, etc.

Further recommendations for the tracer tests

- For the tracer tests and subsequent evaluation and validation of the models, it is advisable to use a discrete fracture, which will enable accurate characterization and subsequent validation of the measured parameters with model approaches. Complicated systems of fault zones and a large number of fractures (fracture networks) complicate more accurate calibration of the models.
- Use “simpler” fracture systems for model validation and uncertainties for tracer experiments.
- Try to make maximum use of natural conditions during the tests (e.g., natural pressure conditions, natural flow, etc.).
- If possible, install a detection system (electrodes, sensors, etc.) directly in the tested interval, when there is a quick reaction to the penetration of the tracer, minimizing the influence of additional instrumentation (e.g., dispersion on piping, pressure losses, etc.). When installing measuring/detection systems in intervals, it is necessary to set up a suitable calibration/verification system of the measuring system (ideally without the need to remove the entire packer system). If it is necessary to remove the multipacker system and then reinstall it, it is necessary to take into account the time needed to establish the hydrogeological conditions.
- Minimize the “dead volume” of both the intervals and the instrumentation.
- Before the experiments, thoroughly test the selected tracers and the test concept under laboratory conditions.
- Use measurement systems that allow low detection limits for accurate measurement of tracer concentrations above background levels. It is also advisable to take samples during the experiment to verify/fine tune the measured concentrations (measurements performed in the laboratory).
- It is advisable to use radionuclides with conservative behavior and low detection limits, the transport of which takes place independently of the environmental conditions (e.g., HTO). For the study of advection, it is advisable to use short-lived radionuclides, which after “extinction” allow the test to be repeated and do not cause contamination of the surrounding environment with radioactive substances.

- If the design of the experiment allows it (e.g., borehole diameters, packer system), when testing permeability intervals (with high flow rates), choose pipes with a larger diameter (minimizing pressure losses due to the resistance of the pipes vs. "dead volume") or, ideally, use the measurement of the studied parameters directly in the studied interval (e.g., conductivity, ISE electrodes, etc.). This is influenced by the overall instrumentation, e.g., the dimensions of the packer system for laying cables, etc.

Use of hydrogeological modeling for evaluating the fracture system:

- The primary basis for hydrogeological modeling in a fracture environment (HydroDFN) is a geometric model of the fracture network compiled based on a geological model and data from hydraulic tests, well-logging measurements, etc. For model evaluations in computer software, it is simpler to process a stochastic model of the fracture network based on variability parameters and statistical sets of input data. For the needs of the model evaluation of the work in this project, the main basis was a semi-deterministic model, where the fracture, or their intersections with boreholes and tunnels, are entered in the model with specific coordinates. This approach is necessary due to the model solution and evaluation of the tests performed on specific fracture connections. On the other hand, the creation of a semi-deterministic model is quite subjective, and dependent on the developer of the model, the interpretation of the data, and may be burdened with a large rate of error, which is then transferred to the entire modeling process. Therefore, at the stage of processing the geometric (geological) model, it is necessary to deal with the issue of determining uncertainties in the model and its validation, which is often neglected and is only addressed in connection with hydrogeological modeling and calculation of flow and transport. The creation of semi-deterministic models also requires specific tools for the geometric processing of the generated networks, which are not a standard part of computer software (e.g. entry of non-intersecting fractures, stochastic generation of fracture centers on a 2D surface, etc.).
- Another basis for the hydrogeological model is outputs from the WPT and the evaluation of the transmissivity of the fractures, or the tested intervals. The results from the model calibration for transport tests show that the fracture transmissivities evaluated in this way may only be apparent, or rather they may represent a wider area of the network than the specific fracture on which the test is performed, or they may be affected by more complex boundary conditions than assumed. The output from the implementation of the optimized model and the transport model was several times higher calibrated values of fracture transmissivity compared to the WPT results. From the WPT outputs, we recommend using directly measured flow values rather than evaluated transmissivities in the models and during their calibration (use these as input estimates).
- The evaluation of tests and the application of mathematical models are conditioned by the range and quality of the input data. For example, if the test is evaluated in an interval in which multiple fractures are interpreted within the geometry of the network, it is necessary to provide data for all the individual fractures for the DFN model. If this is not the case, evaluation of tests with the same or very similar result may be implemented on an "equivalent" DFN model, where the set of fractures in the interval is replaced by a single fracture with corresponding "equivalent" properties (EDFN is not commonly used for this type of simplification, but it is offered as an analogy to ECPM).
- When using ECPM models in a fracture environment, which is usually recommended for optimization and acceleration of the calculation, relatively large homogenization of the

pressure field in the rock and different flow simulation results were found, compared to the results of DFN models. We recommend using and developing the possibilities and capabilities of DFN modeling, even at the cost of a longer calculation time. Alternatively, verify the calculation on a complex ECPM model. The numerical calculation and mathematical apparatus verified on a simple task may not fully function on a more complex network on a larger scale.

- The model evaluation of the transport experiment may be significantly influenced by input uncertainties in the geometry of the task, the hydraulic description (boundary conditions) and the instrumentation of the experiment. Depending on the purpose of the test, e.g., if the output is to be the evaluation of transport parameters, we recommend performing transport experiments in a well-described fracture system and with appropriate test instrumentation. However, these conditions cannot always be ensured during the design of the project, their fulfillment should not be "bound" by the work time schedule.
- Comparison of breakthrough curves from the calculation of transport by the particle tracking method (transport by advection, 1D trajectory) and "full" transport (advection and dispersion in a 2D network) showed the comparability of the results, i.e., the same times for reaching the maximum concentration were calculated. Therefore, due to its speed of calculation, the particle tracking method, which can be used directly in DFN networks (in contrast to the calculation of full transport), is a very effective tool for predictive simulations or evaluation of tests and determination of basic transport parameters.

11.2 Recommendation of Further Work

In conclusion, recommendations are given for further use of the existing workstation ZK-2 with instrumented boreholes S-27, S-31, S-36, and S-8, as well as recommendations for possible implementation of the program at a completely new workstation.

11.2.1 Possible Use of the Workstation in ZK-2

- Use the existing instrumentation for long-term tracer tests on the fracture mesh24 between intervals S31_2 and S36_3, at lower flow rates and pressure gradient, which are closer to natural conditions. These conditions more accurately simulate the natural flow of water in the fracture system.
- Perform further and additional experiments for fractures with different properties (less conductive fractures, fracture zones, etc.), to obtain a range of values for different types of fractures and fracture zones.
- Test the flow and transport in multiple intervals, e.g., tracer injection into a selected interval with measurement of tracer penetration in multiple intervals at the same time, which will enable a more accurate evaluation of the total balance of the tracer, evaluation of dispersion in the fracture system, "cleaning" time of the environment, and determination of sorption properties on the surfaces of fractures depending on the tracer used.
- Test various tracers. For example, use a cocktail of tracers (sorbing, slightly sorbing short-lived radioactive tracers, DNA nano-tracers, etc.) to determine not only the transport characteristics of fractures, but also for testing and developing new measurement methodologies.
- Test with redox-sensitive tracers (to study the influence of redox conditions).

- Tracer tests with radionuclides (HTO, ^{22}Na). Verification of the permitting process, setting conditions for working with radionuclides, studying the transport of radionuclides in natural conditions.
- Use the existing system and selected fractures to study the transport of bentonite colloidal particles.
- “Dilution” tests – circulation of the tracer in the interval and evaluation of the drop in concentration due to natural flow (in an interval with a permeable fracture) or diffusion (in a poorly permeable interval).
- Test detection systems. Tests may focus on the development and testing of new measuring systems in natural conditions (e.g., the effect of pressure, microbiology, salinity of the solution, ionic strength, interference of various elements). Attention may be focused primarily on online measurement systems, or systems that may be installed directly into the studied intervals (with an emphasis on online recording of measured parameters, signal stability, detection limits, sensitivity and accuracy, online calibration options, etc.).
- Study/test the redrilling of active samples (e.g., after sorption of ^{134}Cs, ^{133}Ba) – preparation for further experiments. After the tracer tests with sorbing RN, take a sample (fixation and shaving) of the fracture zone. The experiment will examine the possibilities of studying the distribution of activity in fracture zones, sorption processes of fractures and their fillings, diffusion processes into the rock matrix, etc.
- Study gas migration. Another associated transport medium may be gases and colloids. Tests may focus on gas transport at the same intervals as tracer tests with conservative tracers (solutions). For the tests, it is advisable to use gases that enable both the measurement of hydraulic conditions and the transport and detection of gas (e.g., measurement of Rn, Ar, H).
- The results of future in-situ experiments may be applied in the creation of models of the part of the transport path through the rock environment, into which the properties of the flow paths (fractures) and the retention properties of the rock matrix are entered as input parameters.
- Verify the manipulation of the multipacker system – technical options for adjusting the instrumentation, removing the multipacker system from the borehole and changing the monitored intervals in borehole S-27, where the lower section of the borehole is more suitable for testing, adjusting the input/output pipes.
- Study the hydraulic properties of individual fractures/fracture zones. For more accurate characterization of the GeoDFN and HydroDFN model for individual fractures/fracture zones. In the proposed experiment, a multipacker would be removed from a borehole, e.g., S-36 (if technically possible), and detailed water pressure tests and hydraulic tests would then be performed in this borehole using a double packer with a short defined interval (e.g., 1–2 m). During the tests, measurements would be made in other boreholes and multipacker intervals. Alternatively, it would subsequently be possible to perform tracer tests on the selected fracture of interest. Dual packer instrumentation could be optimized for a specific fault (i.e., minimizing dead volume, intra-interval optimization of the measurement system).

11.2.2 Recommendations for Further In-Situ Experiments

- Optimal selection of the studied block with regard to the objective of the project. For example, for transport experiments, select a simpler and clearly defined fracture system, well described in advance in terms of geometry and hydraulics, i.e., one discrete fracture, simpler connection to the surrounding network of fractures.

- Long-term monitoring of groundwater pressure and flow as a basis for describing the rock environment and for planning experiments.
- Fracture system characterization – for the fracture of interest or fault zones on which experiments will be performed, perform pressure tests with a simple packer (classical WPT) or another type of hydraulic test (e.g., using PFL). We recommend surveying of the entire borehole and identifying all significant conductive structures, including their correlation with the geological description and other measured data (e.g., from well-logging). The aim of the characterization is to obtain a larger statistical set of input data that may be further used for a stochastic description of the site.
- Based on the hydrogeological monitoring and structural-geological mapping, choose monitoring components, e.g., dimension of pipes for expected inflows, choose the number of packers based on the complexity of geological conditions. Set the appropriate drilling diameter to these conditions.
- Tracer tests with radionuclides and study of reactive transport. Perform tracer tests with a "cocktail" of tracers to study the conservative flow (e.g. NaCl, HTO, KI, fluorescein), or slightly sorbing (Rhodamine WT, ^{22}Na) in the framework of a single test (i.e., guaranteeing the same input conditions). To minimize possible contamination of the rock environment with radionuclides, the use of short-lived radionuclides (e.g., ^{24}Na, ^{42}K, ^{198}Au, ^{166}Ho, ^{188}Re) is advisable. Short-lived radionuclides significantly reduce the environmental impact on the rock environment, and comply with safety and legislative requirements for releasing the source into the environment. As part of the development, new on-line detection systems following the Rademet project would be tested and applied (Zuna et al. 2021b).

When conducting experiments, the following is recommended:

- Use mathematical modeling options as a tool for design or detailed evaluation. The basis and input to the models are relevant data from the characterization of the rock environment, processed for further use (evaluated and processed raw data) and with an evaluated degree of uncertainty. Parameters with greater uncertainty may be modeled statistically.
- In the case of multi-year or complexly assigned projects with a larger number of implemented works (stages), enable and simplify changes to the work time schedule depending on the achieved outputs and identified uncertainties, perform additional works or repeat those already implemented. Alternatively, divide more complex projects into several separate units (projects), designed and written gradually.
- Transport tests and subsequent visualization of the transport path, i.e., study the distribution and transport through a discrete fracture, e.g., with sorbing tracers. After the test, the fault zone/fracture would be injected with fluorescent resin, redrilled and then tracer retardation and penetration into the rock matrix would be studied and evaluated. This would make it possible to describe the retardation processes in the fracture zone, as well as the penetration of the tracer into the rock matrix (effect of diffusion), which is affected by fracture fillings, etc.
- "Dilution" test, during which the tracer circulates in a defined interval and the concentration/activity gradually decreases due to natural flow (in an interval with a permeable fracture) or diffusion into the rock environment (in the case of a poorly permeable interval) or retardation. Based on mathematical modeling, it would be possible to optimize transport-diffusion models and obtain transport parameters from the real environment.

- Study advection-diffusion processes on a less fractured block (discrete fracture) (long-term experiment with the possibility of studying diffusion into the rock matrix – validation of mathematical models).
- We recommend examining the values of hydraulic and transport parameters not only for individual fractures, but also for fault zones or structures formed by a series of interconnected subparallel fractures. These structures may have similar hydraulic properties (permeability), but due to their faulting they have a larger surface area and higher porosity. They may contain fracture fillings with a higher sorption capacity and have completely different transport properties.

12 References

BUKOVSKÁ Z, VERNER K. (EDIT) (2017): Komplexní geologická charakterizace prostorů PVP Bukov, Závěrečná zpráva, MS, SÚRAO. 2017.

BUKOVSKÁ Z., SOEJONO I., VONDROVIC L., VAVRO M., SOUČEK K., BURIÁNEK D., DOBEŠ P., ŠVAGERA O., WACLAWIK P., ŘIHOŠEK J., VERNER K., SLÁMA J., VAVRO L., KONÍČEK P., STAŠ L., PÉCSKAY Z., VESELOVSKÝ F. (2019): Characterization and 3D visualization of underground research facility for deep geological repository experiments: A case study of underground research facility Bukov, Czech Republic.– Engineering Geology, 259, 105186.

ConnectFlow Team (2020): ConnectFlow, Technical Summary, Version 12.2. Jacobs.

ConnectFlow Team (2021): ConnectFlow, Technical Summary, Version 12.3. Jacobs.

CRAWFORD J. (2008): Bedrock transport properties Forsmark. Site descriptive modelling SDM-Site Forsmark. SKB R-08-48, Svensk Kärnbränslehantering AB.

FIELD, M. (2002): The QTRACER2 program for Tracer Breakthrough Curve Analysis for Tracer Tests in Karstic Aquifers and Other hydrologic Systems. – U.S. Environmental protection agency, hypertext multimedia publication in the Internet at http://cfpub.epa.gov/ncea/cfm/recordisplay.cfm?deid=54930

FISHER N.I., LEWIS T., EMBLETON B.J.J. (1993): Statistical analysis of spherical data. 329 s. Cambridge University Press (CUP).

GVOŽDÍK L., KABELE P., ŘÍHA J., ŠVAGERA O., TRPKOŠOVÁ D., VETEŠNÍK A., A KOLEKTIV. (2020): Transport radionuklidů z hlubinného úložiště/Testování koncepčních a výpočetních modelů – Závěrečná zpráva. Závěrečná zpráva, SÚRAO – Správa úložišť radioaktivních odpadů, Praha.

KABELE P., ŠVAGERA O., SOMR M., NEŽERKA V., ZEMAN J., BUKOVSKÁ Z., FRANĚK J., JELÍNEK J., SOEJONO I. (2017): Mathematical Modeling of Brittle Fractures in Rock Mass by Means of the DFN Method. Final report, SÚRAO – Radioactive Waste Repository Authority, Prague, Czech Republic.

KRYL J., ŠVAGERA O., BUKOVSKÁ Z., SOEJONO I., ZELINKOVÁ T. (2020): Výzkum puklinové konektivity v PVP Bukov - Průběžná zpráva č. 1 - část 2 - Charakterizace zájmového místa. SÚRAO 459/2020

KŘÍBEK B., ŽÁK K., DOBEŠ P., LEICHMANN J., PUDILOVÁ M., RENÉ M., SCHARM B., SCHARMOVÁ M., HÁJEK A., HOLECZY D., HEIN U., LEHMANN B. (2009): The Rožná uranium deposit (Bohemian Massif, Czech Republic): shear zone-hosted, late Variscan and post-Variscan hydrothermal mineralization. – Mineralium Deposita, 44, 1, 99–128.

MOYE D.G. (1967): Diamond drilling for foundations. Aust. Civil Eng. Trans., CE 9(1): 95–100.

ŠVAGERA O., BUKOVSKÁ Z., FRANĚK J., JELÍNEK J., SOEJONO I. (2017): Metodika dokumentace výchozových partií pro účely DFN modelování. Technická zpráva, SÚRAO – Správa úložišť radioaktivních odpadů, Praha.

TERZAGHI R. (1965): Sources of error in joint surveys. Geotechnique, 15(3), 287–304.

ZUNA M., HAVLOVÁ V., KOLOMÁ K., JANKOVSKÝ F., GRECKA M., ŠVAGERA O., HOLEČEK J., ŘIHOŠEK J., SOSNA K., GVOŽDÍK L. (2020): Výzkum puklinové konektivity v PVP Bukov - Průběžná zpráva č. 1 - část 1- Rešerše. SÚRAO 459/2020.

ZUNA M., HAVLOVÁ V., ŠVAGERA O., HOLEČEK J., SOSNA K., MILICKÝ M., GVOŽDÍK L. (2020): Výzkum puklinové konektivity v PVP Bukov - Průběžná zpráva č. 1 - část 3 - Realizační projekt. SÚRAO 459/2020.

ZUNA M., HAVLOVÁ V., JANKOVSKÝ F., ŠVAGERA O., KRYL J., ZELINKOVÁ T., HOLEČEK J., ŘIHOŠEK J., SOSNA K., KOŘALKA S., GVOŽDÍK L. (2020b): Výzkum puklinové konektivity v PVP Bukov - Průběžná zpráva č. 2. SÚRAO 521/2020.

ZUNA M., HAVLOVÁ V., JANKOVSKÝ F., ŠVAGERA O., SOSNA K., GVOŽDÍK L., HOLEČEK J., ŘIHOŠEK J., HOFMANOVÁ E., KOČAN K., KRYL J., ZELINKOVÁ T., KOŘALKA S. (2021): Výzkum puklinové konektivity v PVP Bukov - Průběžná zpráva č. 3. SÚRAO 551/2021.

ZUNA M., JANKOVSKÝ F., ŠVAGERA O., SOSNA K., GVOŽDÍK L., KABELE P., SKALA V., MILICKÝ M., POLÁK M., HOLEČEK J., ŘIHOŠEK J., KRYL K., ZELINKOVÁ T., HAVLOVÁ V. (2022): Výzkum puklinové konektivity v PVP Bukov – Průběžná zpráva č. 4. SÚRAO 630/2022.

ZUNA M., JANKOVSKÝ F., GVOŽDÍK L., MILICKÝ M., SOSNA K., ŠVAGERA O., DOBEŠ P., KABELE P. (2023): Výzkum puklinové konektivity v PVP Bukov – Průběžná zpráva č. 5. SÚRAO 702/2023.

Zuna M., Dobrev D., Jankovský F., Havlová V., Kůs P., Šoltés J., Vratislavská H.A., Jakůbek J., Doubravová D., Palušák M. (2021b): Využití krátkodobých RAdiostopovačů a vývoj jejich DEtekčních METod pro popis procesů, ovlivňujících transport kontaminantů v životním prostředí (RADEMET) MPO TRIO FV30430. Závěrečná zpráva projektu – Technická zpráva, ÚJV Z5628

SÚRAO | SPRÁVA ÚLOŽIŠŤ RADIOAKTIVNÍCH ODPADŮ | NAŠE BEZPEČNÁ BUDOUCNOST

info@surao.cz | **www.surao.cz**